Vision-Based Control of Flexible Robot Systems

Von der Fakultät für Ingenieurwissenschaften,
Abteilung Maschinenbau und Verfahrenstechnik
der
Universität Duisburg-Essen
zur Erlangung des akademischen Grades
eines
Doktors der Ingenieurwissenschaften
Dr.-Ing.
genehmigte Dissertation

von

Mustafa Turki Hussein
aus
Babylon, Irak

Gutachter: Univ.-Prof. Dr.-Ing. Dirk Söffker
Univ.-Prof. rer. nat. Josef Pauli
Tag der mündlichen Prüfung: 05. August 2014

Dedicated to the memory of my father

Turki Hussein

Acknowledgement

I would never have been able to finish my dissertation without the guidance of my committee members, help from friends, and support from my family.

I would like to express my deepest gratitude to my first advisor, Prof. Dirk Söffker, for his excellent guidance, caring, patience, and providing me with an excellent atmosphere for doing research. I would also like to thank Prof. Josef Pauli my second advisor, for guiding my research for the past three years and helping me to develop my background in computer vision. Special thanks go to Prof. Yan Liu, I am thankful for her aspiring guidance, invaluable constructive criticism and friendly advice during the work.

I would like to thank my committee members in the chair of dynamics and control, which as good friends were always willing to help and give their best suggestions. I am sincerely grateful to them for sharing their truthful and illuminating views on a number of issues in the university and in social life. It would have been a lonely life without them, and my research would not have been possible without their helps.

I also want to thank Ministry of Higher Education in Iraq and German Academic Exchange Service (DAAD) for their financial support granted through MoHESR/DAAD scholarship program.

Finally I would also like to thank my family; they were always supporting me and encouraging me with their best wishes.

Duisburg, November 2014 Mustafa Turki Hussein

Abstract

This thesis covers the controlling of flexible robot systems by using a camera as a measurement device. To accomplish the purpose of the study, the estimation process of dynamic state variables of flexible link robot has been examined based on camera measurements. For the purpose of testing two application examples for flexible link have been applied, an algorithm for the dynamic state variables estimation is proposed.

Flexible robots can have very complex dynamic behavior during their operations, which can lead to induced vibrations. Since the vibrations and its derivative are not all measurable, therefore the estimation of state variables plays a significant role in the state feedback control of flexible link robots. A vision sensor (i.e. camera) realizing a contact-less measurement sensor can be used to measure the deflection of flexible robot arm. Using a vision sensor, however, would generate new effects such as limited accuracy and time delay, which are the main inherent problems of the application of vision sensors within the context. These effects and related compensation approaches are studied in this thesis. An indirect method for link deflection (i.e. system states) sensing is presented. It uses a vision system consisting of a CCD camera and an image processing unit.

The main purpose of this thesis is to develop an estimation approach combining suitable measurement devices which are easy to realize with improved reliability. It includes designing two state estimators; the first one for the traditional sensor type (negligible noise and time delay) and the second one is for the camera measurement which account for the dynamic error due to the time delay.

The estimation approach is applied first using a single link flexible robot; the dynamic model of the flexible link is derived using a finite element method. Based on the suggested estimation approach, the first observer estimates the vibrations using strain gauge (fast and complete dynamics), and the second observer estimates the vibrations using vision data (slow dynamical parts). In order to achieve an optimal estimation, a proper combination process of the two estimated dynamical parts of the system dynamics is described. The simulation results for the estimations based on vision measurements show that the slow dynamical states can be estimated and the observer can compensate the time delay dynamic errors. It is also observed that an optimal estimation can be attained by combining slow dynamical estimated states with those of fast observer-based on strain gauge measurement.

Based on suggested estimation approach a vision-based control for elastic ship-mounted crane is designed to regulate the motion of the payload. For the observers and the controller design, a linear dynamic model of elastic-ship mounted crane incorporating a finite element technique for modeling flexible link is employed. In order to estimate the dynamic states variables and the unknown disturbance two state observers are designed. The first one estimates the state variables using camera measurement (augmented Kalman filter). The second one used potentiometers measurement (PI-Observer). To realize a multi-model approach of elastic-ship mounted crane, a variable gain controller and variable gain observers are designed. The variable gain controller is used to generate the required damping to control the system based on the estimated states and the roll angle. Simulation results show that the variable gain observers can adequately estimate the states and the unknown disturbance acting on the payload. It is further observed that the variable gain controller can effectively reduce the payload pendulations. Experiments are conducted using the camera to measure the link deflection of scaled elastic ship-mounted crane system. The results shown that the variable gain controller based on the combined states observers mitigated the vibrations of the system and the swinging of the payload.

The presented material above is embedded into an interrelated thesis. A concise introduction to the vision-based control and state estimation problems is attached in the first chapter. An extensive survey of available visual servoing algorithms that include the rigid robot system and the flexible robot system is also presented. The conclusions of the work and suggestions for the future research are provided at the last chapter of this thesis.

Contents

List of Figures

Nomenclature

Mathematical terms

e	Estimation error
f_c	Focal length of the camera
f, f^*	Estimated and desired features
$g(t)$	Dynamic accounting equation
p_2	Wind force disturbance signal
q	Elastic crane displacement variable vector
s_x, s_y	Effective pixel size
t_{ext}	Translational extrinsic vector
u, y	Input and output signal
u_i , v_i	Image coordinate frame
v	Displacement vector after applying the boundary conditions
v_T	Displacement vector
x_0, y_0	Origin center of projection
x_p, y_p	Point position image plane
z	Elastic crane state vector
A, B, C, D, E, F	State space model matrices
F_f	Force vector after applying the boundary conditions
F_T	Force vector
K_z, K_Δ, K_2	The controllers gain matrices
L_1, L_e	The observers gain matrices
M_0, K_0, $B_{1,\cdots,5}$	Elastic crane dynamic model matrices
M_f, D_f, K_f	Flexible link dynamic model matrices after applying the boundary conditions
M_T, D_T, K_T	Flexible link dynamic model matrices
OG	State estimation gain
P^c	Point position with respect to camera coordinate
${}^C P_T$, ${}^C P_T^*$	Estimated and desired target pose
Q_e, Q_{m1}, R_e, R_{m1}	Symmetric positive definite weighting matrices
R_{ext}	Rotational extrinsic matrix
X_g, Y_g, Z_g	Point position global coordinate
X_P, Y_P, Z_P	Point position camera coordinate
β	Boom base luff angle
χ	Single flexible link state vector

η	Measurement noise
τ	Time delay
w_i, θ_i	Translational and rotational displacements flexible link
$\Delta\delta$	Sea waves rolling force
Δw_3, $\Delta\alpha_2$, $\Delta\phi_2$	Elastic crane measurement variables
$\Delta\rho$, ΔL, ΔD	Elastic crane control input signals
$\dot{}$	Derivation with respect to time
$\hat{}$	Estimation
$\tilde{}$	Transformed matrix or vector

Important abbreviations

2D	Two Dimensions
3D	Three Dimensions
CCD	Charged Coupled Device
CSM	Camera System Manipulation
DOF	Degree of Freedom
EKF	Extended Kalman Filter
HBVS	Hybrid Visual Servoing Approach
IBVS	Image-Based Visual Servoing
LQR	Linear Quadratic Regulator
MIMO	Multi Input Multi Output
PI	Proportional Integral
PD	Proportional Derivative
PBVS	Position-Based Visual Servoing
RGB-D	Red Green Blue - Depth
SRS	Lehrstuhl Steuerung, Regelung und Systemdynamik

1 Introduction

In this chapter, a detailed overview of the intended study is outlined. Problem definition and objectives of the study are delineated. Finally, the outline of thesis is described.

1.1 Background

Besides the studies on the human/animal vision with the goal of understanding the operation of biological vision systems, vision technology is a popular research topic in robotic realm. There is a paradigm shift on developing vision systems for the application in an industrial environment such as navigation, recognizing, and tracking objects.

Machine vision system can not perform all the functions of human eyes. However, robot vision technology provides a combination of flexibility, adaptability, precision, non-contact measurement, and object recognition for robotics. Generally, using a vision system two questions can be answered: "What it is?" and "Where it is?". Here "it" refers to the observed object in the scenery. A robot visual servoing system can answer both questions, but often focuses on one of them.

During the past decades industrial robots have become very important facet in the manufacturing industry. Robots are applied to new areas each day, and in order to be able to go into more new applications the robots often require better performance or lower price. In order to meet these demands the physical robot structures are built lighter and flexible materials (flexible robots). Therefore the demands on the accuracy of the robot controllers have been growing. Good models are also needed for model-based diagnosis of robots. A fundamental property in flexible robot control is that the amount of sensors is limited. Usually, in the rigid robot joint encoder signal is the only available feedback. But in the flexible robot with infinite number of degree of freedom which come from the deformation of the flexible links, a comprehensive measurement system is needed to compensate for these flexibilities.

Flexible robots are now widely applied in various areas; especially in space plants where pick and place processes are often required. A flexible robot system is a special type of robots, the feedback signal in this system can be easily affected by any uncertainty such as: robot calibration errors, lack of link stiffness, poor

fixturing, and predictable target motion which can pose of the robot end-effector or target object. Considerable effort and cost are expended to overcome the above issues, e.g., to design and manufacture special-purpose end-effectors and intelligent jigs and fixtures. Another difficulty with such systems is the preparation of the robot for new tasks requires considerable reprogramming effort.

In order to overcome the above disadvantages, the most straight forward solution is to add additional sensors to the conventional robot control system, which can directly measure the relative motion between the robot end-effector and the target. The vision sensor is one of the low cost, acceptable accuracy, and versatile sensors that are well suitable for this application. Vision-based flexible robot control, or visual servoing for flexible robot, has been one of the major research areas in flexible robotics for more than a decade. The task of robot visual servoing is to control the pose of the robot end-effector relative to either a world coordinate frame or a target object being manipulated, using real-time image measurements extracted from the distinguishable visual features.

The advantages of flexible robot visual servoing can be summarized as follows:

- It can reduce the requirement for the exact specification of the target pose. Therefore, it can reduce the costs associated with robot teaching and special-purpose fixtures. One of the significant improvements is that it can allow operations on arbitrarily moving or randomly placed target object.
- The requirement for exact positioning of the robot end-effector can be relaxed. In other words, the robot operations are not completely dependent on mechanical accuracy and stiffness of the robot structure. Hence, robot mechanisms could be built lighter. This can lead to reduced cost of robot manufacturing and operation, and decreased robot cycle time.
- Task specifications in a flexible robot visual servoing framework would be supported. That means it is relatively robust to many disturbing effects in unstructured environments, and can be easily adapted to monitor changes in the task or target object without requiring extensive reprogramming efforts.

1.2 Description of the Research Area

The main objective of this work is to improve the robust control performance (state estimation capability) of an existing flexible robot by equipping the flexible robot

system with a vision system. In order to achieve the goal of this dissertation, the vision-assisted dynamic state variables estimation and vision-based control; for flexible robot systems are studied. The purpose also is to study the dynamic error of state estimation process for flexible robot with a vision sensor. The vision system can be used as a good failure inspector by combining the data of other sensors with vision sensor measurements. For state estimation of a flexible link robot the camera system is proposed as a robust substitute for the strain gauge sensors. Here robustness is defined as: the measurements are not effected by the change of the internal dynamics. Vision-based flexible robot state estimation is applied in a direct visual servo control method, which has been proposed for an elastic ship-mounted crane type manipulator in this thesis. The main problems related to the vision sensor have been addressed in the dynamic state estimation of the flexible robot system theoretically and experimentally.

1.3 Outline

This thesis is organized as following:

Chapter 2 outlines the literature survey on the visual servoing theories. Applications of vision-based control related to the flexible robot are discussed. Chapter 3 describes the state estimation process of dynamical systems based on vision sensor data. Suggested estimation approach is applied using flexible link beam as a case study. Subsequently, in Chapter 4 the estimation approach is used with the elastic ship-mounted crane system. The mathematical model of the elastic ship-mounted crane is re-derived. The state estimation process and control is simulated. In chapter 5 The elastic ship-mounted crane test-rig is used to verify suggested estimation approach using different types of measurements through experiments. The camera modeling and calibration process is done. The deflection measurements through camera and combination of the camera system in the test-rig are also detailed. Finally, the conclusions and considerations regarding further research are presented in Chapter 6.

2 Literature Review

Robots are widely applied in various areas, especially in industrial assembly processes. One major source of uncertainty that often leads to poor performance or even failure of the assembly tasks is the absolute motion control used in the conventional robotic systems [JS02]. Using this type of control, the target object is required to be accurately placed at fixed world coordinate frame, and therefore, only absolute pose (3D position and orientation) of the robot end-effector in the base frame is controlled to operate with respect to the target object. Usually, the robot joint encoder is the only available measurement in rigid manipulator system. So the operation can be affected by uncertainty or errors regarding the pose of the robot end-effector or target object, e.g. due to robot calibration errors, lack of link stiffness, and unpredictable target motion. These conflicting requirements between high speed and high accuracy lead to the use of flexible robots.

Here the challenge lies in the incorporation of flexibility effects in the system model leading to increase in complexity which, in turn, complicates the problem of controller synthesis. Due to the flexibility the controller must be able to control the motion of the rigid-body mode of the arm and to suppress the vibration modes. Flexible link robots are distributed parameter systems and have an infinite number of degrees of freedom; hence many researchers have tried to solve the control problem by improving the dynamic models and incorporating different control strategies. Due to the structural flexibility of flexible robots; specific control approaches are required to affect their vibrations. Another difficulty with such systems is that the preparation of the robot for new tasks requires considerable reprogramming effort [CLG+12].

In order to overcome the above issues, a straightforward solution is to add additional sensors to the flexible robots control system, which can directly measure the relative motion between the robot end-effector and the target, and at the same time can also measure the vibration in the flexible link. Vision sensors are cheap, may have specific high accuracy; versatile sensors are well suitable for a wide range of robot control. This has been one of the major research areas in robotics for more than two decades. The task of flexible robot visual servoing are to control the pose of the robot end-effector relative to either a world coordinate frame or a target object being manipulated, and to damp out the vibration in the structure by implementing real-time image measurements extracted from the distinguishable visual features.

This chapter is organized as follows. Section 2.1 describes the general vision-based control process. Visual servoing approaches are addressed in section 2.2. In section 2.3, visual servoing of flexible robot is discussed in detail. Applications and classification of visual servoing of flexible robot is detailed in section 2.4. The state of art is summarized in section 2.5.

2.1 Vision-Based Control

Machine vision [Cor11], which is originated from photogrammetry, is thought to have the ability to sense, store, and recover a virtual space that matches the original space as closely as possible. Based on photogrammetry, machine vision technologies expanded into new research areas such as object recognition. The application of machine vision in robotics is robot vision (visual servoing), which concentrates on recognition, positioning, inspection, and modeling of objects. Two questions about the objects what $\cdots$? (recognition) and where $\cdots$? (precision) could be solved using the vision system [JS02]; in robot applications it should solve both of them. It is often focused to one of these two aspects, to realize the robot system to solve tasks of recognizing special objects (marks) or to evaluate its movement accuracy relative to the environment.

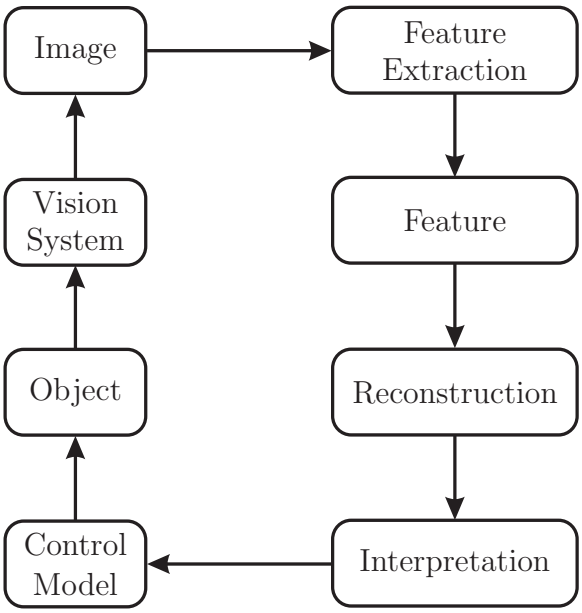

Figure 2.1: General vision-based control procedure

In figure 2.1 a typical robot vision procedure based on the characteristics of robot applications is presented. Different parts of this procedure could be investigated to produce various practical technologies suitable for different applications. The elements in figure 2.1 represent [Cor11]: 3D-world (object), the vision data-2D (image), the data extracted from 2D image (features), the 3D model description of objects or targets (interpretation), the camera (vision system), the image processing (feature extraction), transformation from 2D to 3D algorithm (reconstruction), and the method giving the decision about how to use the results from all elements (control model).

This typical form of the robot vision system can be adjusted based on the following factors: the kinds of images required, features found in the images, the mathematical form of these features as obtained from the images, and how to use the image features recovering the observed objects.

2.2 Visual Servoing System

In 1979, visual servoing is introduced by [HP79], in order to distinguish a new control approach. This technology merges the vision information into the usual control loop of a robot. This type of control system is not only a simple feedback system but a result of the fusion of many areas such as high speed image processing, kinematics, control theory, and real-time computing ([Has03], [JS02]). Incorporated with sensor fusion technology, many vision-based controllers have been investigated which realizing industrial, surgical, space, and military applications. The kinematics-based methods work with the assumption that the velocity of the manipulator can be controlled precisely. While dynamic visual servoing directly provide joint inputs based on visual feedback and the nonlinear robot dynamics. The visual servoing methods have been briefly discussed, compared, and reviewed by many researchers [CH08], [Mal02], [KC02], [Has03], [JS02]. Visual servoing systems were classified with respect to several aspects:

- the position of the camera as eye-in-hand and eye-to-hand [Has03];
- the feedback representation mode position based, image based, and hybrid visual servoing [KC02];
- the combination of vision sensor and controller of the joint: dynamic look-and-move system and direct visual servo system [KC02]; and

- the use of the visual information (control model) distinguishes two types of visual servoing systems: kinematics-based visual servoing and dynamic visual servoing [WLW08a],

in this review only the characteristics and drawbacks of the methods will be presented.

2.2.1 Position-Based Visual Servoing (PBVS)

The 3D-visual information used in PBVS, define the position and orientation of the object (target) with respect to the camera (robot) coordinate system as a desired reference input. Figure 2.2 shows the basic block diagram for PBVS system. Here ${}^{C}P_{T}$ is the target pose with respect to the camera, and ${}^{C}P_{T}^{*}$ is the desired target pose. The error between the desired pose and the pose of the target represent the motion required to move the robot from its initial pose to the desired pose. The position-based methods have been investigated and discussed by many researchers ([DJSW02], [WHB96], [HDAG08], [JF09]).

The practical applications of this method have the advantage that it allows the error computation from the desired relative pose in the 3D workspace. The second advantage is that the end-effector cartesian trajectory can be controlled to move along a straight line in the cartesian space. In addition, the controller design can use the advantage of classic robot control problem; due to the separating of the pose estimation problem from the control design problem [JS02].

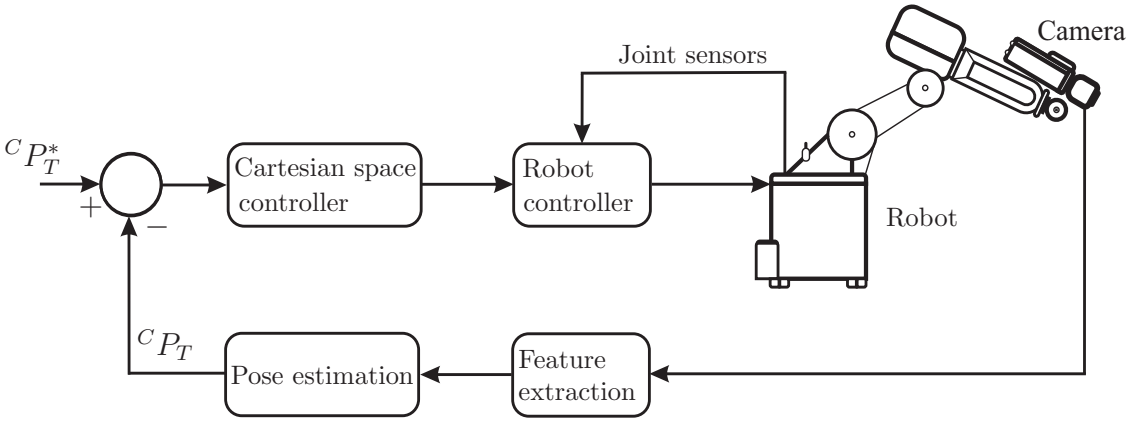

Figure 2.2: Position-based visual servoing

One of the inherent problems of the position-based method is that the geometric model of the object should be known for pose estimation ([Cha98], [HHC96], [MCB99]), which makes it a "model-based" method in comparison with the image-based method. The second problem related to PBVS is the sensitivity of the camera calibration error; the camera calibration is needed to get the unbiased cartesian positioning.

2.2.2 Image-Based Visual Servoing (IBVS)

The image-based visual servoing defines the desired reference input using the 2D-visual information (image features) figure 2.3. In IBVS the relative pose is estimated based on the features f provided by the camera. The control goal is fulfilled by coinciding the desired f^* and estimated f features. In this method, control error function is computed in the 2D space based on the image Jacobin matrix that shows the characteristics of movement in image space. The image-based method have been investigated and discussed by many researchers ([Cha98], [DJSW02], [Esp93], [HHC96], [KC02], [Mal02]). The practical advantage of this method is that it represents a "model-free" method, this means there is no need for a full object model and also no camera model. The positioning accuracy of the image-based method is robust to the camera and target modeling errors ([HHC96], [Mal02]). The stability of the image-based method is known to be robust with respect to camera calibration errors [Esp93].

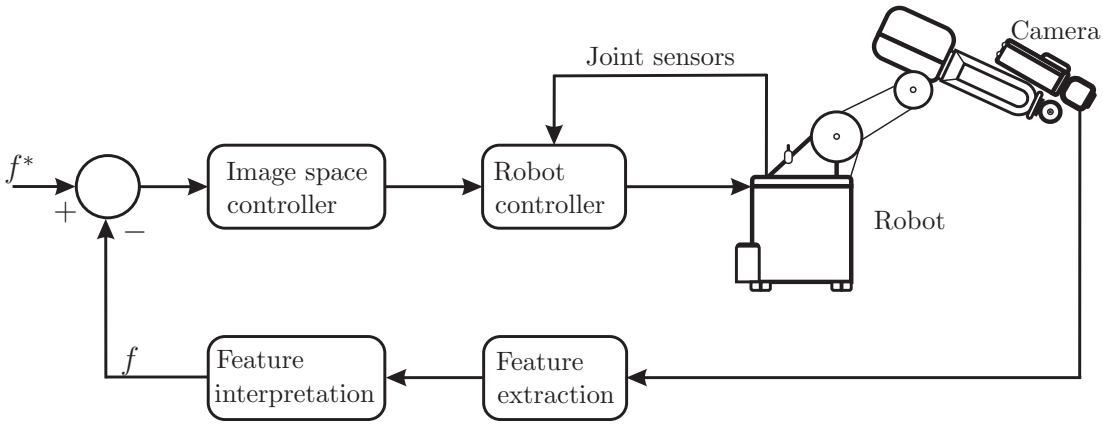

Figure 2.3: Image-based visual servoing

The major disadvantage of the image-based method it is local asymptotic stable, where the control error function decreases exponentially ([Has03], [DJSW02]). It

has been stated [Cha98] due to the coupling between the end-effector translational and rotational motions the image-based visual servoing suffers from typical problem representing the motion coupling, when the camera moves away from the target in a depth direction and then returns (camera retreat). Also in the presence of camera modeling errors the analytically described robustness domain of the stability of the system dynamics can not be determined due to the fact that the system is highly coupled ([Cha98], [Esp93]). There are disadvantages of existing image singularities and image local minima induced from the image Jacobian matrix, which may lead to potential failure of the method [Has03]. These control law drawbacks arise especially when the initial and the goal camera images respectively corresponding to the actual and desired system configurations are very different (i.e for large system displacements).

2.2.3 Hybrid Visual Servoing Approach (HVSA)

Using the advantages of both of the two earlier approaches and in order to overcome their disadvantages a hybrid visual servoing ($2\&\frac{1}{2}$ D) which represents a new visual servoing system is presented by [MCB99]. Hybrid visual servoing represents a system which does not need a complete 3D model of the object, and also can be used in the whole work space of the system. Several hybrid visual servoing approaches have been proposed ([MC02a], [MCB99], [HJ07]). The aim is to get hybrid visual servoing approach which gives a partial control in the same time for both of cartesian and image trajectories. This approach realizes model-free visual servoing; it still uses the recognizable feature in the image but does not require a full object model. Unlike to image-based approaches the analytical robustness domain of system dynamic stability can be determined, in other words camera modeling errors can be expressed by closed form analytical function. Finally this method is free of singularities and local minima.

Another hybrid approach is the partitioned approach [Hut01]. Within the approach the rotation around and translation along the optical axis from all other DOFs are decoupled. This is specifically developed to avoid problems related to a pure rotation around the optical axis. Although the partitioned approach is a very suitable method to keep the object in the field of view. This method has one drawback: the two IBVS rotational degrees of freedom are controlled in image space, they do not take cartesian space into account [GH07]. Another work which executes visual control by combining or partitioning the visual control structure [CH08]. The

methodology of switching control is presented in [CH08], the method allows switching of the controller (i.e. switching between IBVS and PBVS) based on the situation of the system or based on measurements in image space. The switching control encompasses the idea that in each iteration it should be decided which controller should be used, based on performance criteria.

In the last decade many researcher proposed several developments for visual servoing to overcome the drawbacks of previous developed approaches. A virtual visual servoing enabling the calculation of camera parameters iteratively is proposed in [MC02b]. Using a special calibration rig [PCT07] investigated a calibration method to determine varying intrinsic parameters. Fuzzy techniques are used to estimate the robot-camera model [SMSC08] which presents a new eye-to-hand visual servoing method using inverse fuzzy modeling. This method can be used with unknown camera and/or robot parameters. [SY09] also uses a fuzzy controller and applied it on a specific class of IBVS. Here the camera moves in the depth axis, for the sake of finding the image moment to reflect the object depth.

A new method for image-based visual servoing approach with eye-in hand configuration and not calibrated camera parameters proposed in ([WLW08a], [WLW08b], [WLZ08]). Depth independent interaction matrix have been developed and extended, the asymptotic stability of this method has been proved by using Lyapunov theory. The asymptotic stability condition is: the elements result from multiplication of depth interaction matrix and its inverse are greater than zero. The inverse of depth interaction matrix approximated model is determined using offline step. The interaction matrix and the depth are updated at each iteration using the measurements of the features. Each feature is constrained to reach its desired position through straight line. In these studies a new algorithm has been developed to estimate the unknown camera and geometric parameters. An introduction to sensor fusion approach by using a combination of two cameras (eye-in-hand, and eye-to-hand) is presented by [AJSMM10]. Here reduces the inaccuracy of the estimation of the end-effector pose. As a result the robustness of visual servoing is improved.

In the recent years many problems in visual servoing got more and more attention from the researchers. There are many points related to the visual servoing need further studies, e.g., stability analysis of visual servoing systems, uncalibrated visual servoing, time delay in the measurements, sensor data fusion, and stereo visual servoing.

2.3 Visual Servoing of Flexible Robots

A vision sensor (camera) represents a contactless virtual movable measurement sensor, or a set of sensors working at the same time (i.e. getting a set of data from the camera), therefore vision-based control can improve the control performance and can be extended to other application areas such as flexible robot manipulators. In the last three decades the researchers stimulated to study flexible manipulators due to the need of large load capacities, low energy consumption, the use of small actuators, the requirements related to high-speed, and also to high precision robot's operations. Recently there has been an increasing research interest in this area. A number of research reports concentrating in visual servoing of flexible robot applications have been published in order to study related issues problems (see applications in section 2.4).

Flexible robots have been employed not only in space shuttles, but also in industrial, surgical, and maintenance applications. However, due to the structural flexibility and inertial forces, flexible robots have very complex static deflections, they show dynamic vibrations, especially in high speed operations. Static deflection adds the initial condition value to the system which should be taken into account in the control design process. In many cases, there will be very large path tracking or positioning errors. The dynamic models of flexible robot available till date can not take care of large elastic deflections of the manipulator. Internal resonances due to modal interactions are almost ignored, and in most analyses of multi-link manipulators, only linearized models are considered [DE06]. Many control techniques were proposed to isolate the dynamic errors based on the dynamics models [DE06], but they seem not very suitable for real-time application due to the very complicated and time consuming computation of the dynamics of flexible manipulators. Compared to rigid robots the end effector position of flexible links can not be obtained precisely enough based on the kinematics and joint variables, because the position of any point of a flexible link is not only related to the joint angles but also to the link flexural displacements.

2.3.1 State Variable Estimation of Flexible Robot Using Vision Sensors

In case of rigid manipulators, the state variables consist of joint angles and their velocities, which can be measured by encoders, potentiometers, tachometers, and so on. In case of flexible manipulators, however, the state variables also include

elastic deformations and their velocities due to flexibility. In order to control a flexible manipulator based on dynamic model, the state variables should be accurately estimated.

Flexible link robots are distributed parameter systems and have an infinite number of degrees of freedom. Each degree of freedom can be represented by using time related variable and flexible mode shape function. A mode shape function represents the shape of the beam related to a specific natural frequency. This mode shape can be determined by the Eigenvalue problem of the vibration equation. In flexible link robot case the modes are modeled using elasticity theory in order to describe the shape of the link. In general the frequencies of the individual modes have no simple relation to each other. For control purposes the approximation of the dynamical behavior is typically truncated to a finite number of flexible modes [DlB08]. To sense these modes, the sampling frequency has to be at least twice the frequency of the highest mode of interest. Further, the vision system resolution needs to be high enough in order to detect the small vibration amplitudes of higher modes [OB96]. The work on vision-based control for flexible robot is first presented in [TWL90]. The image feedback of the tip displacement and estimated vibration states are used in [TWL90] to improve the overall performance of end-effector position control. The main disadvantages of this work are the limited abilities of data processing and analyzing, camera properties, and image processing software. Several image processing schemes are proposed by [TWL90] to increase the operational speed. The researchers had overcome these disadvantages in the following years through the generation of powerful processing and new vision systems. In [YOK01] the camera is used to measure the state variables of flexible link, and then using these measured states to identify the physical parameters of flexible link dynamic model. The idea is to use the camera sensor to measure the real elastic deformation related to markers along the link and transform these positions (markers position) as virtual passive joint angles.

The issues of vibration measurement and control, the end-effector trajectory tracking control, and Cartesian space trajectory tracking control of robot arms with link flexibility using vision sensor data are addressed in ([JG05], [JE07], [Jia08]). The control strategies used are: regulation of end-effector trajectory tracking error to zero based on visual feedback, compensation of nonlinear forces, and to damp out the vibrations of the flexible links using a PD plus controller based on feedback of link deflections. Since the time derivatives of the end-effector position, joint angles, and link deflections are needed in calculation of the control input, the estimation

algorithms are used to estimate the value of the velocities in order to calculate the control input.

2.3.2 Output Feedback Control of Flexible Robot Using Vision Sensors

As an alternative to state feedback control method, the camera is used as a sensor to measure the output of the system and provide the controller with the information about the target in order to generate the required input. In [OB96] and [OB99], a landmark tracking system-based position sensor with fast sampling rate and good position resolution was proven effective and economical. With this sensor the first two natural modes of the studied long-reach manipulator were identified. The direct sensing of the end point position of a flexible positioning system using this sensor can provide a feedback signal that can always ensure accurate tip placement. The landmark tracking system works even with link inaccurate construction and in the case of uncertain placement of equipment. The analytical criteria for selection of the number, type and location of suitable sensors for robust control of mechanical systems with flexible bodies is presented in [SMVP99]. In the criteria, a dynamic sensors data fusion approach is developed to integrate additional sensors such as vision based sensors in the active control of flexible robots.

The eye-in-hand IBVS of flexible manipulators is studied in [BR06b]. The IBVS approach was chosen as it computes the feedback control directly from the visual information, and does not require any further knowledge of the physical parameters of the manipulator. In [BR06b] the IBVS approach implemented by combining the two-time scale control of flexible structures and the task space control. Dynamic effects of both the rigid and the flexible motion of the manipulator are fully taken into account. The "fast" subsystem uses the joint sensors information, while the visual information is used in the "slow" subsystem for a task-space-oriented control law. Since the control law in this case is related to work space, the computationally expensive operations such as generating the inverse and also the time derivative of the Jacobian, are avoided. The results related to this approach are simulated and implemented experimentally in ([BR03], [BR04], [BR06b]).

2.3.3 Sensor Data Fusion

In the last decade the problem of data fusion sensor (i.e. strain gauge, vision sensor,$\cdots$) in the control of flexible link robots, is strongly addressed by several researchers. The vision sensor data can be used effectively in cooperation with

other types of sensors for control of the flexible robot system due to the versatility of vision sensor. Nowadays the vision sensor can be represented as set of sensors and not only as plain visual feedback. Several measurements can be accomplished in the same time using single vision sensor (i.e. the same image frame) by augmenting the image processing software and without needing to change the sensor position.

The estimation of the elastic coordinates as a problem of sensor data fusion is presented by [BR06a]. Although Kalman filter can be effectively used to weigh the measurements coming from different sensors. The approach developed in [BR06a], allows the design of a complete visual servoing control law which can be applied using a digital camera, a standard image acquisition, and processing hardware. Three dimensional range sensor is proposed in ([LD04], [LD05], [LUD06]) for estimating the vibration of large scale flexible structure. In this scheme, a set of synchronously working satellites is employed to observe the vibrations that appear in various parts of the structure. The measured vibrational data range from the satellites are fused by using Kalman filter. This method is validated by experiment where stereo camera is used as the range sensor in order to estimate the vibration of a quadruple pendulum composed of four links and low friction rotational joints. The method presented consists of three parts: kinematic data fusion, Kalman filtering, and shape estimation. The advantage of this method is that it needs only coarse kinematic surrogate measurements to be provided to the Kalman filter, but on the other hand it assumes that the dynamic model is accurately known and the mode shapes are approximately known a priori.

2.3.4 Improving the Control of Flexible Robot Using Vision Sensors

The most common problems related to vision sensors are that of the noise and time delay of measurement data. Thus the less noisy measurement from the camera can help improving the quality of deflection measurements. On the other hand, to deal with delays in a control system the actuator gains should be increased to increase the damping and making the system more robust against the time delays. However, some approaches are not based on time delay robust controllers but on the accurate estimation of the delay itself. The vision-based two-time scale controller (fast and slow) to track a desired tip position while suppressing oscillations in the single flexible link is described in [XR09]. The vision sensor (slow) is used in combination with motor encoder (fast) to estimate the full states of the system. The effect of noise is removed using a Kalman filter, and the time delay effect is accounted using the

dynamics of the system. The information obtained from end-effector camera (eye-in-hand) used by [JYKU08] to estimate the tip vibration using modified two-time scale Kalman filter takes into account the constant delay due to the image processing time. The estimator is modified in order to deal with image features of unknown objects. The image Jacobian matrix used in measurement equation can not be obtained easily when no prior information available for the detected image features. In [DDM09] two-time scale Kalman filter is used considering a variable delay which is estimated on the basis of time stamps. The variable time delay estimation based on time stamps represents a robust method against visual sensor troubles such as partial occlusions or failure of the camera sensor. The problem by considering sinusoidal regression instead of a Kalman filter to reconstruct the vibration from visual data is addressed in [DDM10]. Using a eye-in-hand configuration, the problem of vibration suppression by using visual features without any markers, or priori knowledge on the environment is developed by the authors of [DDM10]. The tip displacement induced by vibrations is estimated exploiting a simple physical model of the manipulator.

The time delay was estimated in [DDM09], [DDM10] by exchanging timestamps between real-time high sampling rate controller and the non-real time supervisor whose sampling rate is aligned to the camera frame rate. An alternative method described in [Dub10] consists of using a secondary concurrent sensor to estimate the delay. The cross-correlation technique is used to compute the time-delay between the two signals. These signals are: first free of noise, but delayed visual data to estimate the tip displacement and the second is noisy, but concurrent inertial data to correct these visual data in time. An approach to combine suitable measurement devices easy to realize with improved reliability was proposed in [HS12b]. In this work the compensation of time delay and noise effects in the estimated states of the flexible link dynamics is addressed. The approach is based on combination of the two estimated fast and slow dynamical parts of the flexible link dynamics by combining the estimations of the slow observer (based on vision measurements) with those of the fast observer (based on strain gauges).

2.4 Applications

As has been pointed out before, flexible manipulators can find many applications, but since the main problem is to control their vibrations, many researchers have tried to solve this problem by improving the dynamic models and incorporating different control strategies. The study on the control of a flexible arm manipulator started

as a part of the space robots research, as a space manipulator should be as light as possible in order to reduce its launching cost. Another application for large robotic manipulators are needed in nuclear maintenance, e.g., to perform decontamination tasks. The nozzle dam positioning task for maintenance of a nuclear power plant steam generator is an example of a task that requires a strong manipulator with very fine absolute positioning accuracy.

In order to ease the design procedure of flexible space robot systems a method developed in [SMVP99] to select the type and the location of sensors for flexible robotic applications is used. The sensors meeting this criteria are called 'hyperstability sensors'. The criteria is implemented practically on special three revolute joints and a very flexible link designed to simulate the dynamic characteristics of Space Station Remote Manipulator System (SSRMS). A control positioning for flexible link using Camera Space Manipulation (CSM) is developed in [KPB04]. In comparison with the visual servoing method presented by [SMVP99], CSM provides a less computationally intensive method which is imperative for flexible manipulation. Also the amount of image data required for CSM makes it a vigorous method for unknown environments.

2.4.1 Visual Servoing of Flexible Robot Configuration

Any visual servoing systems using typically one of the two camera configurations: (1) Eye-in-hand and (2) Eye-to-hand configurations. The detailed applications for visual servoing of flexible manipulator are described below.

2.4.1.1 Eye-in-hand configuration

Despite of the structural flexibility of flexible manipulators, the eye-in-hand vision-based control which is more complicated than the eye-to-hand approach is addressed by many researchers in the last ten years due to the development of the vision systems and controllers. The concept of the eye-in-hand is used in [MKU03], [MKU04] to design an automated object capturing with a two-arm flexible manipulator. In this work basic technology in space for automated object capture with a two-arm spatial flexible manipulator is presented. A small CCD camera and a laser displacement sensor are mounted at the end-effector of the arm. The camera is utilized to detect the distance to an object and relative orientations at long and middle range,

while the laser displacement sensor precisely measures the distance from each end-effector to the surface of the object at close range. Feature based visual servoing is applied to control the end-effector positions relative to the object positions.

In [FS04] the eye-in-hand approach is used to control the position of a flexible robot end-effector. In [FS04] the flexibilities of the manipulator links was assumed as small disturbances to be counteracted by the feedback control loop. A vision-based training for a neural network control model of a planar, large-deflection robot manipulator is developed by [LF04]. The training data are acquired from images by moving the motors to a randomly selected motor position. This method which requires no previous knowledge of the kinematics or dynamics of the manipulator suffers from several disadvantages: not robust to sudden disturbances, time consuming process of training the neural network, and it is applicable only on planar robot. An approach which is composed of an end-effector position control based on eye-in-hand visual servoing and a vibration suppression control is proposed in ([JKU06], [JKU07]). High and low pass filters are used to decouple the end-effector position control and the vibration control. This modified approach applied practically based on an impedance control used with 3D flexible link manipulator which succeeds to insert the peg into the hole whose clearance is 0.1mm. In [JKU07], also studied the trajectory and vibration control by using an endpoint camera, where a two-time scale discrete Kalman filter is used to estimate the deflection and vibration of the links using the endpoint camera.

Most of vibration control strategies proposed so far assumes that the structural vibration is directly measured (or it can be measured) by sensors such as strain gauges or accelerometers. Specific applications such as Articulated Inspection Arm (AIA) [GBB+09], which works in high temperature and highly level of radiation need special type of sensors. The eye-in-hand camera system used in corporation of other sensor as stated in ([DDM09], [DDM10], [Dub10]) to damp the vibration of the end effector of AIA. A novel approach for active vibration damping of the TUDOR (3-Dof flexible link robot arm) using RGB-D-sensor based on the eye-in-hand configuration is adressed by several articles ([JAR+10], [JAB12], [JAT12b], [JAT12a]). The limitations such as frame rate and camera resolution are studied practically using TUDOR test rig. The end-effector oscillations of TUDOR system are suppressed using energy-based model free in conjunction with damping controller.

The RGB-D camera [JAB12], which is different from RGB sensor by providing per-pixel depth (D) values computed from a reflected pseudo-random structured infrared light pattern. The authors compared six different visual oscillation sensing

approaches on scenes, including sparse texture and poor geometrical profiles as well as static and dynamic contents, by utilizing the per pixel depth measurements to reconstruct the 6D vector of the camera motion between two subsequent acquired images. The method involving the image Jacobian, the homography and the rigid transformations after back projection rely on a previously extracted set of point feature correspondences from subsequently acquired images. The problem of time delay compensation for the TUDOR system has been studied in [JAT12b]. Fourier extrapolation, sinusoidal-regression and auto-regression, signal processing approaches to compensate for the sensor inherent delay are compared. TUDOR system is used under gravitational influence to catch multiple balls sequentially thrown by a human in [JAT12a]. The ball detection, tracking as well as the prediction of the ball intercept location is based on a wall-mounted Kinect RGB-D sensor. Varying payload and flexible link deformations are damped out using model free independent joint controller.

The application of the IBVS algorithm has been validated to a space manipulator for an eye-in-hand camera using a software simulation tool, and then by means of the experimental test-bed in ([SMGP13b], [SMGP13a]). In their works and due to its simpler arrangements, the IBVS have been adopted to control three flexible links with eye-in-hand camera. An image processing algorithm is developed for adapting itself to different lighting conditions. However, in their papers only fixed targets are considered. Since the camera affected by the flexible vibration and visual distortion, an Extended Kalman Filter (EKF) is not only used for the estimate of the feature motion, but also account the camera measurements in the case of camera failure. The usage of a camera system for navigation and flexible vibration control is analyzed in the work.

2.4.1.2 Eye-to-hand configuration

In the eye-to-hand configuration, the camera is fixed in the workspace and its continuously focusing on the robot end effector. In this case the camera image is independent of the robot motion, the weight of the camera is not representing an additional payload to the system, and the auto focus feature is not necessary, in contrast to the eye-in-hand configuration. The main disadvantage here is the limitation of the workspace; the robot can be controlled by keeping it in the field of view during the visual servoing. The eye-to-hand high-speed camera configuration which available for visual servoing is used by [CLGM05], [CLG$^+$06]; to identify the dynamic model of two-link flexible robot around a particular position. Using the identified

model a Generalized Predictive Controller (GPC) in the frequency domain, and H∞ controller are implemented practically for validation of the model. The main disadvantage is the arm generally has to remain around particular position, which makes the model only appropriate for medical application. An advanced MIMO control strategy is designed in [CLG$^+$12] for high-speed visual servoing based on recomputing model after camera displacement, and the robustness due to a change in the working position is evaluated.

In [KMM10] results of ground-based experiments on the assembly of flexible space structures using the hardware developed under the Self-Assembling Wireless Autonomous Reconfigurable Modules (SWARM) program is presented. Two estimation systems are introduced for observing the dynamics of flexible beam using vision measurements. The Kalman filter is used to estimate the internal beam joint angles, while the steady state filter is used to estimate the angular position and angular velocity of the total beam deflection. Adaptive control is used to generate the control signal by using the measurements and the model information. The SWARM program has successfully demonstrated the maneuvering and docking of a flexible beam in a 2D flat floor environment. In [HS12a], [HS12c] illustrated the problem related to state variable estimation of Elastic Ship-Mounted Crane by using vision sensor data, the main goal of the work was to develop an approach to combine suitable measurement devices easy to realize with improved reliability. The task which be solved was estimations of the variable gain observer (based on vision measurements) with those of the variable gain observer (based on potentiometers) are combined. By realizing a multi-model approach the variable gain controller uses the variable gain observer's estimated states and the roll angle to generate the required damping to control the system to reduce the payload pendulations.

2.5 Summarized State of Art

The main inherent problem regarding visual servoing are the limitations of vision sensor, long time image processing, image resolution, and frame rate. Although relatively fast cameras and visual algorithms exist, the sampling rates of visual measurements are still lower than the frequency of positional encoders and joint angle sensors. In a flexible robotics context, the visual measurements are often needed to provide a feedback for control, or measurements to estimate the dynamic state variables of the system. In feedback control to attain controller stability, the sample rate needs to be high enough and the low sensor delay. The sensor delay

of the visual measurements must be taken into account when estimating the state variables of the system for state feedback control. By combining the visual measurements with high frequency position information the control loop can be run with higher frequency to allow better stability and faster convergence. In addition, the sensor delay of the visual measurements must be taken into account when fusing the measurements. Especially, eye-in-hand configuration requires precise synchronization of the traditional measurement and visual measurement. Otherwise vision give erroneous information while the end-effector is in motion.

In addition to low sample rate and sensor delay the visual measurements are uncertain. The resolution of a camera is limited, image noise is present and motion blur adds error to the image. The dynamics and control of 3D flexible robot motion are more complicated when using a single measurement at each time instant as is it typical in visual servoing. More than one camera (scenario) can be used effectively in the 3D visual servoing of flexible robot system. The uncertainty in visual measurements can cause undesired oscillations and hinder the accuracy, by fusing multiple measurements together more accurate estimates of target motion can be made compared to a single image.

3 Dynamic State variables Estimation Using Vision Sensor Data

In the last chapter a detailed overview for the visual servoing for flexible manipulator is presented. The main challenges, and applications of the this kind of robots are also addressed. The state estimation process using vision sensors; which represents the core of the state feedback control method in visual servoing will be addressed in this chapter.

3.1 Dynamic State Variables Estimation

State estimation in dynamical systems is crucial in state feedback control real world applications, because the designed control systems using full-state feedback required the true state of the real system. However, it is rarely possible to measure all the state variables. Some state variables are not even physical quantities [Tew02]. Even in such cases where all the state variables are physical quantities, accurate sensors may not be available, or may be too expensive to construct for measuring all the state variables. Also, sensors provide only specific output measurements which are sometimes a sequence of noisy and delayed measurements that a control system based on such measurements would be unsuccessful. Hence, it is invariably required to estimate rather than measure the state vector of a system. The state estimation process contains observing the output of the system for a known input and for a finite time interval, and then reconstructing the state-vector from the record of the output [HDRT04]. The mathematical model of the process by which a state-vector is estimated from the measured output and the known input is called an observer (or state estimator). The estimation (observation) of the state of a process is a fundamental part of modeling, monitoring and control strategies. Consider a noise free, linear, time-invariant plant described by the following state and output equations:

$$\begin{aligned} \dot{\chi}(t) &= A\,\chi(t) + B\,u(t) \\ y(t) &= C\,\chi(t) + D\,u(t). \end{aligned} \tag{3.1}$$

Here: A, B, C, and D are the system state space model matrices, χ represents the state vector of the system, u, and y are the input and the output of the system respectively. The general schematic diagram of an observer is shown in figure 3.1.

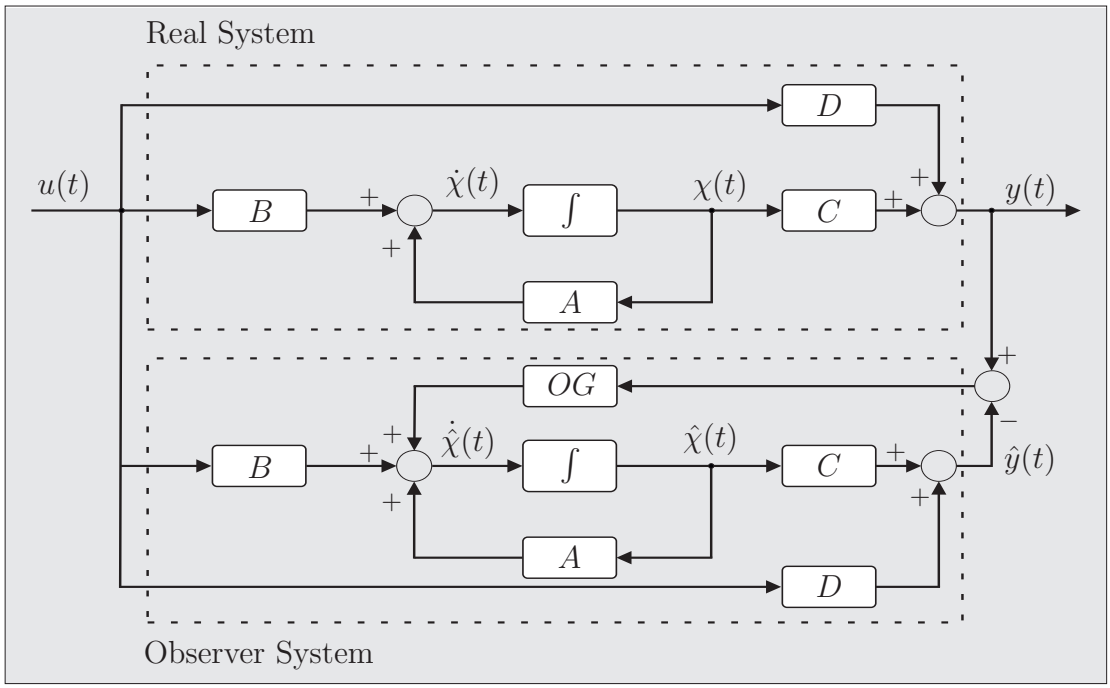

Figure 3.1: General structure of observer

Based on the measured output, a known input, and plant dynamics there are different types of state observers. If the plant for which the observer is required is linear, the observer's dynamics would also be described by linear state-equations. The states of the system must be determinable at any initial state, $\chi(0)$ in order to design an observer for a system, of a free motion system. This is called the observability of the system; which is an important property of physical systems to decide whether the states of the system can be reconstructed based on the output and a known input or not [Tew02]. The linear time-invariant state-equation which describes the dynamics of an observer can be expressed as follows:

$$\dot{\hat{\chi}}(t) = A\ \hat{\chi}(t) + B\ u(t) + OG\ (y(t) - \hat{y}(t)), \tag{3.2}$$

where $\hat{\chi}$ is the estimated state-vector, OG is the observer gain matrix, and $\hat{y}$ is the observer output ($\hat{y}(t) = C\ \hat{\chi}(t) + D\ u(t)$). The matrix OG must be selected in a design process such that the estimation error $e_o(t) = \chi(t) - \hat{\chi}(t)$ is brought to zero in the steady state. From Eqs. (3.1 and 3.2) the error dynamic equation of the observer can be derived as:

$$\dot{e}_o(t) = (A - OG\ C)e_o(t). \tag{3.3}$$

According to (3.3) the Observer gain OG should be chosen to ensure the asymptotic stability of the error dynamics (i.e. $e \to 0$ as $t \to \infty$).

Estimation theory discussed above is a model-based. Hence, the need for an appropriate model is imperative. "Appropriate" means a model that is well suited for its intended purpose [HDRT04]. The model must describe the essential properties of the underlying system. In other words, when a model is developed it must always be kept in mind what it should be used for. It should also be simple enough to make sure that it can be used to devise an efficient estimation algorithm. If the underlying model is not appropriate it does not matter how good the estimation algorithm is. Hence, a reliable model is essential to obtain good estimates. When referring to a model, this means a system of equations describing the evolution of the states and the measurements associated with the application. Other models are for instance impulse responses, transfer functions and Volterra series. A state-space model is used in the rest of the work, to model the mechanical systems.

3.2 State Variables Estimation Using Vision Sensor Data

With the evolving technology of digital video and communication, come new demands and new ways to utilize the technology. Increasing number visual or video based control systems can be seen in several areas. A vision sensor (i.e. camera) realizing a contactless measurement sensor can be used to measure the deformations of flexible mechanical systems [HS12b]. On the other hand, the estimation of dynamic state variables plays a significant role in the control of flexible link robots. The camera system can be used effectively to estimate the states of mechanical systems. The application of visual servoing for flexible robots has several drawbacks like limited accuracy, time delay occurs, and relatively low frame rate, which are the main inherent problems of vision sensors.

3.2.1 Noisy Measurements

Because of the limited accuracy of the camera systems, the measuring process used normally produces noised measurements, which are not suitable data to use with traditional types of observer. On the other hand the filtering problem of measurements is in general difficult, especially if the underlying system is nonlinear and/or the noise sources are non-Gaussian [JU05]. In many cases the filtering process can not be done in real time, which leads to a need for estimation process based on these

noisy measurements. The Eq. (3.1) after adding the noise term to the output can be written as

$$y(t) \;=\; C\,\chi(t) + D\,u(t) + \eta, \tag{3.4}$$

where η represent the noise generated during the measurement process (Image Processing). The term η in the measurements which is unknown in the real time applications, will lead to the failure of the estimation process in the traditional state observer. In this work the Kalman filter is used later to estimate the states of the dynamic model, in order to avoid the effects of noise in the estimation process. This is because one important property: which is the covariance matrices of the filter are independent of the measurement.

3.2.2 Delayed Measurements

Filtering methods, such as the extended Kalman filter (EKF) and the particle filter, are commonly used to acquire an estimate of the true state from noisy measurements. In general, it is assumed that the measurements are transmitted to the filter without any delay. In other words, a currently available measurement reflects the current state. Thus, the current state can be corrected by the current measurement. In practice, however, in the case of vision sensor this assumption may be unjustified. For instance, when an observation processor is connected to a camera sensor through a network, there is a fundamental communication time. Moreover, the raw sensor data require post-processing (image processing). In order to update the state of the dynamic system, processing time is needed, resulting in a delay between the acquisition of a measurement and its availability for the filter. The basic conceptual design is similar for all cameras [Cor11], meaning that all camera types contribute the delay in the same way, as basically the same things happens in the process of capturing, processing and dispatching an image. A measurement sequence without delay is represented in figure 3.2(a). When, however, both instants does not coincide, there is a time difference, called delay, between them. Figure 3.2(b) shows a sequence of this situation. The measurement equation is rewritten, by adding the time delay to the output Eq.(3.4) as:

$$y(t) \;=\; C\,\chi(t-\tau) + D\,u(t-\tau) + \eta(t-\tau), \tag{3.5}$$

here τ is the time delay in the measurements. The researchers have used many special techniques in order to reduce the data processing and transfer time of the measured data. In the next section the dynamic state estimation of flexible link robot will be addressed.

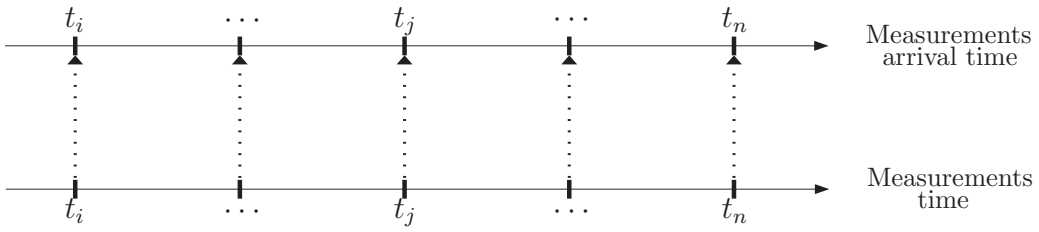

a) Measurements with neglected delay

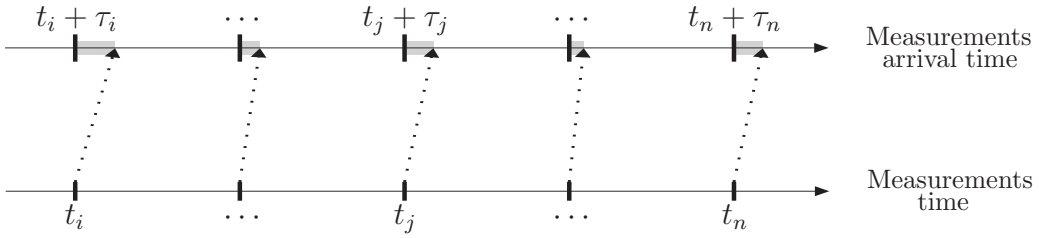

b) Camera measurements

Figure 3.2: Measurements sequence [CCPK09]

3.3 Case Study: Flexible Link Robot

As stated in the second chapter vision based control of flexible robots have been presented in several researches. An analytical criterion for the selection of suitable sensors for the control of structures with flexible bodies was developed in [SMVP99]. The state estimation of a single link flexible manipulator was studied in [YOK01]; the vision system was used to estimate the state variables of the virtual joint model of a flexible link. Due to the slow image processing operation in comparison with the real time control several researchers used a two time scale control ([BR06b]), [JKU07]. Other researchers developed new approaches of state estimators dealing directly with time delay and noise [ZLC06], [LZW+08].

In this chapter the effect of time delay and noise in state estimation process of flexible robot arm are shown through the comparison between the estimated states based on different measurements data. The flexible link model used, is based on finite element method. The separation of the dynamics is based on the frequencies of the system. The slow dynamic is chosen using assumed camera specifications. Two observers are designed, the first one to estimate the higher modes of the vibration using strain gauges, the second one represents an estimator using the camera as a sensor to estimate a modal set of slow dynamics based on the measurable frequencies of the modes.

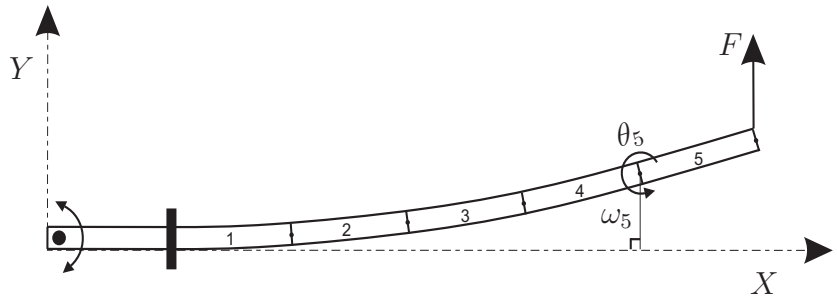

Figure 3.3: Flexible link

3.3.1 Mathematical model of flexible link robot

The basis of the dynamic model used in this case study is related to the elastic ship mounted crane. The flexible part of the boom is modeled as flexible link. The derivation of the dynamic model can be divided into two main parts: the finite element (FE) analysis, and the state-space representation.

The dynamic model of a flexible link shown in figure 3.3 is utilized using the FE method ([HS12b]), the effects of rotary inertia, transverse shear deformation, axial forces, and torsion are neglected. The link is assumed to be clamped at $x = 0$. The elementary dynamic model matrices related to the elastic vibration for a beam consisting of five elements can be written as

$$M_T\ddot{\upsilon}_T + D_T\dot{\upsilon}_T + K_T\upsilon_T = F_T, \tag{3.6}$$

where the M_T, D_T, K_T matrices represent the 12×12 mass, damping, and stiffness matrices respectively, F_T represents the 12×1 force vector, υ_T represents nodal translational and rotational displacements variables as

$$\upsilon_T = [\omega_1\ \theta_1\ \omega_2\ \theta_2\ \cdots\cdots\ \omega_6\ \theta_6]^{\mathrm{T}}, \tag{3.7}$$

ω_i , θ_i denote the translational and rotational displacements at each node along the flexible link. The translational and rotational displacements at $x = 0$ must be zero (ω_1=0 , θ_1=0). The complete system is described by

$$M_f\ddot{\upsilon} + D_f\dot{\upsilon} + K_f\upsilon = F_f, \tag{3.8}$$

where M_f, D_f, K_f represent the global 10×10 mass, damping, and stiffness matrices respectively, F_f represents the 10×1 force vector, and $\upsilon = [\omega_2\ \theta_2\ \omega_3\ \theta_3\ \cdots\cdots\ \omega_6\ \theta_6]^{\mathrm{T}}$.

The matrix differential equation (Eq. 3.8) is represented in a state-space form as

$$\begin{aligned} \dot{z} &= Az + Bu, \\ y &= Cz + \eta, \end{aligned} \tag{3.9}$$

with $z = \begin{bmatrix} v \\ \dot{v} \end{bmatrix}$, $A = \begin{bmatrix} 0_{n\times n} & I_n \\ -M_f^{-1}K_f & -M_f^{-1}D_f \end{bmatrix}$, $B = \begin{bmatrix} 0_{n\times 1} \\ M_f^{-1}I_1 \end{bmatrix}$, $C = \begin{bmatrix} C_1 \\ C_2 \end{bmatrix}$,

here z denotes the $(2 \times n) \times 1$ state vector and η represents the measurement noise, with $n = 10$. The values of the elements of matrix C are depending on the sensor gain of the measuring sensor.

In order to separate the state space model (Eq. 3.9) to fast and slow subsystem, the state transformation is defined as

$$z(t) = Tx(t), \tag{3.10}$$

with T as nonsingular transformation matrix, the state space model is written by replacing z in equation 3.9

$$\begin{aligned} \dot{x} &= T^{-1}ATx + T^{-1}Bu, \\ y &= CTx + \eta. \end{aligned} \tag{3.11}$$

to obtain

$$\begin{aligned} \dot{x} &= \tilde{A}x + \tilde{B}u, \\ y &= \tilde{C}x + \eta. \end{aligned} \tag{3.12}$$

In (Eq. 3.12), $\tilde{}$ sign means the transformed matrix and the resulting state matrix from this equation is diagonal/block-diagonal. By reordering the system states are separated to slow and fast subsystems. The state space equations corresponding to the dynamic separation can be expressed in vector form as

$$\begin{aligned} \begin{bmatrix} \dot{x}_1 \\ \dot{x}_2 \end{bmatrix} &= \begin{bmatrix} \tilde{A}_1 & 0 \\ 0 & \tilde{A}_2 \end{bmatrix} \begin{bmatrix} x_1 \\ x_2 \end{bmatrix} + \begin{bmatrix} \tilde{B}_1 \\ \tilde{B}_2 \end{bmatrix} u, \\ \begin{bmatrix} y_1 \\ y_2 \end{bmatrix} &= \begin{bmatrix} \tilde{C}_1 \\ \tilde{C}_2 \end{bmatrix} x + \begin{bmatrix} 0 \\ \eta \end{bmatrix}. \end{aligned} \tag{3.13}$$

In equation 3.13 the slow dynamical system can be generated from the overall system according to the frequency of the modes. The state components related to the slow dynamics should be estimated by using the signal from the camera system. An augmented predictor for the delay and noise compensation described in the next section can be used for overall optimal estimation.

3.3.2 State Variables Estimation

In this work, the flexible link model is observed with two types of sensor: strain gauge sensor to observe the fast dynamic states, camera sensor to observe the slow motion of the beam. The vision data, which provide direct measurements of the deflection with respect to inertial coordinate, prove to be a good substitute for strain gauges if the slow modes of vibration are considered. Related to the description (Eq. 3.13) two different measurement vectors

$$\begin{aligned} y_1(t) &= \tilde{C}_1 x_1(t), \\ y_2(t) &= \tilde{C}_2 x_2(t-\tau) + \eta(t-\tau), \end{aligned} \tag{3.14}$$

are used. Here τ denote the time delay between the two sensor types, which is equal to the time of the image frame transfer and processing.

Practically there will be time delay and noise in the all types of measurements; here the delay and the noise for the strain gauge signal are neglected in comparison with the camera signal. Due to the limitations of the sampling rate, and the resolution of the camera to detect all modes of the system; two different observers are designed to estimate the dynamical behavior of the system. The first one is a standard one, while the second one is not used only to estimate the states, but also for time delay compensation. The dynamic model is divided in slow and fast dynamic parts (3.13) in accord to consider the maximal natural frequencies which are related to the cameras sensor limit. In this work the camera measurement is used to estimate the modes; which are not only related to the first mode, but also to the remaining modes of the flexible slow modes up to the camera sampling rate. This contributes significantly to the beam tip deflection estimation using the vision sensor.

3.3.2.1 State Estimator for Non-delayed Measurement

For the non-delayed measurement (based on the strain gauges), the modes are estimated using classical observer approach as

$$\dot{\hat{x}}_1 = (\tilde{A}_1 - K_1\tilde{C}_1)\hat{x}_1 + \tilde{B}_1 u + K_1 y_1, \tag{3.15}$$

with $K_1 = P_1\tilde{C}_1^{\mathrm{T}}R_1^{-1}$ and P_1 as the solution of the Riccati equation [HDRT04] described as

$$\tilde{A}_1 P_1 + P_1\tilde{A}_1^{\mathrm{T}} - P_1\tilde{C}_1^{\mathrm{T}}R_1^{-1}\tilde{C}_1 P_1 + Q_1 = 0, \tag{3.16}$$

where Q_1 and R_1 are positive definite weighting matrices for the non-delayed states and measurements respectively.

3.3.2.2 State Estimator for Noised-delayed Measurement

The advantage of using the camera as a tip sensing device is the direct inertial measurement. The disadvantage is a delayed and noisy measurement signal. The delay is due to the time used in the vision processing and video signal transmission. In this section the method of defining states using an augmented predictor for the delay and noise compensation is described. Here, a Kalman filter is proposed for the delayed estimation. According to [Rob86], and assuming that the estimated states are delayed by τ, the Kalman filter equation can be written as

$$\dot{\hat{x}}_2(t-\tau) = (\tilde{A}_2 - K_2\tilde{C}_2)\hat{x}_2(t-\tau) + \tilde{B}_2 u + K_2 y_2(t), \tag{3.17}$$

where $K_2 = P_2\tilde{C}_2^{\mathrm{T}}R_2^{-1}$ and P_2 is the solution of the Riccati equation described as

$$\tilde{A}_2 P_2 + P_2\tilde{A}_2^{\mathrm{T}} - P_2\tilde{C}_2^{\mathrm{T}}R_2^{-1}\tilde{C}_2 P_2 + Q_2 = 0, \tag{3.18}$$

where Q_2 and R_2 are positive definite covariance matrices for the noised-delayed measurement.

To remove the delay effect from the estimated states, a equation g is defined as

$$\dot{g}(t) = \tilde{A}_2 g(t) + \tilde{B}_2 u, \tag{3.19}$$

derived using the slow modes dynamic, is used to account the effect of delay in the estimated states, and the non delayed state estimate can now be found as

$$\hat{x}_2(t) = g(t) + e^{\tilde{A}_2\tau}[\hat{x}_2(t-\tau) - g(t-\tau)]. \tag{3.20}$$

3.3.2.3 Combination of the Estimated States

The schematic diagram for the estimation approach is shown in figure 3.4. Each estimator described before is used to predict the related modes of vibration. The full state estimation can be found by using equation 3.10 as

$$\hat{z} = T\begin{bmatrix}\hat{x}_1\\ \hat{x}_2\end{bmatrix}, \tag{3.21}$$

However, in practical implementation the states of the system can be estimated from different measurements by combining all of the corresponding estimated states. In this work for the sake of comparison the full system states are also estimated based

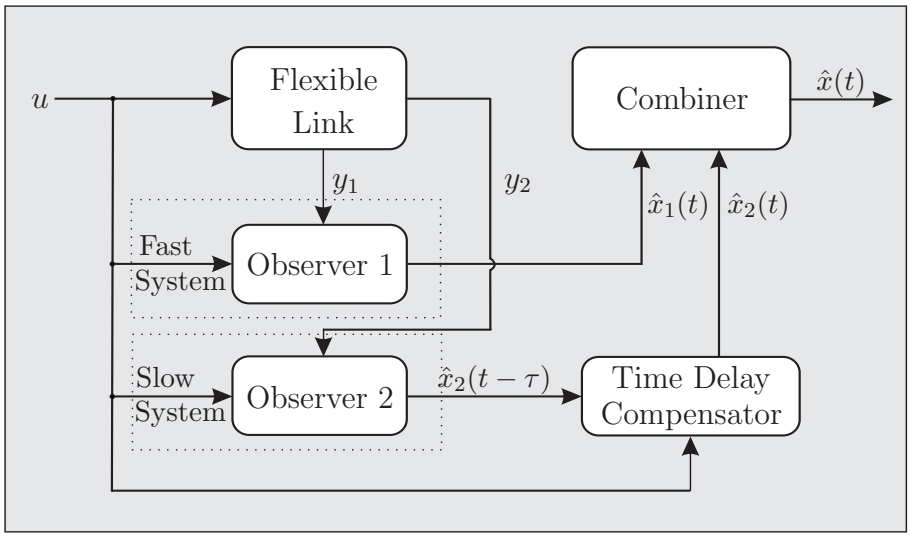

Figure 3.4: Schematic diagram for observation approach

on the strain gauge measurement and this can be done by changing the variables in Eq. 3.15 by the complete system dynamics. The states from the second estimator are combined with the same set of states, which are estimated using the full observer using the minimum mean-squared error $\hat{x}_i$ with

$$\hat{x}_i = \frac{(p_{ii}\hat{x}_{1,i} + q_{ii}\hat{x}_{2,i})}{(q_{ii} + p_{ii})}, \; i = 1, \ldots, n_1, \tag{3.22}$$

here n_1 denotes the number of slow modes. An optimal estimation can be achieved, when they are combined properly. The derivation process of $q_{i,i}, p_{i,i}$ is explained in detail in [Rob86]. Note, that the subscripts '1' and '2' in the states represent cases that the states are estimated based on measurements '1' and '2', respectively. The transformed states are used in (Eq. 3.22) due to the parameters $q_{i,i}, p_{i,i}$; which are related to transformed states.

3.3.3 Simulation Results

The parameters used in this work for the system illustrated in section 3.3.1 are:

- $L = 0.5$ m,
- $A = 0.00125$ m^2,

- $EI = 54.6$ N.m^2, and
- $\rho = 7850$ Kg/m^3.

Here L, A, E, I, ρ denotes length, cross sectional area, elastic modulus, cross section moment of area, and mass density, of the elastic link. Assuming two measurement points as, node 3 (using the strain gauge) and node 6 (using the camera sensor), two different input signals are used in the simulation, these two input signals are placed in the same position. The first one is an impulse force, deflecting the beam for 0.01 sec. with 10 N, the second one is vibrating the flexible beam with different frequencies according to the equation

$$u = a\ sin(2\pi t^2). \tag{3.23}$$

Here a denotes the amplitude of the sweep function. The simulation for the measurements of the camera sensor for the 6th node after the applying the input forces is illustrated in figure 3.5 and figure 3.6. Here node 6 denotes the end effector point of the flexible link. The noise in the signal is generated by adding the random number to the white noise signal and the results is multiplied by an appropriate factor related to the measurement signal. The time delay is assumed equal to 0.15 sec. Practically the total delay time can be determined by comparing the camera measurement to the strain gauge measurement for the same node. In this work the time delay is used as constant value due to the fact that the time delay can only be calculated based on the comparison between camera measurement and another sensor measurement. The time delay can be set as constant if there is no problem related to the camera measurement such as camera failure. The delay calculation can be done continuously (real time) during the operation of the real system in case of variable time delay.

3.3.3.1 Effect of Noise and Delay on Estimated States

The strain gauge simulated measurement for the 3rd node is used to estimate the full states of the system by using a full state observer. The simulated camera measurement is used also to estimate the full states of the system. The estimation of the full states using the camera measurement is to show the effect of the noise and the time delay in the estimated state variables figure 3.7 and figure 3.8. These figures show the error in the set of estimated states based on simulated camera measurement for each input type. In these two figures e represent the difference

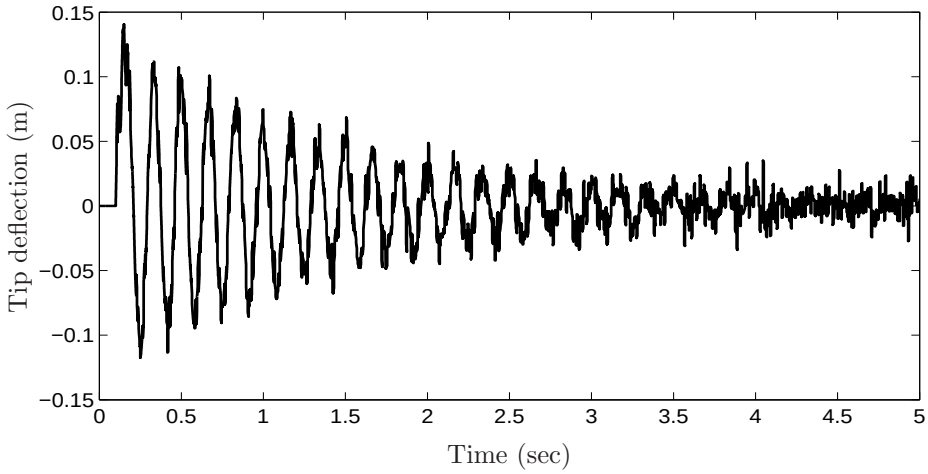

Figure 3.5: Simulated measurement of the camera sensor (impulse input)

between the two cases of estimation ($\hat{z}_c - \hat{z}_s$), where c, s represent camera and strain gauge respectively, for each type of inputs. Where $e - \hat{z}_i$ represents the error between the two cases for state number i.

3.3.3.2 Compensation of Noise and Delay

It can clearly be seen from the estimated tip point error in figure 3.9 and figure 3.10 that the slow and fast state estimators compensate the noise and delay from the estimated states for the each type of input. The state estimates which are designed in this work follow the states and remove the effects of noise and time delay very fast. The estimated states of the slow dynamic are combined with the estimated states from the observer to get an optimal augmented state estimation figure 3.11 and figure 3.12.

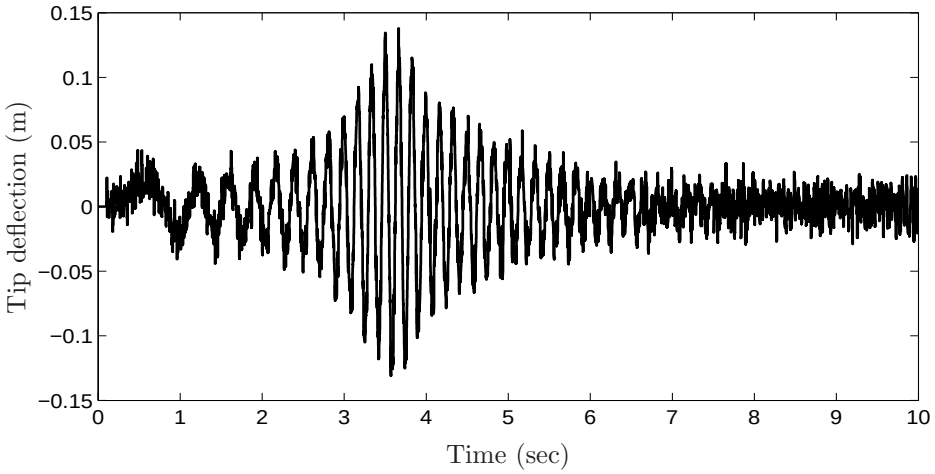

Figure 3.6: Simulated measurement of the camera sensor (sweep input Eq. 3.23)

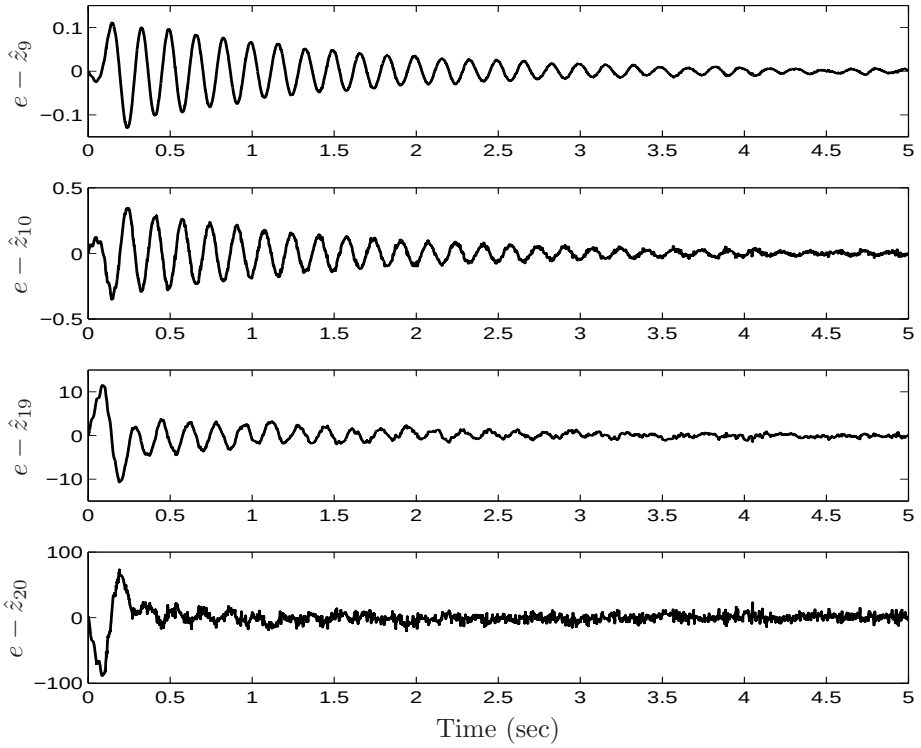

Figure 3.7: Effects of noise and time delay on the estimated states (impulse input)

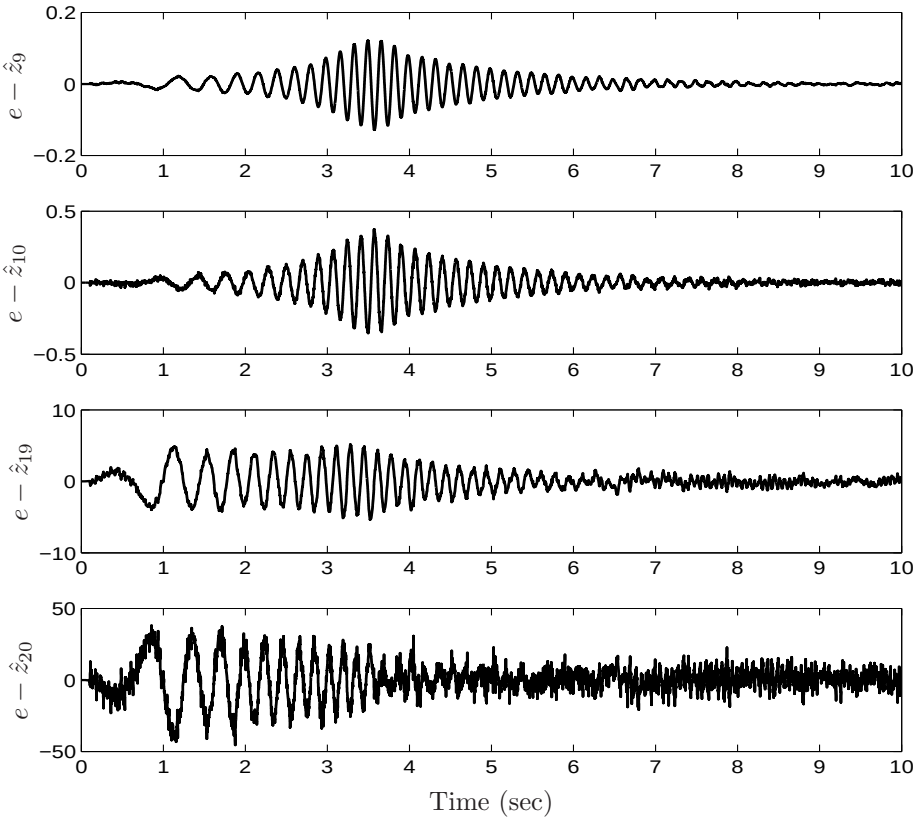

Figure 3.8: Effects of noise and time delay on the estimated states (sweep input)

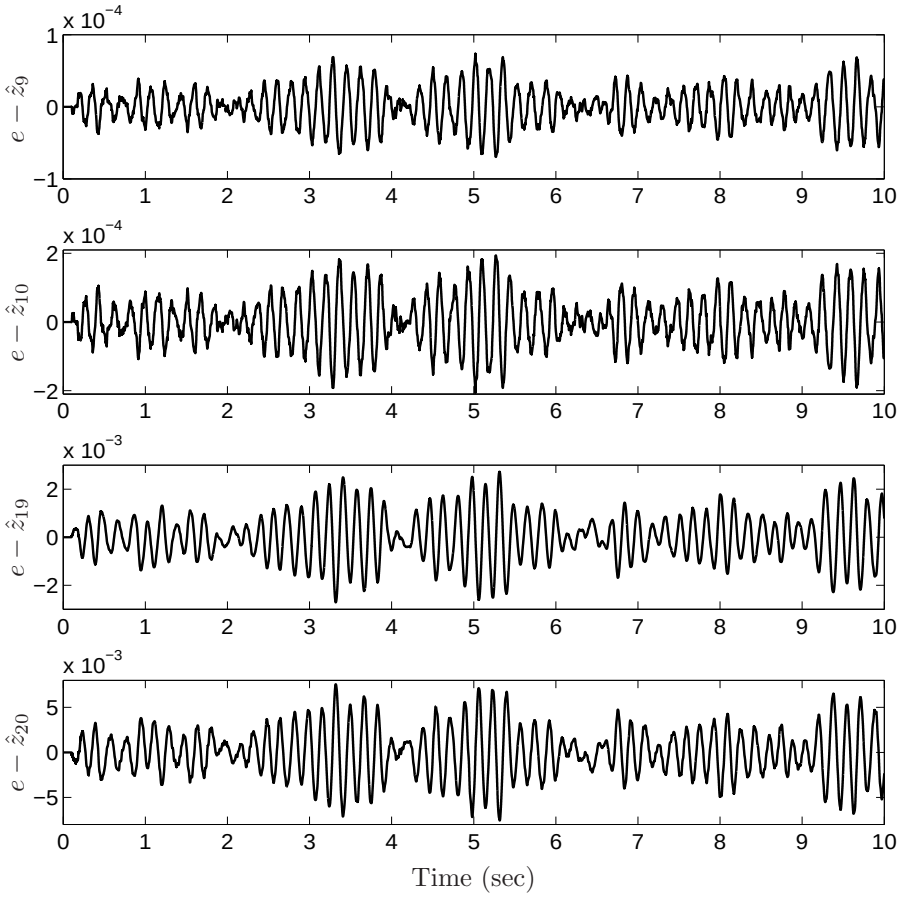

Figure 3.9: Compensation of the effects of noise and time delay on the estimated states (impulse input)

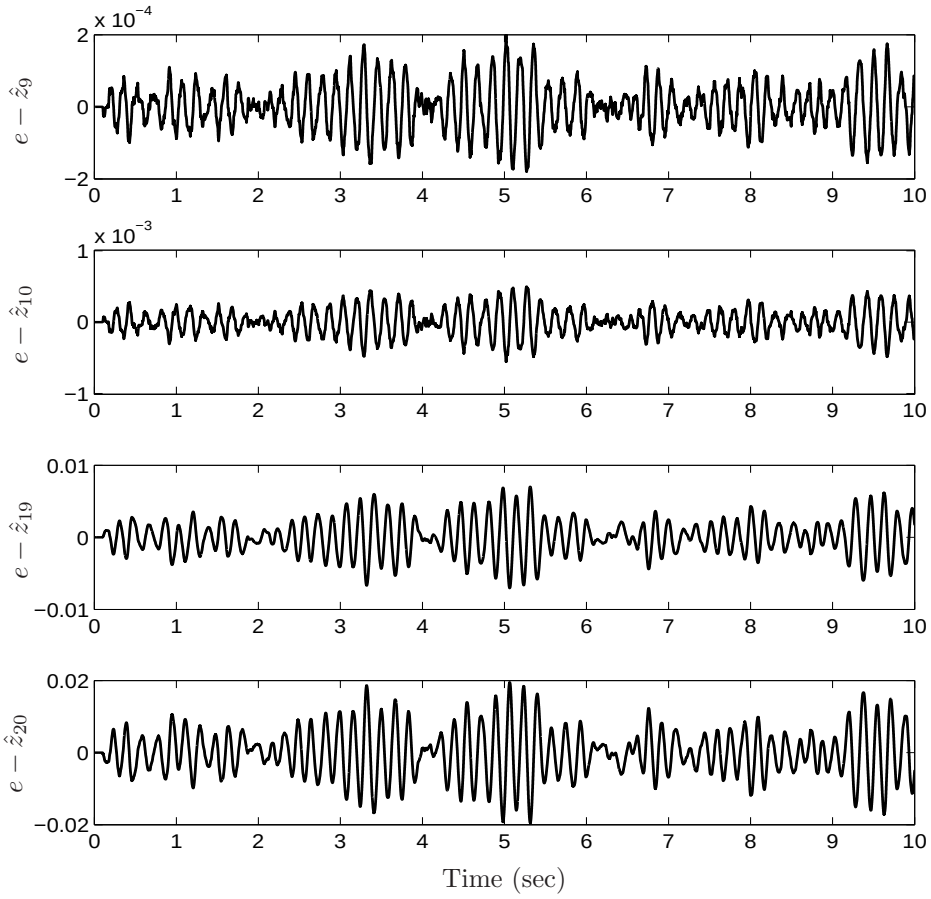

Figure 3.10: Compensation of the effects of noise and time delay on the estimated states (sweep input)

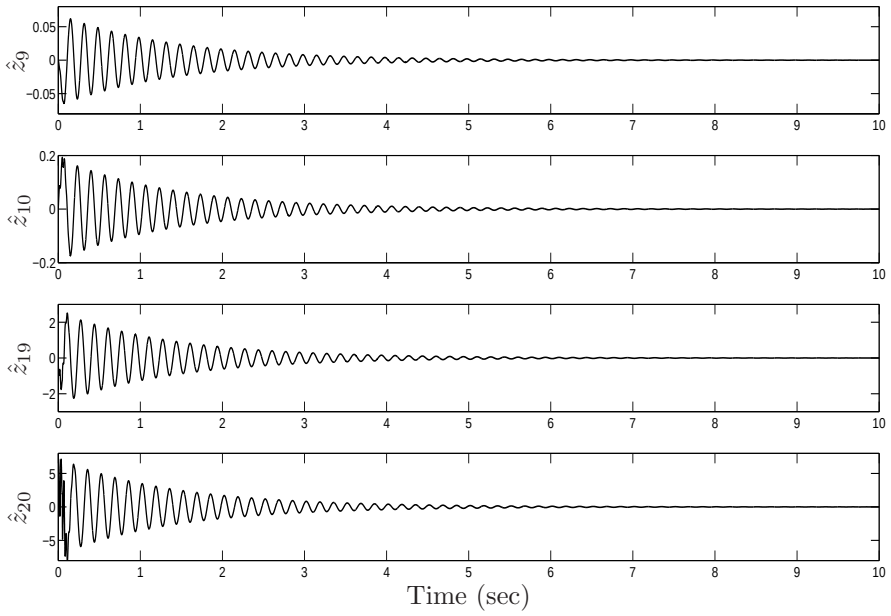

Figure 3.11: Combination of the estimated states (impulse input)

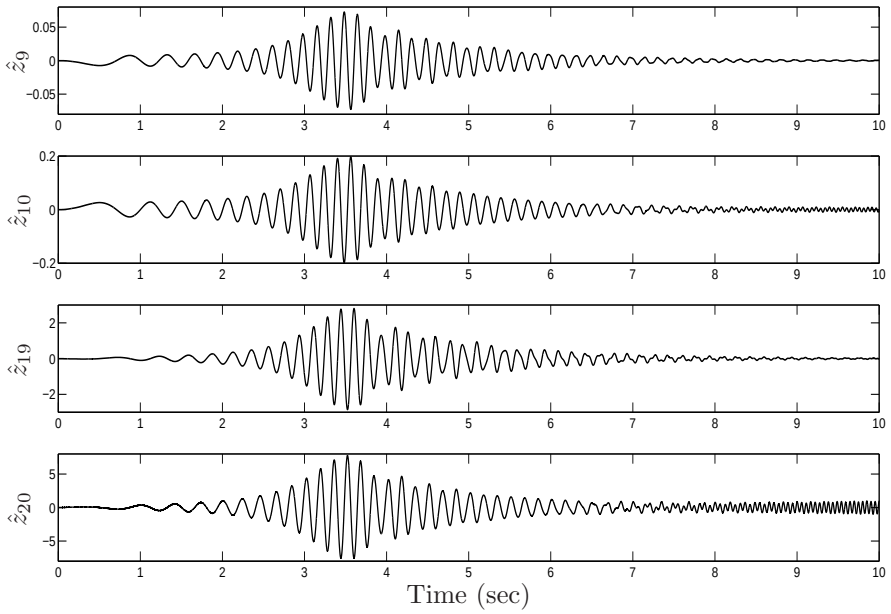

Figure 3.12: Combination of the estimated states (sweep input)

3.4 Summary

In this chapter the effects and compensation of limited accuracy and time delay occur on the state estimation process based on noised and delayed measurements are studied. The effects of time delay and noise in states estimation are shown by the comparison of the states from different measured input data. The main goal of the work is to develop an approach to combine suitable measurement devices easy to realize with improved reliability. After a brief overview of dynamical state observation systems, a flexible link mechanical systems has been studied in this chapter as examples for flexible robot systems. The dynamic model is separated to slow and fast dynamics based on assumed camera specification. Two observers are designed using the fast and slow dynamics, the first one to estimate the higher modes of the vibration using strain gauges, the second one represent an estimator using the camera as a sensor to estimate a modal set of slow dynamics based on the frequency of the system states. The combination of the two estimated dynamical parts of the system dynamics of flexible link robot is described. The solved task is combining the estimations of the slow observer (based on vision measurements) with those of the fast observer based on strain gauges. The simulation is done in order to verify the effectiveness of the state estimation proposed approach. The proposed method of states estimation will be used later for the more complicated system, by integrating the flexible link with the overall dynamics of the elastic ship mounted crane.

4 Visual Servoing of an Elastic Ship-Mounted Crane: Theory

The model used in this work is based upon SRS[1]-designed elastic ship mounted crane (Fig. 4.1). The flexible part of the boom can be represented as a flexible link robot. As compared to rigid boom of the cranes, the end effector position of flexible links can not be obtained precisely enough based on the kinematics and joint variables. The position of any point of a flexible link is not only related to the joint angles but also to the link flexural displacements. Elastic cranes can have very complex dynamic pendulations during the operation, due to the flexibility in the boom of the crane [ASS07]. The boom in this crane consists of a flexible and of a rigid part. The flexible part is coupled with the dynamics of the pulley and the payload. The dynamic model of the lower part of the boom (flexible link) is utilized using the Finite Element method neglecting the effects of rotary inertia, transverse shear deformation, axial forces, and torsion. The link is assumed to be clamped at $x = 0$.

4.1 Mathematical Model of Elastic Ship-Mounted Crane

The mathematical model used in this work is related to the elastic crane designed by SRS. The mathematical model is briefly presented, the development as well as the full model are given in [ASS07]. In this work, the mathematical model is re-derived with the only unique change from the original model, where the flexible link is divided into two elements instead of five elements (Fig. 4.2). The vision feedback can provide the actual tip point position, but only for low modes of vibration. Then there is no need to include negligible (in terms of pixel size) high frequency modes. Detection of higher order modes is limited by the camera resolution, so in this contribution only lower order model is used.

The linear equations of motion [ASS07] of the crane using two elements for flexible parts of the boom can be rewritten as

$$M_0\ddot{q} - B_2\ddot{u} - B_4\Delta\ddot{\delta} = -K_0 q + B_1 u + B_3\Delta\delta + B_5 p_2, \tag{4.1}$$

where

$$q = \begin{bmatrix} \Delta w_2 & \Delta\theta_2 & \Delta w_3 & \Delta\theta_3 & \Delta\alpha_2 & \Delta\phi_2 \end{bmatrix}^{\mathrm{T}} \tag{4.2}$$

[1]SRS: Chair of Dynamics and Control, University of Duisburg-Essen.

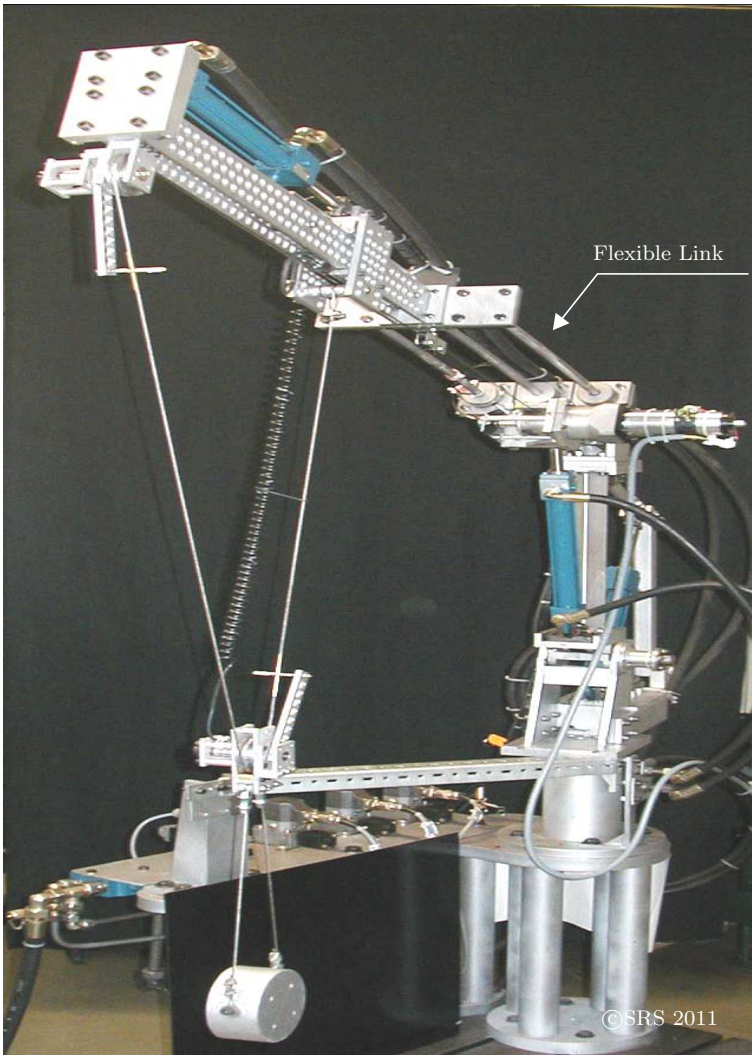

Figure 4.1: Elastic ship mounted crane, SRS

denotes the 6×1 generalized displacement vector, Δw_i describes the translational displacement at the nodes along the flexible link, $\Delta\theta_i$ describes the elastic rotational displacement at each node, $\Delta\alpha_2$ the angle of the right hand side of the cable (L_2) with respect to the horizontal plane, $\Delta\phi_2$ the angle of payload with respect to the vertical plane, and

$$u = \begin{bmatrix} \Delta\rho & \Delta L & \Delta D \end{bmatrix}^{\mathrm{T}} \tag{4.3}$$

represents the control input vector, with $\Delta\rho$ as a luff angle of the boom, ΔL the total length of the cable, and ΔD the position of the movable suspension point B', M_0, K_0 as the total mass and stiffness matrices respectively of order 6×6, B_1, B_2 are input matrices of order 6×3, B_3, B_4 and B_5 are disturbance matrices of order 6×1.

The measurement vector is specified as

$$y_m = \begin{bmatrix} \Delta w_3 & \Delta\alpha_2 & \Delta\phi_2 \end{bmatrix}^{\mathrm{T}} = C_1 q, \tag{4.4}$$

where C_1 is the measurement matrix of order 3×6; describing the position of the sensors of the crane. The state space equations corresponding to the current equilibrium point, can be expressed as

$$\begin{aligned} \dot{z} &= Az + Bu + E\Delta\delta + Np_2, \\ y_m &= Cz + Du + F\Delta\delta + \eta, \end{aligned} \tag{4.5}$$

with

$$A = \begin{bmatrix} 0_{6\times6} & I_6 \\ -K_0M_0^{-1} & 0_{6\times6} \end{bmatrix}, B = \begin{bmatrix} 0_{6\times3} \\ B_1 - K_0M_0^{-1}B_2 \end{bmatrix}, \tag{4.6}$$

representing the corresponding system and input matrices respectively,

$$E = \begin{bmatrix} 0_{6\times1} \\ B_3 - K_0M_0^{-1}B_4 \end{bmatrix},\ N = \begin{bmatrix} 0_{6\times1} \\ B_5 \end{bmatrix}, \tag{4.7}$$

representing the disturbance input matrix for the rolling and the disturbance matrix N for the forces acting on the payload respectively. The matrix

$$C = \begin{bmatrix} C_1M_0^{-1} & 0_{3\times6} \end{bmatrix} \tag{4.8}$$

denotes the output matrix, the matrices D and F as

$$D = [C_1M_0^{-1}B_2]_{12\times3}\ , \quad F = [C_1M_0^{-1}B_4]_{12\times1}, \tag{4.9}$$

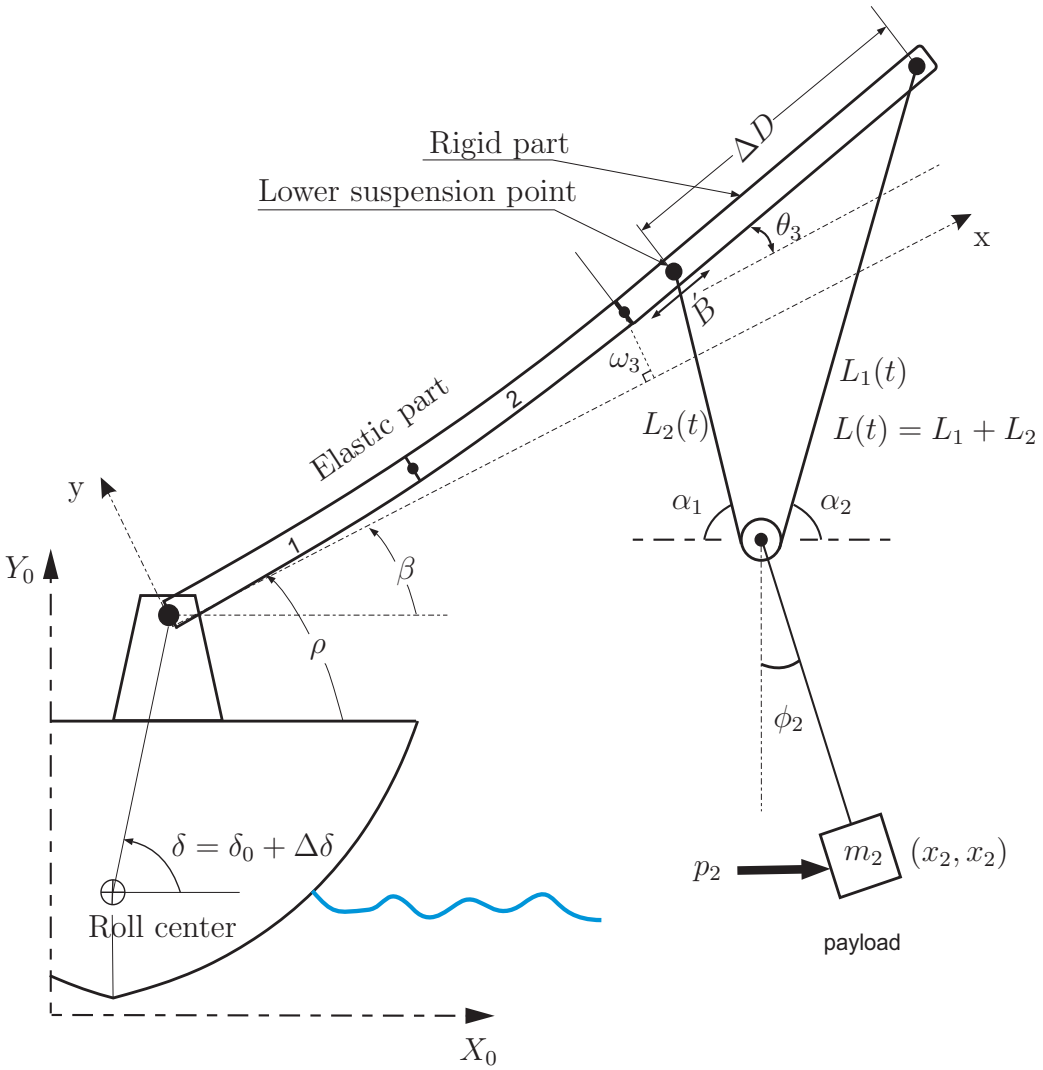

Figure 4.2: Modified elastic ship-mounted crane configuration [ASS07]

representing the input and disturbance direct transmission matrices respectively. The input matrices E, F are used to relate external effects to the dynamics. The modeled displacement vector q can be obtained using state variables vector as

$$q = \begin{bmatrix} M_0^{-1} & 0 \end{bmatrix} z + M_0^{-1} B_2 u + M_0^{-1} B_4 \Delta\delta, \tag{4.10}$$

where $\Delta\delta$ denotes the external movement of the system. The noise in the measurement signal and the wind disturbance force are specified in (Eq. 4.5) by the terms η, p_2.

4.1.1 Measurements

Due to economic or practical reasons not all the state variables are measured, only 3 out of 12 states can be easily measured. In this work the system is observed with two types of sensors. The vision sensor represents the first type of sensors, which provides direct measurements of the flexible link deflection with respect to inertial coordinates, as a good substitute for strain gauges. Related to (Eq. 4.4) two different types of measurements

$$\begin{aligned} y_m &= \begin{bmatrix} \Delta w_3 \\ \Delta\alpha_2 \\ \Delta\phi_2 \end{bmatrix} = \begin{bmatrix} y_1(t-\tau) \\ y_2(t) \\ y_3(t) \end{bmatrix} + \begin{bmatrix} \eta_1(t) \\ \eta_2(t) \\ \eta_3(t) \end{bmatrix} \\ &= \begin{bmatrix} C_{m1} \\ C_{m2} \end{bmatrix} z + \begin{bmatrix} D_{m1} \\ D_{m2} \end{bmatrix} u + \begin{bmatrix} F_{m1} \\ F_{m2} \end{bmatrix} \Delta\delta + \begin{bmatrix} \eta_1 \\ 0 \end{bmatrix} \\ &= \begin{bmatrix} y_{m1} \\ y_{m2} \end{bmatrix}, \end{aligned} \tag{4.11}$$

are used. Here τ denote the time delay between the two sensors, which is equal to the time of the image frame transfer and processing.

The angle of the right part of the cable with respect to the horizontal and the angle of the payload with respect to vertical α_2 and ϕ_2 measurements are assumed free of noise and delay $\eta_2(t), \eta_3(t) \approx 0$. The two angles can be measured using potentiometers. Practically there will be time delay and noise in the all types of measurements [HDRT04]; here the delay and the noise in the angles signal measurement are neglected in comparison to those of the camera signal.

4.2 State Variables Estimation for Control

4.2.1 State and disturbance estimation using non-delayed measurements

The state space model (Eq. 4.5) of the crane contains the unknown disturbance p_2 (wind force). The state variables and the unknown disturbance can be estimated by using an observer design able to reconstruct system states in presence of additional unknown effects acting on the system. Therefore a Proportional-Integral-Observer (PI-observer) [SYM95] is used. For the non-delayed measurements (based on the potentiometers), the unknown wind force is approximated by

$$p_2 \approx Hv, \tag{4.12}$$

and (Eq. 4.5) can be rewritten as

$$\begin{bmatrix} \dot{z}_2 \\ \dot{v} \end{bmatrix} = \begin{bmatrix} A & NH \\ 0 & S \end{bmatrix} \begin{bmatrix} z_2 \\ v \end{bmatrix} + \begin{bmatrix} B \\ 0 \end{bmatrix} u + \begin{bmatrix} E \\ 0 \end{bmatrix} \Delta\delta, \tag{4.13}$$

$$y_{m2} = \begin{bmatrix} C_{m2} & 0 \end{bmatrix} \begin{bmatrix} z_2 \\ v \end{bmatrix} + Du + F\Delta\delta. \tag{4.14}$$

Due to the difficulty of defining a simple linear model that can adequately describe the unknown disturbance (assumed as unknown) a suitable design procedure is necessary. It is assumed that the rolling motion of the ship $\Delta\delta(t)$ can be measured. Here a model approximation $\dot{v} = Sv$, $S = 0$ is used. A high gain observer to realize $\hat{v} \approx p_2$ [SYM95] is applied. Therefore, the PI-observer model can be written as

$$\begin{bmatrix} \dot{\hat{z}}_2 \\ \dot{\hat{v}} \end{bmatrix} = \underbrace{\begin{bmatrix} A & NH \\ 0 & S \end{bmatrix}}_{A_e} \begin{bmatrix} \hat{z}_2 \\ \hat{v} \end{bmatrix} + \underbrace{\begin{bmatrix} B \\ 0 \end{bmatrix}}_{B_e} u + \underbrace{\begin{bmatrix} E \\ 0 \end{bmatrix}}_{E_e} \Delta\delta + \underbrace{\begin{bmatrix} L_{e1} \\ L_{e2} \end{bmatrix}}_{L_e} (y_{m2} - \hat{y}_{m2}), \tag{4.15}$$

with

$$\hat{y}_{m2} = \underbrace{\begin{bmatrix} C_{m2} & 0 \end{bmatrix}}_{C_e} \begin{bmatrix} \hat{z} \\ \hat{v} \end{bmatrix} + Du + F\Delta\delta, \tag{4.16}$$

where $\hat{y}_{m2}$ is the output of the observer, L_{e1} and L_{e2} are the observer gain matrices of appropriate dimensions. It is necessary that the extended system is full observable, i.e.,

$$\operatorname{rank}\begin{bmatrix}\lambda_i I - A_e \\ C_e\end{bmatrix} = \dim(z_2) + \dim(p_2). \tag{4.17}$$

Here λ_i denotes all eigenvalues of the system (Eq. 4.17). Different design techniques can be used to design the observer gain matrices [SYM95]. Here the well-known LQR approach solving the Algebraic Riccati Equation

$$A_e P_e + P_e A_e^{\mathrm{T}} + Q_e - P_e C_e^{\mathrm{T}} R_e^{-1} C_e P = 0, \tag{4.18}$$

is used, so the gain matrix of the observer is calculated by

$$L_e = P_e C_e^{\mathrm{T}} R_e^{-1}. \tag{4.19}$$

Here Q_e and R_e are symmetric positive definite weighting matrices for the extended states and the non-delayed measurements respectively.

4.2.2 State estimation using noised-delayed measurement

The advantage of using the camera as a tip sensing device is the direct inertial measurement. The disadvantage is a delayed and noisy measurement signal. In this work it is assumed that the camera measurements is highly noised and delayed in order to represent typical practical situations. In order to achieve the objectives of minimizing the effect of measurement noise and time delay, a Kalman Filter is chosen [LS13] as a state estimator. However, the presence of measurement noise and delay challenges this premise. In this section the method of defining states using an augmented predictor for the delay and noise compensation is described. According to [Rob86], assuming a certain delay time τ, the Kalman Filter differential equation can be written as

$$\begin{aligned}\dot{\hat{z}}_1(t-\tau) = A\hat{z}_1(t-\tau) + Bu + E\Delta\delta + N\hat{p}_2 \\ + L_1^{'}(y_{m1}(t-\tau) - \hat{y}_{m1}(t-\tau)),\end{aligned} \tag{4.20}$$

with $L_1^{'} = P_1^{'} C_{m1}^{\mathrm{T}} R_{m1}^{-1}$. Here $P_1^{'}$ is the solution of the Riccati equation described as

$$A P_1^{'} + P_1^{'} A^{\mathrm{T}} + Q_{m1} - P_1^{'} C_{m1}^{\mathrm{T}} R_{m1}^{-1} C_{m1} P_1^{'} = 0, \tag{4.21}$$

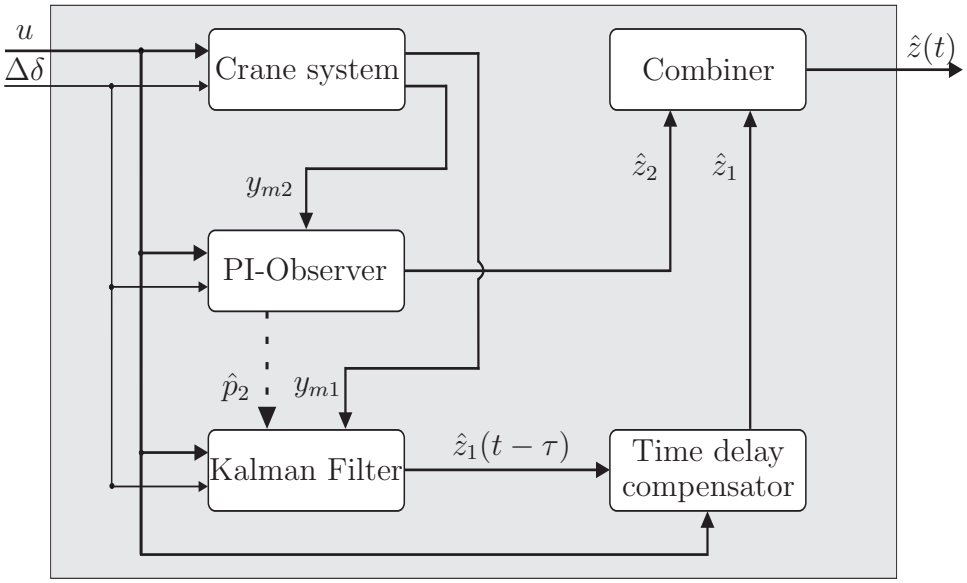

Figure 4.3: Schematic diagram for observer approach

where Q_{m1} and R_{m1} are positive definite covariance matrices for the system states and the delayed measurements respectively. The wind disturbance p_2 can be estimated based on other measurements, because the disturbance is not related to system dynamics. It is assumed, that the rolling motion of the ship $\Delta\delta(t)$ is measured. According to [Rob86], to remove the delay effect from the estimated states, a function g which is derived based on the mathematical model of elastic crane, and the non delayed state estimate $\hat{z}_1(t)$ are given by

$$\dot{g}(t) = Ag(t) + Bu + E\Delta\delta + N\hat{p}_2, \quad \text{and} \tag{4.22}$$

$$\hat{z}_1(t) = g(t) + e^{A\tau}[\hat{z}_1(t-\tau) - g(t-\tau)]. \tag{4.23}$$

In (Eqs. 4.23) $g(t)$ is used as a defined function to account the time delay, $\hat{z}_1(t-\tau)$ as defined above and $g(t-\tau)$ is obtained by a time delay of $g(t)$. Here the initial value for $g(t)$ is $[0\ 0\ 0\ 0\ 0\ 0\ 0\ 0\ 0\ 0\ 0\ 0]^T$.

The estimation error dynamic from equations (Eq. 4.5) and (Eq. 4.23), after filtering and predicting can be written as

$$e(t) = \hat{z}_1(t) - z_1(t) = e^{A\tau}(\hat{z}_1(t-\tau) - z_1(t-\tau)), \tag{4.24}$$

$$\dot{e}(t) = (A - L_1^{'}C_{m2})e(t) + L_1^{'}\eta. \tag{4.25}$$

The corresponding error covariance is given by

$$E_c = e^{A\tau} P_1' e^{A^T\tau} + \int_0^\tau e^{As} Q_{m1} e^{A^T s} ds. \tag{4.26}$$

The estimation error dynamic equation is derived by neglecting the internal noise related to the dynamics of the internal states in comparison with the measurements noise [HDRT04]. Detailed equations of the error covariance of the error dynamics can be found in [Rob86].

4.2.3 Combination of the estimated states

The schematic diagram for the estimation approach is shown in Fig. 4.3. The state estimators described before are used to predict system states $\hat{z}_1$, $\hat{z}_2$. However, in practical implementation the states of the system can be estimated from different measurements by combining all of the corresponding state variable estimates. The states from the second observer (Eqs. 4.23) are combined with the states estimated using observer (Eqs. 4.15). Let the matrix P_e in (Eqs. 4.18) be $P_e = [p_{i,j}]$ and the matrix E_c of (Eqs. 4.26) be $E_c = [\sigma_{i,j}]$. The combination process is based on the minimum mean-squared error [LS13] as

$$\hat{z}_i = \frac{(p_{i,i}\hat{z}_{1,i} + \sigma_{i,i}\hat{z}_{2,i})}{(\sigma_{i,i} + p_{i,i})}. \tag{4.27}$$

An optimal estimation can be achieved, when they are combined properly. The derivation process is explained in detail in [Rob86]. The process of combination is a weighting process, the two state estimators estimate the states with small differences. The parameter $\sigma_{i,i}, p_{i,i}$ are chosen according to [Rob86]. Note, that the subscripts '1' and '2' in the states represent cases that the states are estimated based on measurements '1' and '2', and therefore observers 1 and 2 respectively.

4.3 Controller Design

The observer discussed in the section before reconstructs the states and the unknown disturbance force p_2 as $\hat{p}_2$. The disturbances are calculated, their effect on the control variables should be canceled or compensated. In this section, the controller is designed for the model given by Eq.(4.5). The controller design is published in previous work [ASS07] and will here be repeated briefly. In order to cancel/reduce

the effect of the disturbances and to ensure safe cargo transfer of the crane, the control input u is decomposed into three parts, as

$$u = u_z + u_2 + u_\delta, \tag{4.28}$$

where u_δ and u_2 are used to act against the disturbance $E\Delta\delta$ and the estimated disturbance Np_2 respectively; u_z is chosen to provide the optimal control for the crane using state feedback, i.e.,

$$u_\delta = -K_\delta \Delta\delta \ , \ u_2 = -K_2 \hat{p}_2 \ , \ u_z = -K_z \hat{z}, \tag{4.29}$$

where $\hat{z}$ and $\hat{p}_2$ are the estimated states obtained from Eqs. (4.5 and 4.5).

4.3.1 Defining K_δ , K_2 , K_z

To define the numerical values of the corresponding three inputs, the changes in the position of the payload (x_2 and y_2) resulting from rolling are set to be zero, i.e.,

$$\begin{aligned}\Delta x_2 \approx \frac{\partial x_{20}}{\partial \delta}\Delta\delta + \frac{\partial x_{20}}{\partial \rho}\Delta\rho + \frac{\partial x_{20}}{\partial L}\Delta L + \frac{\partial x_{20}}{\partial D}\Delta D \\ + \frac{\partial x_{20}}{\partial w_3}\Delta w_3 + \frac{\partial x_{20}}{\partial \theta_3}\Delta\theta_3 = 0,\end{aligned} \tag{4.30}$$

$$\begin{aligned}\Delta y_2 \approx \frac{\partial y_{20}}{\partial \delta}\Delta\delta + \frac{\partial y_{20}}{\partial \rho}\Delta\rho + \frac{\partial y_{20}}{\partial L}\Delta L + \frac{\partial y_{20}}{\partial D}\Delta D \\ + \frac{\partial y_{20}}{\partial w_3}\Delta w_3 + \frac{\partial y_{20}}{\partial \theta_3}\Delta\theta_3 = 0.\end{aligned} \tag{4.31}$$

Here, the subscript 20 denotes the value at $t = 0$, the roll angle $\Delta\delta$ is assumed to be measured. The first control input results to

$$u_\delta = -\left[A_\delta + F_\delta G_\delta\right]^{-1} B_\delta \Delta\delta, \tag{4.32}$$

with A_δ , F_δ , G_δ , and B_δ as given in [ASS07]. From (Fig. 4.2) is concluded that the disturbance p_2 acts only on the payload m_2; from (Eqs. 4.1) it can be seen that the corresponding disturbance matrix is

$$B_5 = \begin{bmatrix}0 & 0 & 0 & 0 & -1 & 1\end{bmatrix}^{\mathrm{T}}. \tag{4.33}$$

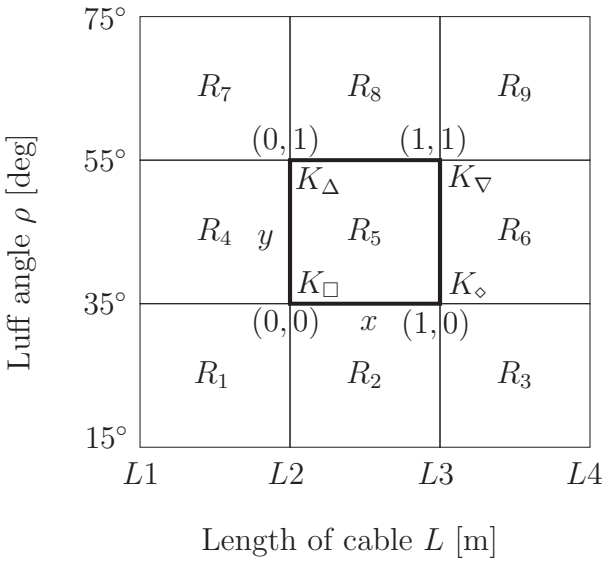

Figure 4.4: Local coordinates and related local gains

From (Eq. 4.33), it can be seen that p_2 affects directly only at the last two states z_{11} and z_{12}, while the structure of the input matrix described by (Eq. 4.10) indicates that the input vector u affects all the last 6 states, which means that any attempt to cancel the effect of the disturbance on the last two states will effect the other states. So no static feedback matrix K_2 can be given to cancel the effect of p_2 without exciting the other states. The effect of the disturbance force p_2 can be reduced by implementing a closed loop state feedback control leading to a dynamical accommodation. It is necessary to estimate the disturbance, because the state feedback controller uses the estimated states obtained by the observer, to reconstruct the states with minimum error only if the disturbances are taken into consideration while reconstructing all states. Using the Introduced PI-observer this can be achieved. Here LQR state feedback matrix K_z is calculated as

$$K_z = R^{-1}B^{\mathrm{T}}P, \tag{4.34}$$

where P represents the solution of the algebraic Riccati equation

$$A^{\mathrm{T}}P + PA + Q - PBR^{-1}B^{\mathrm{T}}P = 0, \tag{4.35}$$

with Q and R as symmetric positive definite weighting matrices of the states and inputs respectively. The controlled system description can be written as

$$\dot{z} = Az - BK_z\hat{z} + (E - BK_\delta)\Delta\delta + Np_2. \tag{4.36}$$

4.3.2 Variable gain observers and controller

It can be seen from Eqs. (4.18, 4.21, and 4.35) that the observer and the controller gain matrices L_e, L_1', K_z, and K_δ depend directly on the system parameters. Additionally the input and measurement matrices (B, C) partly depend on the system parameters. They represent together with the weighting matrices Q_{m1}, Q_e, Q, R_e, R_{m1}, and R the parameters of the Ricatti equations. As a solution a multi model approach is suggested; based on local linearization. The matrices M_0 and K_0 are calculated at different working points, which vary with the length of the cable L and the boom luff angle ρ, so the observers and controller gain matrices are suitable for the local working points.

For the scaled model under consideration, the length of the cable (in meters) and the luff angle (in degrees) are divided such that $L_{0r} = 1 + 0.5r$, $r = 0, \cdots, 3$ and $\rho_{0s} = 15 + 20s$, $s = 0, \cdots, 3$. This results to $3{\times}3 = 9$ operating regions. The operation of the crane is now covered by 9 different observers and controller gain matrices L_e, L_1', K_z, and K_δ. The switching between these gains takes place automatically according to the measurements of the luff angle and the length of the cable to detect the current operating region.

To define the appropriate point inside the region at which the corresponding observers and controller gains should be calculated, special care should be taken. The gains are calculated at each individual region of the whole considered working field; the weighting matrices are chosen to produce nearly the same relative stability and damping at each region, and each local gain set should provide a stable operation of the crane for all possible operating points inside the region. The values of the controller gains are described using a 2D interpolation polynomial

$$K_z = k_1 + k_2 x + k_3 y + k_4 xy, \tag{4.37}$$

where x and y denote the local coordinate axes of the region as shown in Fig. 4.4, and $k_1, \cdots, k_4$ denote the polynomial coefficient matrices, the numerical values of these coefficient matrices depend on the gains associated with the corners of the region. According to [ASS07] the observers and controllers matrices can be calculated based on the interpolution approach as

$$\begin{aligned} K_z(0,0) &= K_\square \rightarrow k_1 = K_\square \\ K_z(1,0) &= K_\diamond \rightarrow k_2 = K_\diamond - K_\square \\ K_z(0,1) &= K_\Delta \rightarrow k_3 = K_\Delta - K_\square \\ K_z(1,1) &= K_\triangledown \rightarrow k_4 = K_\triangledown + K_\square - K_\diamond - K_\Delta. \end{aligned} \tag{4.38}$$

Each corner gain is assumed to satisfy the given interpolation polynomial; therefore, the coefficients of this polynomial can be calculated from (Eqs. 4.37, 4.38) to get

$$L_e = (1 - x - y + xy)L_{\square} + (x - xy)L_{\diamond} + (y - xy)L_{\Delta} + (xy)L_{\nabla}, \tag{4.39}$$

$$L'_1 = (1 - x - y + xy)L'_{\square} + (x - xy)L'_{\diamond} + (y - xy)L'_{\Delta} + (xy)L'_{\nabla}. \tag{4.40}$$

Similarly, the corresponding value of the controller gain matrix can be expressed as

$$K_z = (1 - x - y + xy)K_{\square} + (x - xy)K_{\diamond} + (y - xy)K_{\Delta} + (xy)K_{\nabla}, \tag{4.41}$$

the rolling disturbance compensator gain matrix is described by

$$\begin{aligned} K_\delta = (1 - x - y + xy)K_{\delta\square} + (x - xy)K_{\delta\diamond} \\ +(y - xy)K_{\delta\Delta} + (xy)K_{\delta\nabla}. \end{aligned} \tag{4.42}$$

The subscripts $\square, \diamond, \Delta,$ and $\nabla,$ represent the gain related to the corner of the region as shown in (Fig. 4.4). This includes that the gains are updated continuously according to the local x- and y-coordinates of the current operating point. Therefore, the relative stability and the damping property are preserved for all operating points inside the region.

4.4 Simulation Results of State Variables Estimation and Control

The simulation results are based on the dimensions of a scaled test rig which is designed and constructed at SRS (Figs. 4.1 and 4.2). The following data are used: Boom length = 1.5 m, L_5 = 0.42 m, l = 0.5 m, m_2= 5 kg, and m_1= 0.01 m_2, $\delta_0 = \pi/4$). In the simulation the guided base is subjected to sea-waves-like sinusoidal or chaotic excitations.

As stated earlier simulation of Δw_3 in combination with simulation of the angles $\Delta\alpha_2$, $\Delta\phi_2$ are used to estimate the displacement variable vector q. The simulation of Δw_3 in two cases is shown in Fig. 4.5, the first case noised and delayed Δw_3 the second is free of noise and delay. The noise in the Fig. 4.5 are generated using white noise function. This noise then multiplied by random number. The time delay used here is a variable time delay. Here a mathematical function is used to generate random delay between (0.2 - 0.4) sec. Practically the time delay value can be measured by comparison of the camera measurements and the strain gauge measurements.

4.4.1 Observer and controller gains design

In this work a multi model approach is used for observer and controller design. The Linear Quadratic Regulator (LQR) method [HDRT04] has been applied to design the variable gain PI-observer, and Kalman filter matrices by solving the algebraic matrix Riccati equation. The LQR method is also used to design the variable gains of the controller. The design parameters for the whole working regions is not explicitly described for the sake of conciseness. For a suitable observer design, the feedback matrices L_e, L_1' have to be chosen in such a way that the estimation errors tend to zero ($e(t) \to 0$). The design parameters for the top left corner in working region R_5, Fig. 4.4 have been chosen as $Q_e = \text{diag}(20\ 20\ 20\ 20\ 20\ 10\ 20\ 20\ 20\ 100\ 20\ 10000\ 10e+12)$, and $R_e = \text{diag}\begin{pmatrix}0.5 & 0.5\end{pmatrix}$. For the same region the weighting matrices in (21) for the delayed, noised simulated Δw_3 have been chosen as $Q_{m1} = \text{diag}\ (7e-09\ 10e{-}09\ 8e{-}08\ 10e{-}07\ 10e{-}07\ 3e{-}07\ 4e{-}10\ 2e{-}10\ 8e{-}07\ 1e{-}07\ 2e{-}06\ 2e{-}06)$, and $R_{m1} = 9.26e-5$. the values of Q_e and Q_{m1} matrices are chosen by finding the error covariance for a set of simulated states. While the values of R_e and R_{m1} are chosen by finding the error covariance for a set of simulated outputs. Then these values can be adjusted till get the best results related to estimation gains.

On the other hand, in order to achieve good performance and fast vibration suppression at steady-state, the design terms in (4.35) for the bottom right corner in working region R_5 have been chosen as $Q = \text{diag}\,(10\ 10\ 1\ 1\ 1\ 1\ 0.1\ 0.1\ 1\ 1\ 460\ 370)$, and $R = \text{diag}\,(19000\ 19\times10^{13}\ 250000)$ respectively. With these values the resulting state feedback matrix becomes

$$K_z = 10^{-3}\times\begin{bmatrix} -8.46 & -51.7 & 12.9 \\ -9.55 & -338.3 & -329.3 \\ 0.105 & 1.25 & 3.03 \\ 1.21 & 18 & -35.77 \\ -8e-11 & 3e-08 & -5e-10 \\ 7e-10 & 3e-08 & 3e-08 \\ 7e-10 & 2e-10 & -3.9e-10 \\ 7e-11 & 3e-09 & 4e-09 \\ 0.947 & 16.56 & 2.981 \\ 5.466 & 11.06 & 12.84 \\ 0.301 & 0.265 & -0.0048 \\ 0.297 & 38.56 & 6.728 \end{bmatrix}.$$

4.4.2 State estimation results

The estimated displacement variables $\Delta\hat{w}_3, \Delta\hat{\alpha}_2$, and $\Delta\hat{\phi}_2$ estimation results are shown in Fig. 4.6. Here the crane base is subjected to sinusoidal excitation with

the amplitude of $|\Delta\delta|_{max} = 5$ degree and $\Delta\phi_2 = 30$ degree as initial condition. A sinusoidal wind force affecting the payload is assumed, and the controller is turned off. The estimated displacement variables are compared with the actual states based on the varible dynamic model of the system. The proposed observer estimates the state very well. The Kalman filter removes the noise effect from the states and the dynamic part $g(t)$ accounting the time delay dynamic part very fast. From Fig. 4.6 can be stated that the proposed observer removes the error in the estimated states due to unknown initial condition also.

4.4.3 Controlled motion results

Results for the control based on the developed estimation model are shown in Figs. 4.7, 4.8. The control system is used for a sinusoidal rolling excitation with amplitude of $|\Delta\delta|_{max} = 10$ degree, assuming no wind force affecting the payload. The luff angle is increased in the first 5 seconds from 30 to 55 degree; the length of the cable is decreased from 2.5 to 1.5 meter, the initial conditions are assumed as zero. The controlled and the uncontrolled displacement variables and the position of the payload are shown in Fig. 4.7. In the case the controller is turned on, the vibrations of the flexible link are suppressed very fast. The position of the payload is stays around constant value ($\Delta x_2(t)$, and $\Delta \mathrm{y}_2(\mathrm{t}) \approx 0$). The control system is used to suppress the swing motion of the payload m_2 for a chaotic rolling disturbance (Fig. 4.8). Here the dominant frequency is close to the first eigenfrequency of the crane (2.5 Hz), so the crane vibrates for the first 5 seconds. Then the controller is turned on at t=5 seconds to control the vibrations in the elastic and rigid parts of the crane. The luff angle is increased in the period from $t_{\mathrm{begin}} = 5$ to $t_{\mathrm{end}} = 10$ sec. from 25 to 55 degree, the length of the cable is decreased from 2 to 1.5 meter. The payload swings for the first five seconds, then the controller is turned on. For all of the above mentioned cases, it can be stated that the controller performs very well and the oscillations are reduced significantly without any noticeable secondary effects based on the estimated states.

4.5 Summary

In this chapter the effect of time delay as well as noise in the state estimation process is assumed through the comparison between the states obtained from different measured input data. The main goal of the work is to develop an approach combining suitable measurement devices easy to realize with improved reliability. The dynamic model of elastic crane is used to design the controller for the payload position using three input variables. The state estimators are used based on three measurementsOne of these measurements assumed as camera measurement. Two variable state estimators are designed, the first one to estimate state variables based

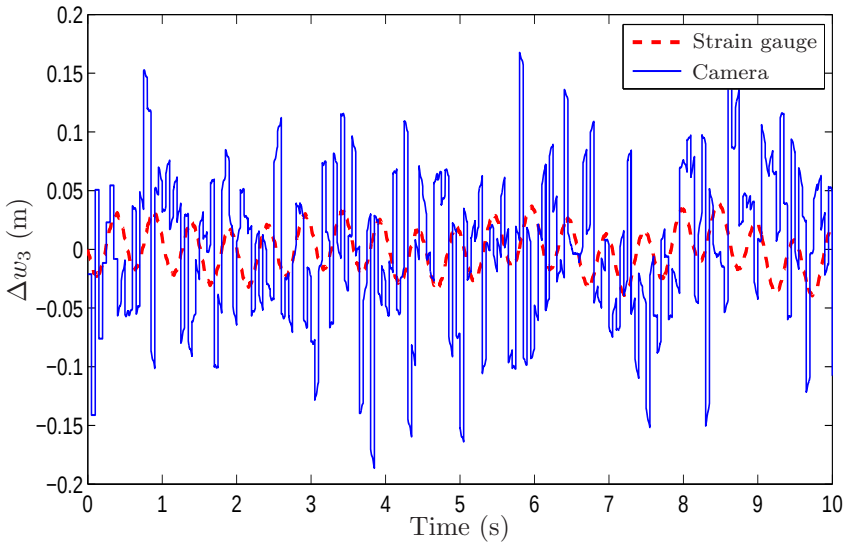

Figure 4.5: Simulation of Δw_3

on the delayed and noised camera measurement, the second one is based on the non-delayed measurements. The states estimated from these two observers are combined in order to get optimal estimation of the required states. A dynamic equation based on the model of the elastic crane is used to account for the time delay in the estimated states. A variable gain controller is designed based on the estimated states to generate the required damping and to compensate for the rolling movement of the ship. As an outline of this chapter, the experimental test of state estimating and controlling of elastic ship-mounted crane using camera measurements will be presented in the next chapter.

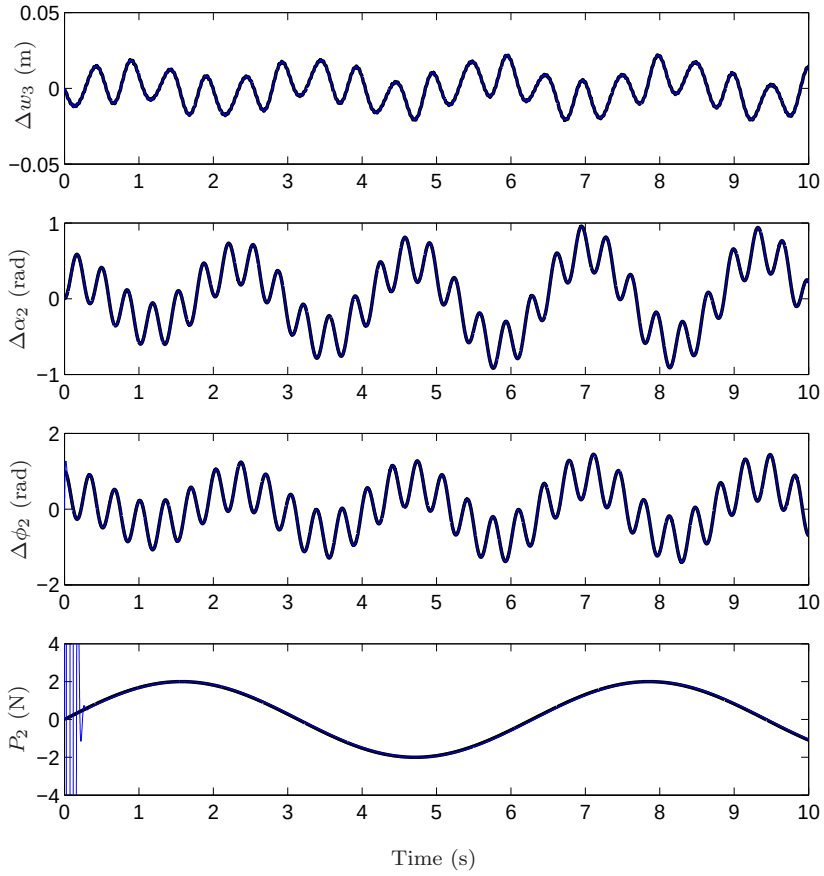

Figure 4.6: Estimation of $\Delta w_3, \Delta\alpha_2, \Delta\phi_2$, sinusoidal rolling, —— actual, —— estimated

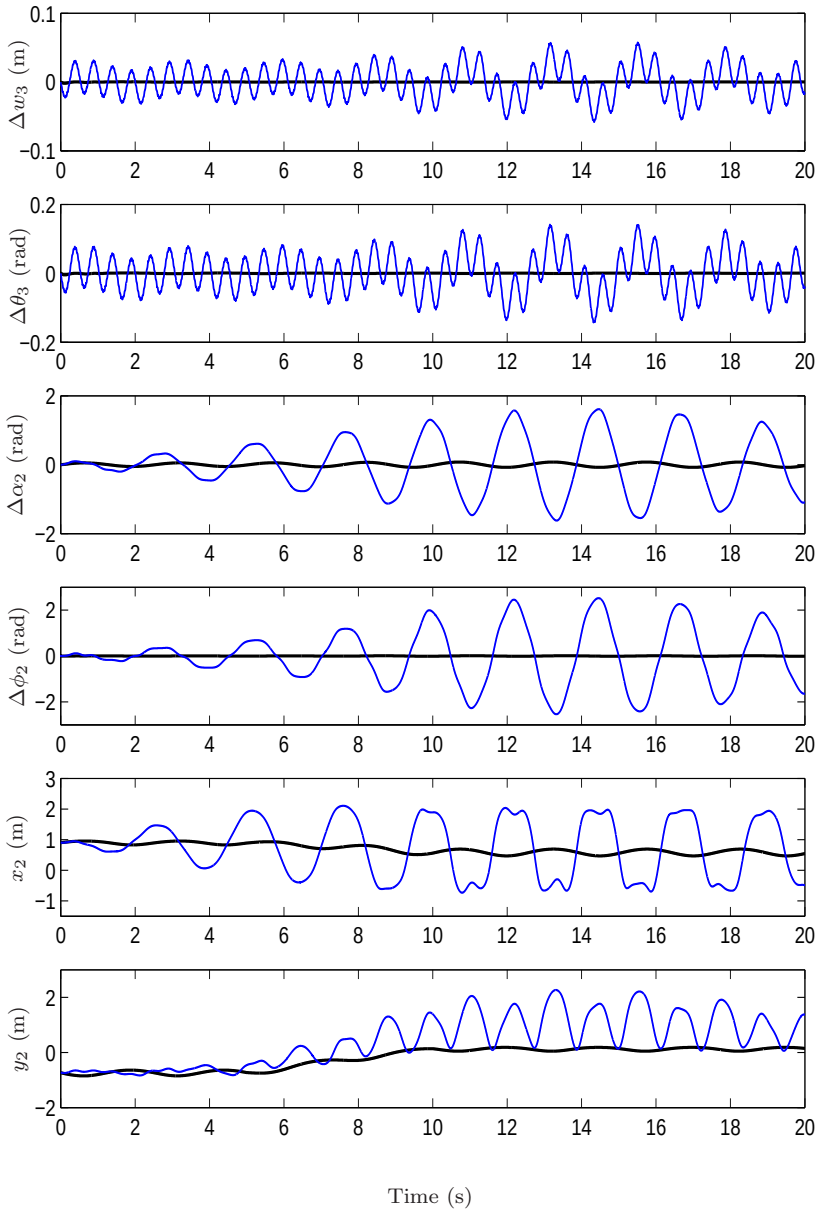

Figure 4.7: Displacement variables and position of the payload, sinusoidal rolling, —— controlled, —— uncontrolled

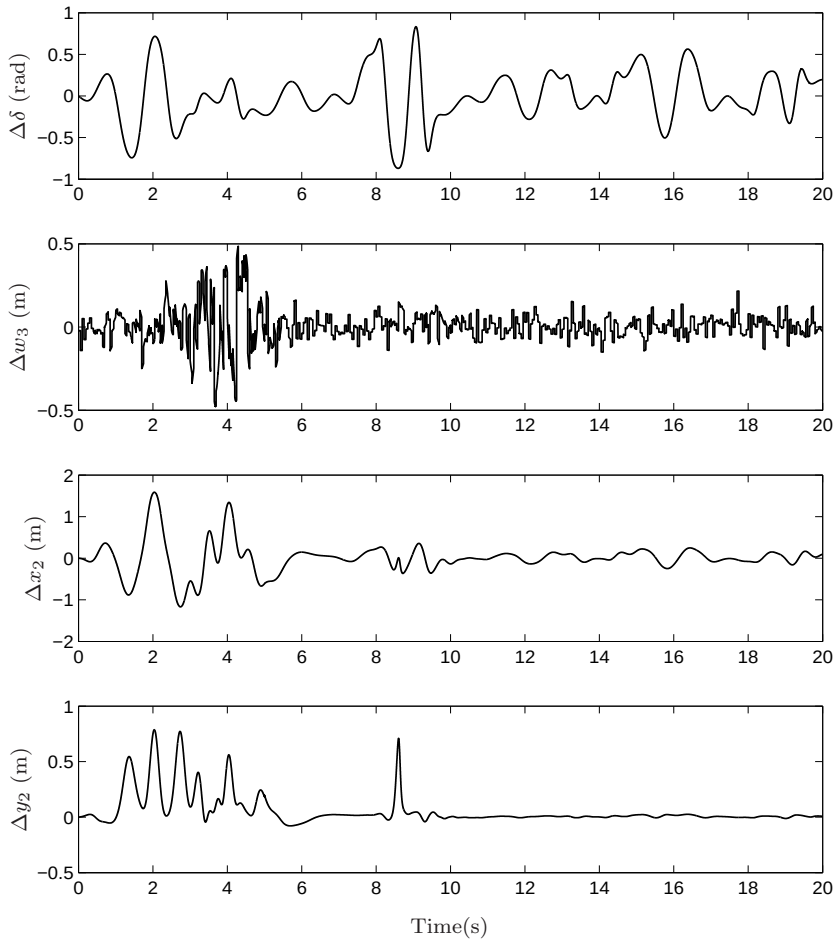

Figure 4.8: Position of the payload and simulated Δw_3 (chaoting rolling, (controller turned on at $t = 5$ sec).

5 Visual Servoing of Elastic Ship-mounted Crane: Experiments

This chapter addresses the experimental results for a vision-based vibration control for elastic ship-mounted crane. Realizing a multi-model approach addressed in the last chapter, the variable gain controller uses the estimated states from variable gain state estimator and the roll angle to generate the required damping to control the system. Experimental work will be explained in detail.

5.1 Experimental Setup: Elastic Ship-Mounted Crane

The configuration of the experimental set up was built at the laboratories of SRS. A scaled test rig is designed and constructed to simulate the operation of an actual elastic ship-mounted crane at sea (Fig. 4.1). The analytic-numerical investigation and the experimentation have been taken in to account in the building process of the test rig, in order to validate the theoretical assumptions and to verify the numerical results. The test rig (components and measurements) are presented in [ASS07]. In this section only brief overview and the additional components presented. The elastic ship-mounted crane test rig consists of the following parts:

1. Three inputs to control the payload during operation:

   - The position of the lower suspension point $\Delta D(t)$, which is controlled using a hydraulic cylinder mounted between the lower suspension point and the tip of the boom as shown in Fig. 5.1(a),
   - the luff angle of the elastic boom $\rho(t)$, The luff angle is controlled by a hydraulic cylinder as shown in Fig. 5.2(a), and
   - the length of the upper cable $L(t)$, is controlled by a DC motor integrated with a spur gear box as shown in Fig. 5.3(a).

   The displacement $\Delta D(t)$ is measured by a linear incremental encoder, while the change in the luff angle $\Delta\rho(t)$ and the change in the upper length cable $\Delta L(t)$ are measured using rotary potentiometer.

2. Three output variables must be known to guarantee the observability condition of the crane and payload:

   - The elastic rotational displacement is measured directly by a strain gauge glued to the elastic boom which is replaced in this work by camera system, as shown in figure 5.5(a).

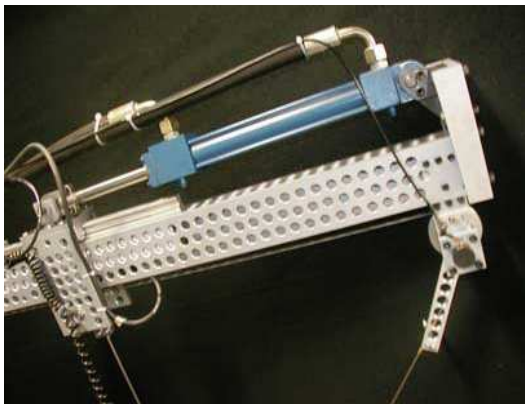

(a) Actuator for $\Delta D(t)$

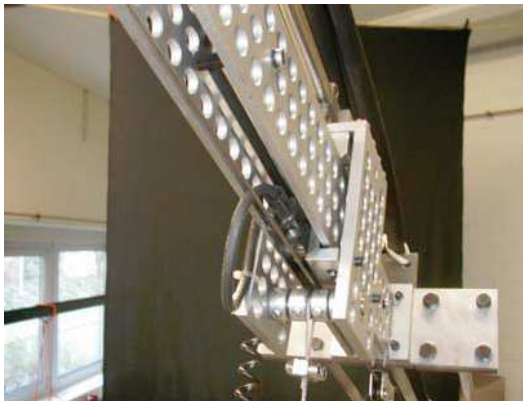

(b) Incremental Encoder for $\Delta D(t)$

Figure 5.1: Lower suspension point measurement and input signal

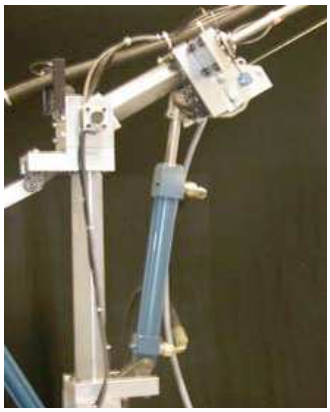

(a) Actuator for $\rho(t)$

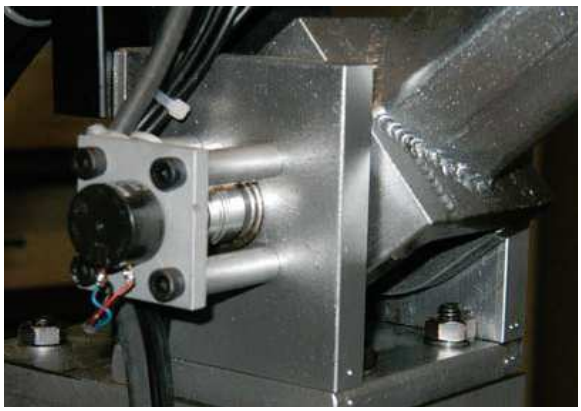

(b) Rotary potentiometer for $\rho(t)$

Figure 5.2: Luff angle measurement and input signal

- The $\Delta\alpha_2$ and $\Delta\phi_2$ angles can be measured indirectly using rotary potentiometers as shown in figure 5.4(a) and figure 5.4 (b).

3. The measuring instruments (the potentiometers and the linear incremental encoder) are connected to the controller (dSpace processor) through a connection block with MIMO channels (Fig. 5.5(b)).

4. The dSpace controller is programmed by MATLAB SIMULINK which includes the multi model PI-Observer and the variable-gain controller. Each actuator of the crane is controlled by a PD tracking controller to ensure that the actuators track the input commands (desired displacements) coming from the MIMO variable-gain controller as illustrated in Fig. 4.20.

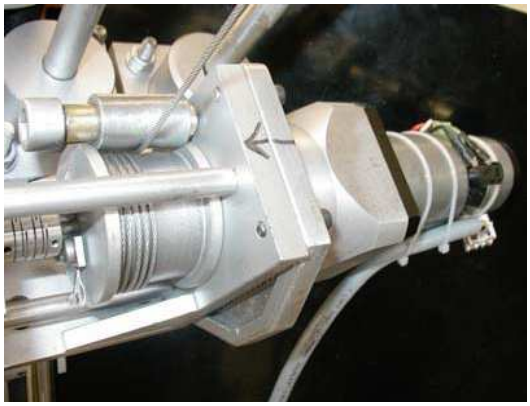

(a) Actuator (DC Motor) for $L(t)$

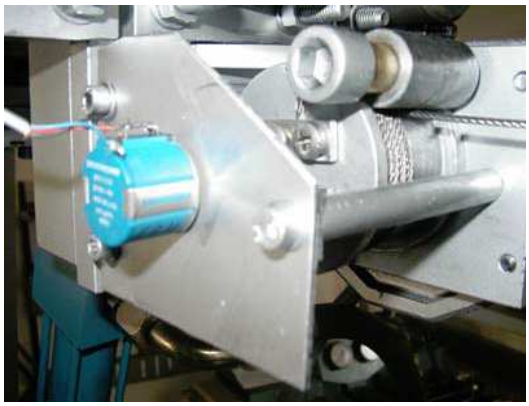

(b) Rotary potentiometer for $L(t)$

Figure 5.3: Cable length measurement and input signal

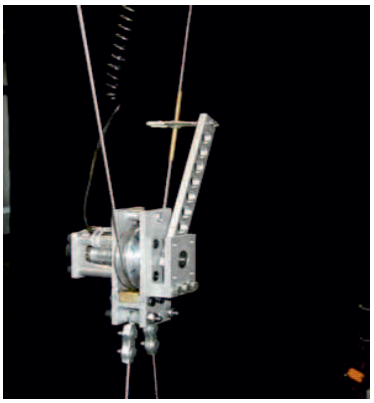

(a) Rotary potentiometer for $\Delta\alpha_2$

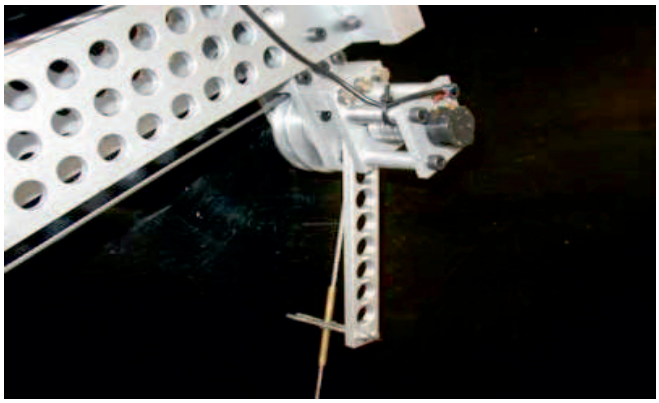

(b) Rotary potentiometer for $\Delta\phi_2$

Figure 5.4: Measurement of angles

(a) Strain gauge

(b) dSpace connection block

Figure 5.5: Deflection measurement and connection block

Figure 5.6: Basler aviator camera, SRS

5. In this work, a high performance CCD camera avA1600-50gc that is made by Basler Company (Fig. 5.6) is used for sensor fusion.

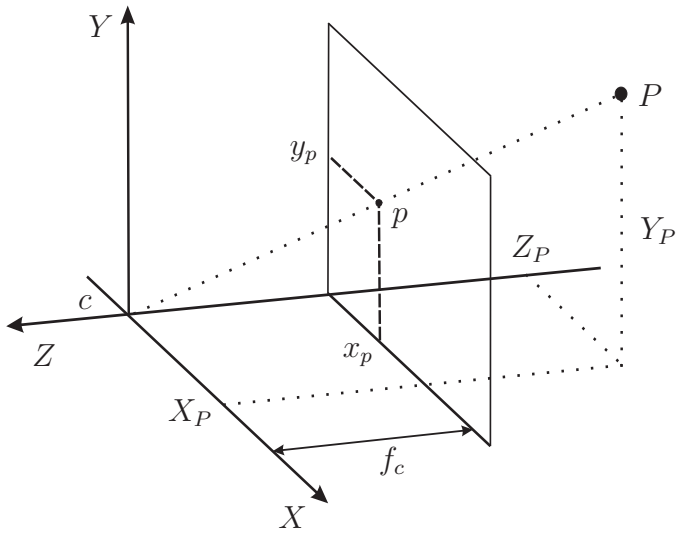

Figure 5.7: Simple camera model

5.2 Flexible Link Deflection Measurement

In the operation of flexible link robot it is important to compensate the tip position and orientation inaccuracies caused by the link deformations through adjustment of the joint variables. Thus, a vision sensor system which is specially dedicated to the measurement of the link deformations in real-time is essential for the accurate control of the flexible link. A combined PI- observer and Kalman filter are used for estimating beam deflection angle in order to address robustness issues and reduce the operation error.

5.2.1 Camera System Modeling

The second type of sensor considered in this work for dynamic state estimation: the camera. When the camera is pointed to a physical object, an image of this object is formed on a photographic film or an image capture device by means of rays reflected from the object passing through the aperture of the camera lens. Digital images are stored as number arrays where numbers represent the intensity of light exposed on the sensor array. By using a camera as the flexible link sensing device, a direct measurement of the deflection can be made. The quality of the camera measurement depends on the properties such as the imaging sensor, lens type and frame rate, which cameras are usually classified according to. However, a significant delay and noise was found between the actual and measured flexible link deflection, which needs to be compensated. In this section the camera model used, is first explained, followed by the adjustment for distortion in the camera lens

and the description of the calibration process. After that how finding the flexible link deflection based on the image frames captured by the camera is discussed. As stated earlier, a high performance CCD camera avA1600-50gc that is made by Basler Company is used for sensor fusion. The image array sensor is up to 1600 pixel by 1200 pixel image size, and highest sampling frequency being 60 Hz. The computer used in the real time image processing captures the frames from camera using a high performance GigE vision interface. The mathematical camera model and calibration procedure is also explained in this section.

A visual sensor system containing: CCD camera and LED markers, is used. Assuming the camera geometry modeled by perspective projection [Cor11], which simplifies the camera lens to its ideal behavior. Mathematical camera models represent the mapping of 3D coordinates of a point in the scene to its 2D projection in the image plane (figure 5.7). The 2D projection of the point is derived by using the similarity of triangles, as

$$(u_i, v_i) = (f_c \frac{X_P}{Z_P}, f_c \frac{Y_P}{Z_P}), \tag{5.1}$$

where u and v represent the components of the image coordinate frame (i-frame) with origin on the center of the image plane, i.e. the center of projection. Here, f_c is the focal length of the camera. Since the digital output of the camera is represented by pixel values pixel coordinates (p-frame). The projection of point P having 3D camera frame coordinates $[X_P, Y_P, Z_P]$ on the image plane is given by

$$(x_p, y_p) = (x + x_0, y + y_0) = (x_0 + f_c \frac{X_P}{Z_P}, y_0 + f_c \frac{Y_P}{Z_P}), \tag{5.2}$$

where x and y represent the components of the image coordinate frame(i-frame) with origin on the center of the image plane, i.e. the center of projection. (x_0, y_0) being the position of center of projection.

This ideal camera model is converted to a more realistic model by employing terms for non-ideal characteristics of a camera. These include the effective pixel size s_x and s_y , and image plane orientation represented by the skew factor. The aforementioned attributes are collected in a matrix form symbolized by K_{int} which is multiplied with the position vector of the observed 3D point. the K_{int} can be written in compact form as:

$$K_{int} = \begin{bmatrix} s_x f_c & \text{skew factor} & x_0 \\ 0 & s_y f_c & y_0 \end{bmatrix}, \tag{5.3}$$

and using K_{int} the projection of point P on the image plane reformulated as

$$(x_p, y_p) = K_{int}\ \mathrm{P^c}. \tag{5.4}$$

Additionally, non-linear image distortion model can be utilized to express the non-ideal lens properties. In more recent works, a distortion model is also suggested by introducing non-linear coefficients to the camera model.

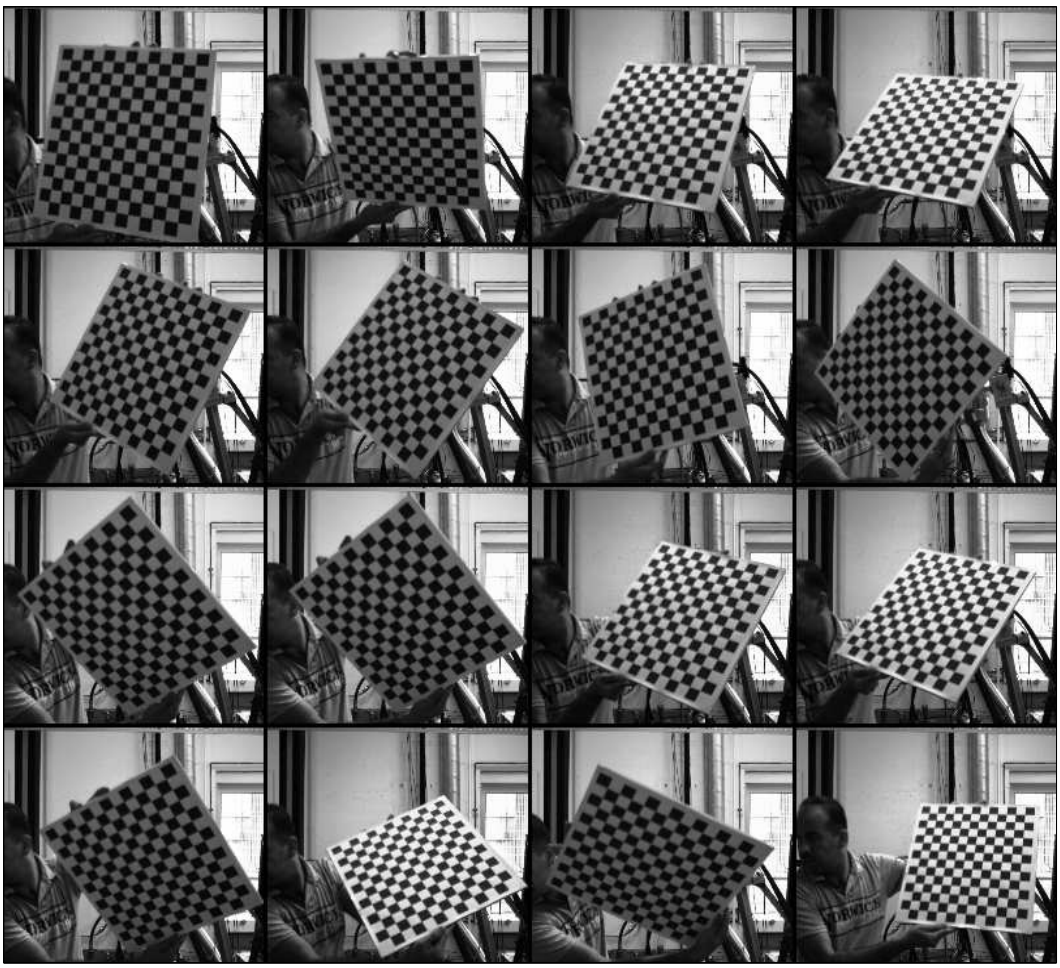

Figure 5.8: Checkerboard pattern images used for intrinsic calibration

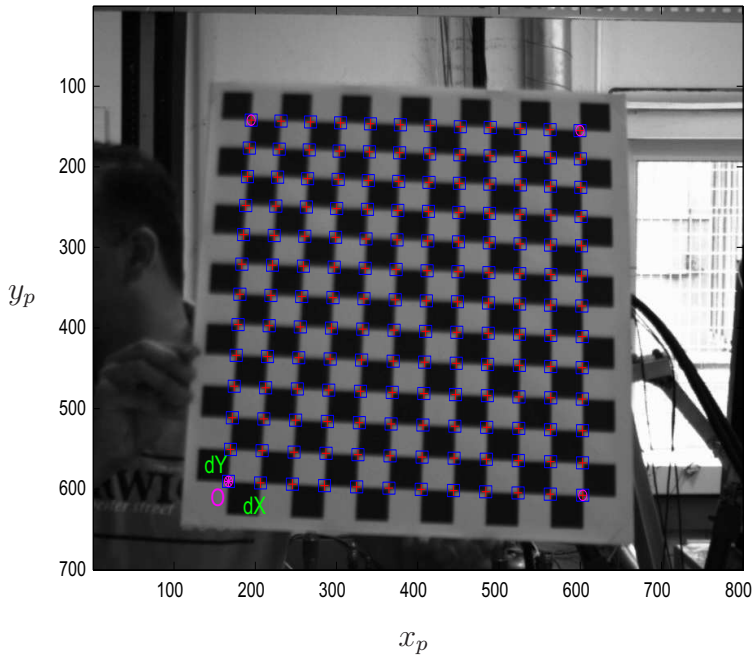

Figure 5.9: Extracted image points for calibration

5.2.2 Camera Calibration

Camera calibration is necessary to relate information obtained from the image plane pixels to objects in the real world through determining the matrix form symbolized by K_{int} and the external calibration parameters. Camera calibration extensively studied with many more techniques presented in the literature. The camera calibration toolbox for matlab developed by Jean-Yves Bouguet at the Vision Laboratory of California Institute of Technology [Bou] for internal and external calibration is used in this work. Internal calibration is used for the determination of pinhole camera model parameters, i.e. K_{int} explained earlier. The relationship between the camera frame and object (point) frame is defined using K_{int}. However, object or point P is represented in global frame $[X_g, Y_g, Z_g]$, since it is not possible to measure the distance from the center of the camera to the point P. Hence, external projection between the camera frame and global frame should be known. Determination of the position of camera in global frame and the rotation between the frames are calculated via external calibration as follows

$$\begin{bmatrix} X_P \\ Y_P \\ Z_P \end{bmatrix} = R_{ext} \begin{bmatrix} X_g \\ Y_g \\ Z_g \end{bmatrix} + t_{ext}. \tag{5.5}$$

The relationships given in Eqns.(5.2-5.5) can be represented with a equation matrix multiplication by combining t_{ext} and R_{ext} in a 3x4 matrix $[R_{ext}|t_{ext}]$ and multiplying

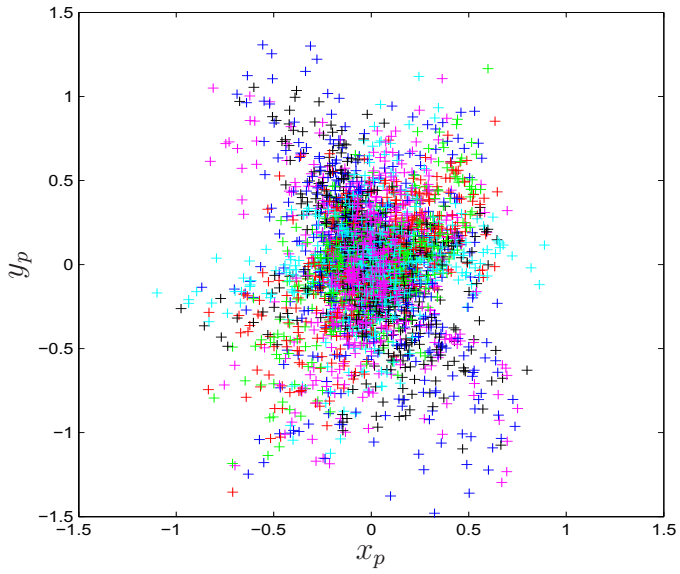

Figure 5.10: Reprojection error of image points for calibration

the resultant with employing homogeneous coordinates, a 4x1 vector. Homogeneous coordinates are formed with augmenting 1 at the end of the coordinate vector:

$$\begin{bmatrix} mx_p \\ my_p \\ m \end{bmatrix} = \begin{bmatrix} K_{int} & & \\ 0 & 0 & 1 \end{bmatrix} [R_{ext}|t_{ext}] \begin{bmatrix} X_g \\ Y_g \\ Z_g \\ 1 \end{bmatrix}. \tag{5.6}$$

The calculated pixel coordinate vector from Eqn.(5.6) is weighted by a factor of m which is the 3rd component. By dividing the first two components of the vector, pixel coordinates are obtained.

As stated earlier intrinsic and extrinsic parameters of the camera are obtained by utilizing the Camera Calibration Toolbox for MATLAB [Bou]. The main internal parameters are estimated using images of a planar checkerboard pattern (Fig. 5.8). This pattern provides a number of points for minimization of the re-projection error. These error patterns represent the estimation of the corners' positions based on the calibration parameters for each frame. Several iteration have to be done, until the error is smallest as possible. One of the images with the extracted and projected corners and the distribution of re-projection pixel error are shown in figures 5.9 and 5.10 respectively. Internal camera parameters for Basler Camera are obtained

as follows:

$$\begin{aligned} \left[s_x f_c s_y f_c\right] &= \left[1480.33\ 1478.77\right] \pm \left[4.504\ 5.531\right], \\ \left[x_0\ y_0\right] &= \left[320.18\ 293.08\right] \pm \left[5.71\ 3.42\right], \\ \text{skew factor} &= \left[0.00\right] \pm \left[0.00\right], \\ \text{Pixel error} &= \left[0.24346\ 0.3497\right]. \end{aligned}$$

Additionally, non-linear image distortion model can be utilized to express the non-ideal lens properties, distortion coefficients D_c are obtained as follows:

$D_c = [-0.104\ 0.474\ 0\ 0] \pm [0.019\ 0.211\ 0\ 0]$.

The unit to the internal parameter values is 'one pixel long'. The external camera parameters of the Basler Camera used in this work are calculated at in the experimental setup. The corner of the checkerboard pattern is marked as the origin of the global coordinate frame. The rotation and translation matrices are obtained as follows:

$$\begin{aligned} \text{Translationvector} : \mathrm{T_cext} &= \left[-85.492828\ 98.748398\ 1236.655272\right], \\ \text{Rotationmatrix} : \mathrm{R_cext} &= \begin{bmatrix} 0.971317 & -0.131396 & -0.198189 \\ -0.018018 & -0.871738 & 0.489641 \\ -0.237105 & -0.472026 & -0.849101 \end{bmatrix}, \\ \text{Pixel error} &= \left[0.22383\ 0.58252\right]. \end{aligned}$$

5.2.3 Deflection Calculation

Control strategy based on image processing is usually done by extracting relevant features that characterize uniquely the target with respect to other objects that could be present in the image. These features can be points, lines, or general shapes. The task of an advanced image processing for complex target detection is not of primary interest in the present work, and the description of the developed algorithm for the target detection is limited to the case of point features. The experimental target is here represented by three red lights mounted on a flexible link. The three red markers to measure the deflection of flexible link is used in order to simplify the detection process of markers, as shown in figure 5.11. In the begin of the experiments three white LEDs are used as markers. Because of the white LED were not appropriate with the scene (as shown in figure 5.12). In order to avoid the requirements of black background, reduce the light of the environment (laboratory), and paint some parts of the crane. The white LEDs are replaced in the progress of the work with red LEDs .

Figure 5.11: LED markers fixed on flexible link

Figure 5.12: White LEDs test

Clearly, in a generic environment, other red pixels could be present but if the other pixels have different intensity, the image processing procedure will not detect the pixels as LED markers. The idea of tip deflection measurements is based on using two point located on straight line and then using the third point to calculate the deflection of the tip point (vertical distance between the line and the third point). In RGB codification, three values are associated to any pixel, corresponding to the red, blue, and green levels. A perfect red should be a $[255, 0, 0]$ triplet. However, due to changing light conditions and sensor imperfections, this value is not expected to be found. A common behavior that has been experimentally observed is that the camera automatic exposition regulation. Meaning, the distance between the camera and the test rig brings to an underexposed image when it is far from the target (i.e. acquired red is darker than perfect red) and to an over-exposed image when it is close to the target (i.e. acquired red almost like white).

Sequences of processes are applied consecutively in real time for the sake of red marker detection: first subtract the red component (R-Image) from the gray scale image to extract the red components in the image. After that the median filter is used to filter out noise. Convert the resulting gray scale image into a binary image. Remove all those pixels region less than 12px, Label all the connected components in the image which represent the red objects, and the image blob analysis is done finally to locate the center of the LED in the image. The image processing steps are shown in figure 5.13, the image processing is done using the Matlab/Simulink software through capture the video signal from GigE vision card using Simulink and by using Matlab/Sfunction for Image processing.

5.3 Experimental Results

The results are based on the dimensions of a scaled test rig which is designed and constructed at the Chair of Dynamics and Control at the University of Duisburg-Essen (Fig. 4.1). The data used are: Boom length = 1.5 m, L_5 = 0.42 m, l =0.5 m, m_2= 5 kg, and m_1= 0.01 m_2, $\delta_0 = \pi/4$). In the experiment the guided base is subjected to two different types of sea-waves like sinusoidal and chaotic excitation. The dSpace controller is programmed by MATLAB SIMULINK which includes the multi-model PI-Observer, Kalman Filter for state estimation and the variable-gain controller. Each actuator of the crane is controlled by a PD tracking controller to ensure that the actuators track the input commands coming from the MIMO variable-gain controller. Two mainframes, one for image processing and the second for the dSpace system are used in the experiments. A User Data-gram Protocol (UDP) in Python program is used as a connection between these two computers to transfer the camera measurements to the dSpace computer. The time delay can be calculated by using the python program by comparing the time of send and the time of receive in the first and second computer respectively; and then the time delay fed

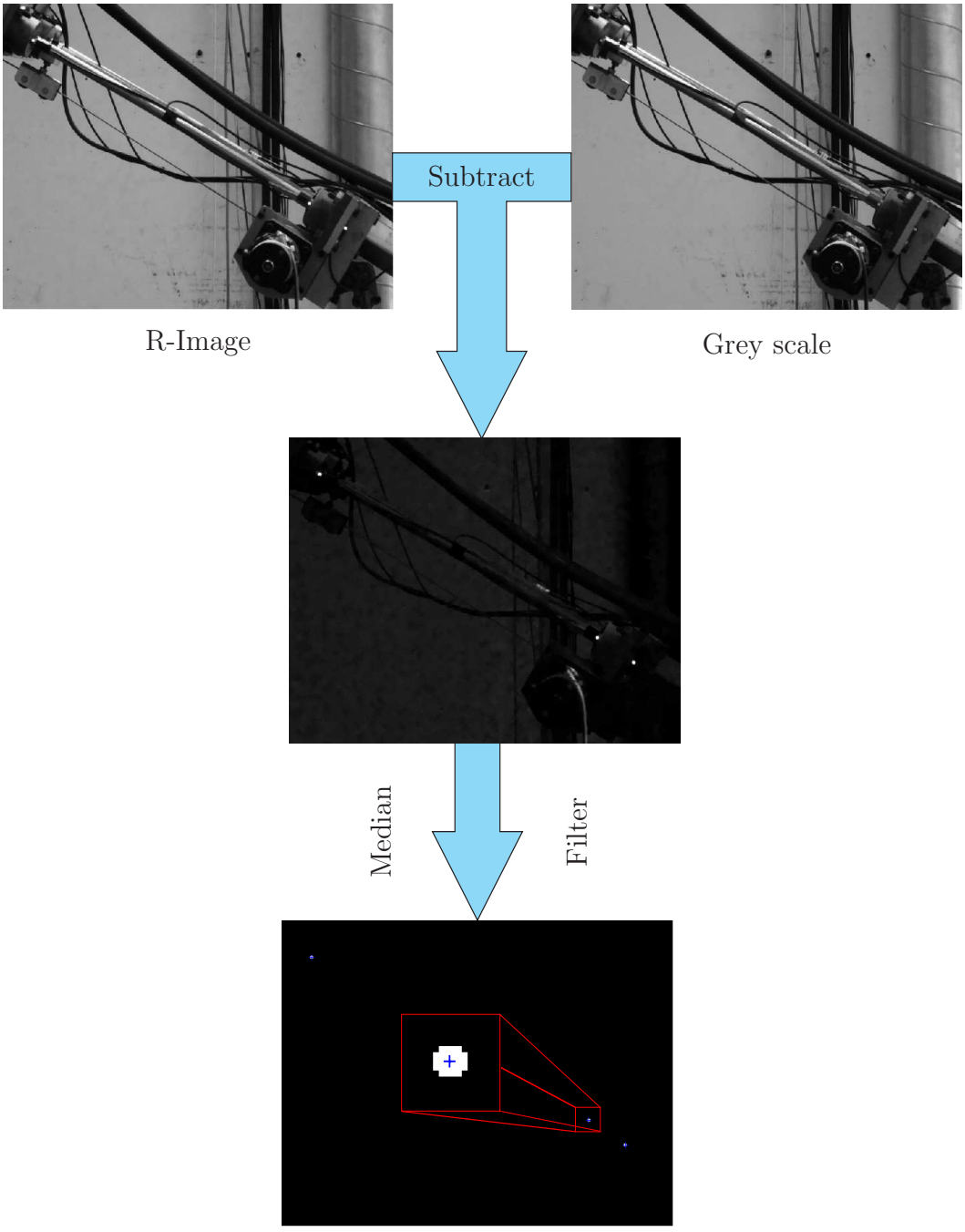

Figure 5.13: LED markers centers using image processing

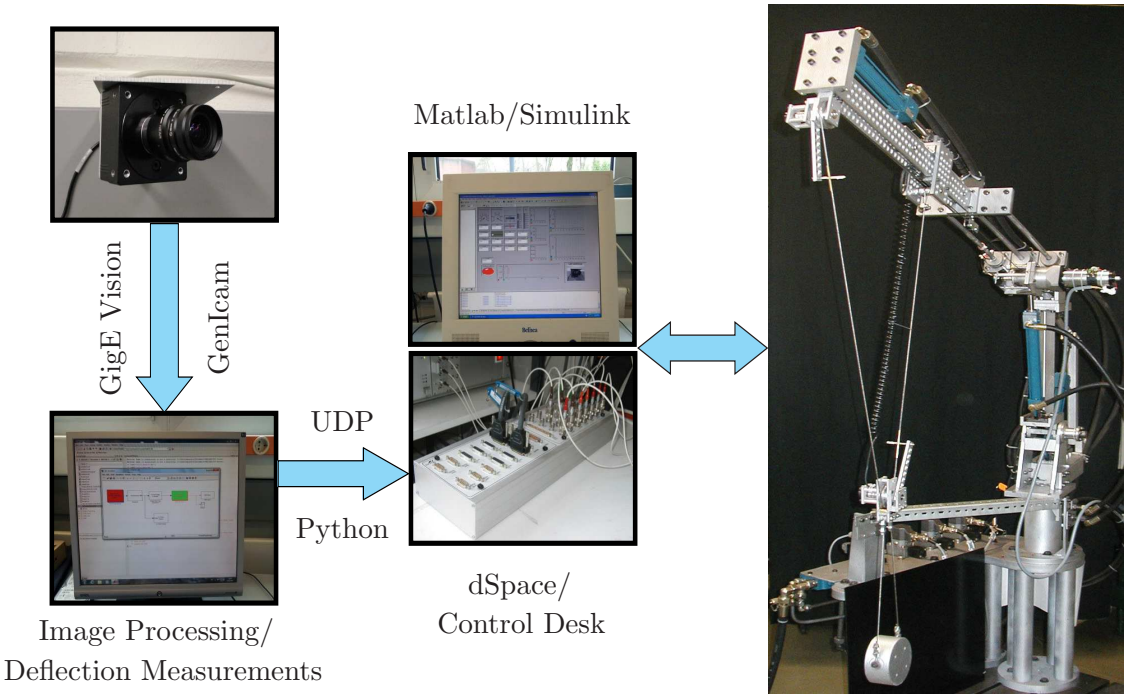

Figure 5.14: Schematic diagram for the test rig (Chair of Dynamics and Control, University of Duisburg-Essen)

to the dSpace model to account delay effect in the state variables. The schematic diagram for the image processing unit and experimental test rig connection is shown in figure 5.14.

5.3.1 Link Deflection Measurement

The tip point position is measured based on image frames. The camera is set on the location in front of the vertical plane in which the crane moves with a distance of 2.25 (m). With this setting, the measurable area of the visual sensor system is 0.8 (m) $\times$ 1 (m), the resolution is 55(μm) $\times$ 55 (μm). The frame rate of the camera is fixed on 30 fps. Deflection of the link is calculated on real-time basis, the main steps of this process are

1. LEDs detection on image plane,
2. Determination of LEDs centroids, and
3. Determination of deflection using the LEDs centroids.

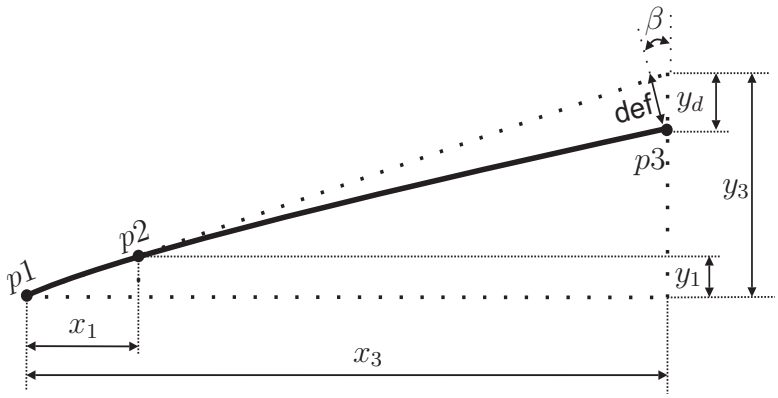

Figure 5.15: Tip deflection measurement

To detect the center of each LED it is necessary to determine its edge. After the detection of each LED centroids, and as shown in figure 5.15, the deflection calculation can be found by

$$\Delta w_3 = def = y_d * cos(\beta), \tag{5.7}$$

where y_d is calculated by

$$y_d = y_3 - (y_{p3} - y_{p1}), \tag{5.8}$$

here $p1$, $p2$, and $p3$ represent the position of the LEDs centroids on the image plane. In order to compare the tip deflection measurement with those given in [ASS07], θ_3 is required which is derived based on the beam model, and as the result is given by $\Delta\theta_3 = 3\Delta w_3/2L_3$. The deflection measurement using the camera system is shown in figure 5.16. The camera is used to measure the slope of the tip deflection when the controller is on. The measurement using the camera system suffer from highly noise (Fig. 5.16) due to the resolution limitation and the error in the LED centroids detection. Due to the limitation of the frame rate, the camera system can not detect the exact deflection of the tip point precisely. Because of coupling between rigid and flexible dynamics; the rigid states of the system affect the flexible dynamics. Then, there is no linear system for the estimator which can be constructed by simply removing their rows and columns from the matrices of dynamic equations. The camera measurement is used in the rest of results instead of strain gauge measurement to estimate the states of the system. The performance of the elastic crane system will be compared in the next section using the camera and the strain gauge measurements.

5.3.2 State Estimation and Control Experimental Results

Results for an actual disturbance in addition to the actual displacements, the estimations based on the illustrated approach are presented in Figs. (5.17−5.26). Results

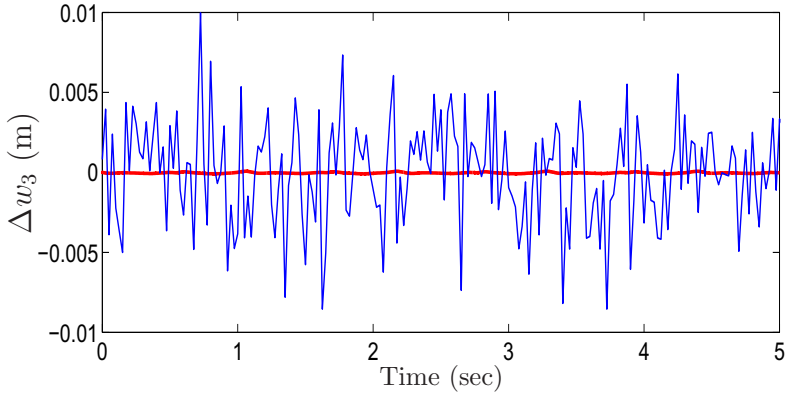

Figure 5.16: Flexible link deflection measurements —— camera, —— strain gauge

presented here are based on the full working range of the elastic crane. In these results the dynamic state variables experimentally estimated based on the estimation approach addressed in chapter 4, where simulated camera and potentiometers measurements are used by different types of state estimators. Then the estimated state are combined in order to get the optimal estimation, and used to generate the control inputs.

In figure 5.17 and 5.18, the crane was subjected to sinusoidal rolling excitation in the neighborhood of the first eigenfrequency of the crane. The controlled (camera and strain gauge measurements) and the uncontrolled dynamic response variables of the crane are presented. In the uncontrolled case, this excitation caused the amplitude of measurements to grow rapidly to a dangerous level. Two different amplitude for the sinusoidal rolling is used in order the see the effect of higher amplitude on the system. Figure 5.17 shows the sinusoidal excitation of the crane with ± 5 degree, the output variables beside the position of the payload are presented. The sinusoidal excitation of the crane with ± 10 degree is presented in Figure 5.18 and the same system output and the position of the payload are presented. The crane also subjected to chaotic rolling excitation the results shown in Figure 5.19. From the earlier mentioned figures it can be seen that the controller based on the estimation approach can be remove the vibration of the payload after few seconds. It is also clear from the presented results that the performance of the system when using strain gauge or camera measurements is quite close. This set was repeated for different luff angles, cable lengths, and payloads (different models) in order to test the operation of the region finder and the behavior of the variable-gain observer and controller in case of camera measurements.

The constant values like initial condition of the cable length L_0, the initial condition of the luff angle ρ_0 (variable-gain), and payload m_2 were changed during the experiments, in order to test the work of the crane under variation of these values Figs. (5.20−5.26). The payload of the crane changed from 5 kg to 10 kg, and the

experiments done using the three sets of rolling conditions, produced the results presented in (5.20−5.22). In figure 5.23 the system to swing for 10 seconds, and then run the controller just to ensure the effectiveness of the controller to suppress the vibration. Two sets of results for sinusoidal rolling with ±5 degree, are presented in figure 5.24. The length of the cable, and the luff angle changed during the operation of the crane from $1.6 - 1.2(m)$, and $30 - 45(Deg)$ and this led observer to change the gain to estimate the states based on the variable gain approach, the controlled and uncontrolled of the output response and the position of the payload are presented in this figure. After that in figure (5.25) the L_0, and ρ_0 are changed during the operation ($L_0 = 1.6 - 1.2(m)$ and $\rho_0 = 30 - 45(Deg)$) of the crane to simulate real world lift process with the value of 7.5 kg payload. System outputs, and the position of the payload are shown in Fig. (5.25).

The chaotic rolling excitation is used in combination with the changes of the L_0, ρ_0, and $m_2 = 10$ kg and the results shown in figure 5.26. The rolling excitation is shown, and the output responses and the position payload for the controlled and the uncontrolled cases are shown in the figure. All results addressed in this section cover all the operations possibility of the crane. The results also shown that the estimation approach based on the camera measurements works well and estimated the states of the system fast in different operation condition which prove the robustness of the estimation approach.

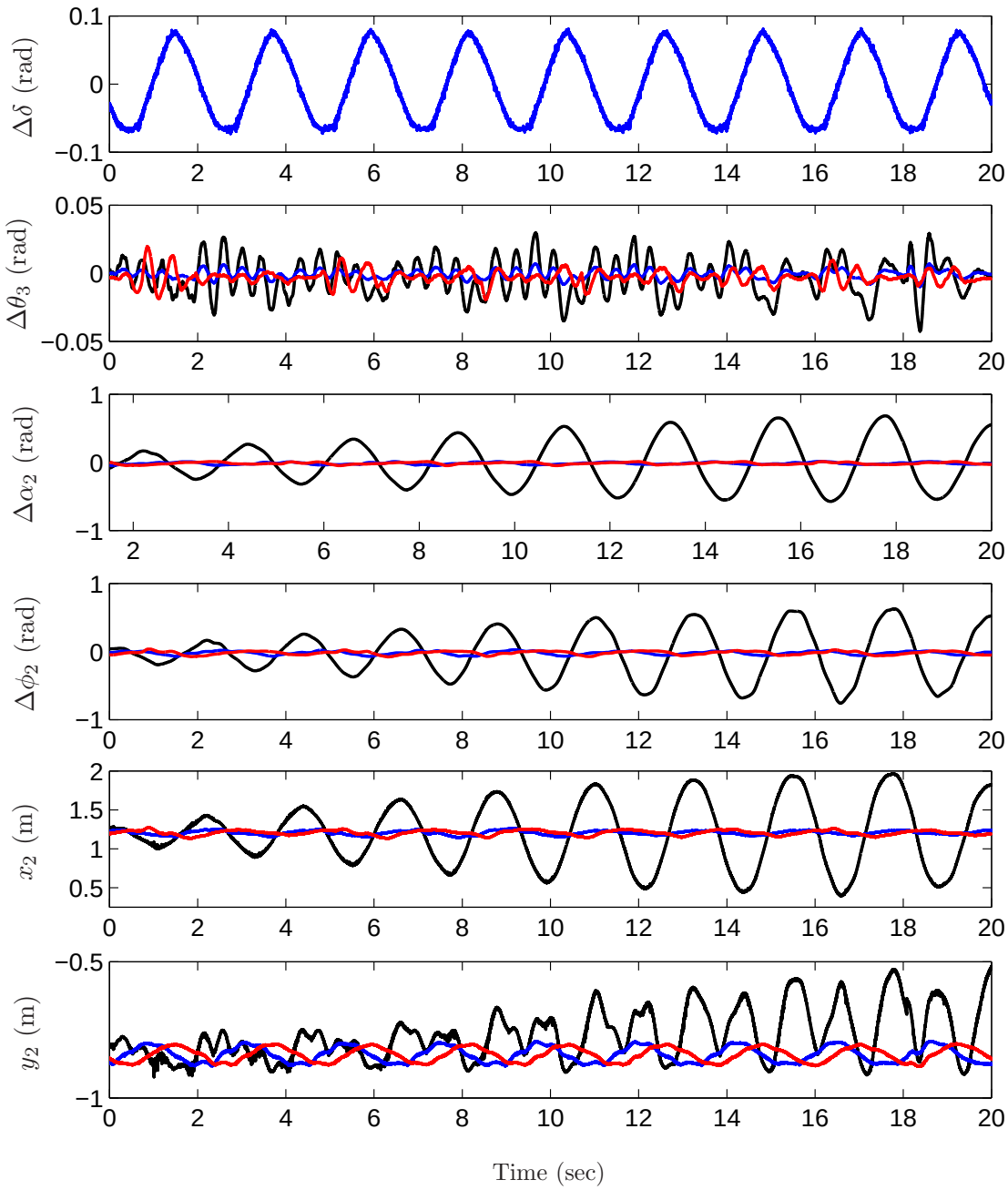

Figure 5.17: Experimental response due to sinusoidal rolling ±5 degree, —— uncontrolled —— controlled (camera), —— controlled (strain gauge)

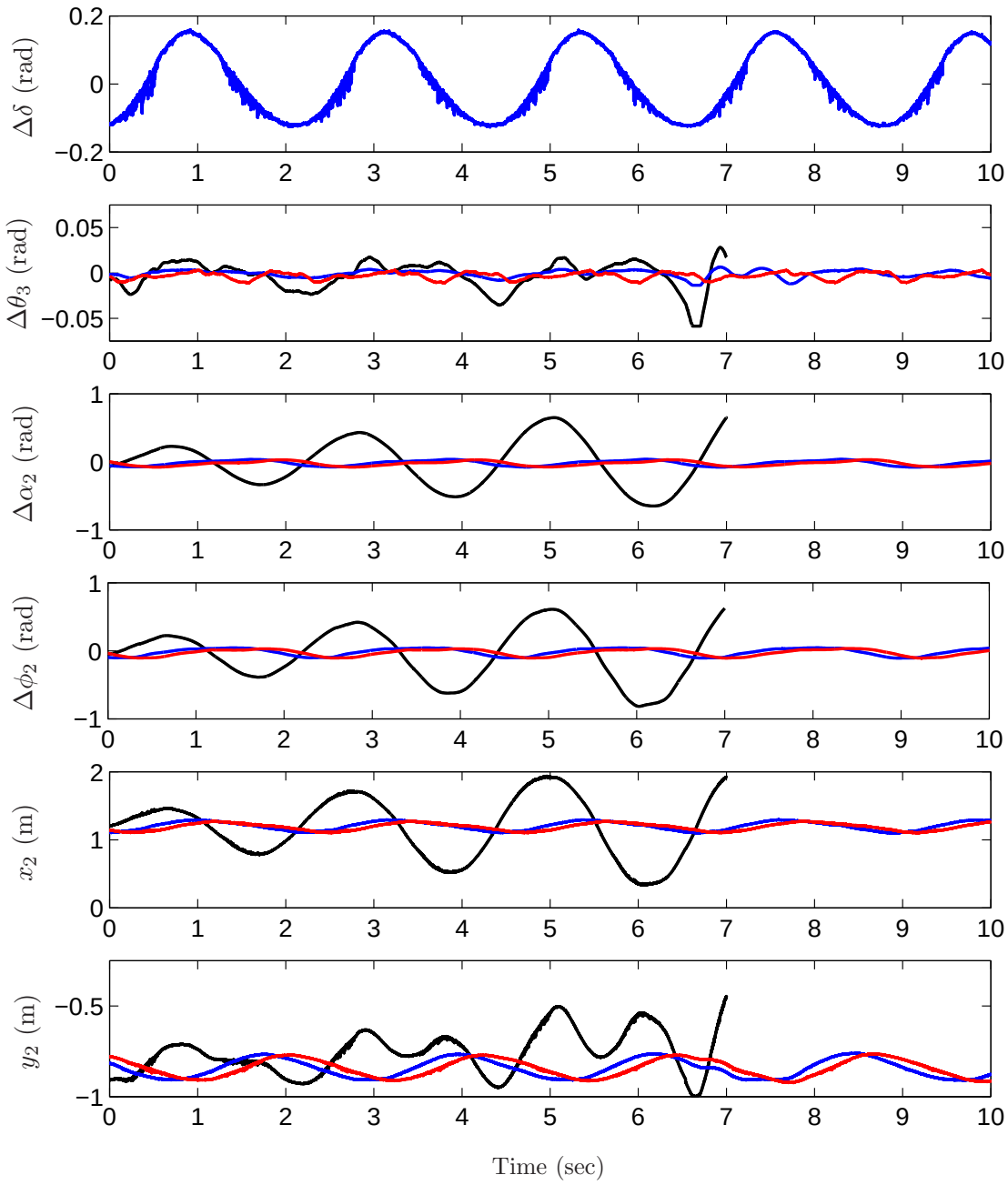

Figure 5.18: Experimental response due to sinusoidal rolling ±10 degree, —— uncontrolled —— controlled (camera), —— controlled (strain gauge)

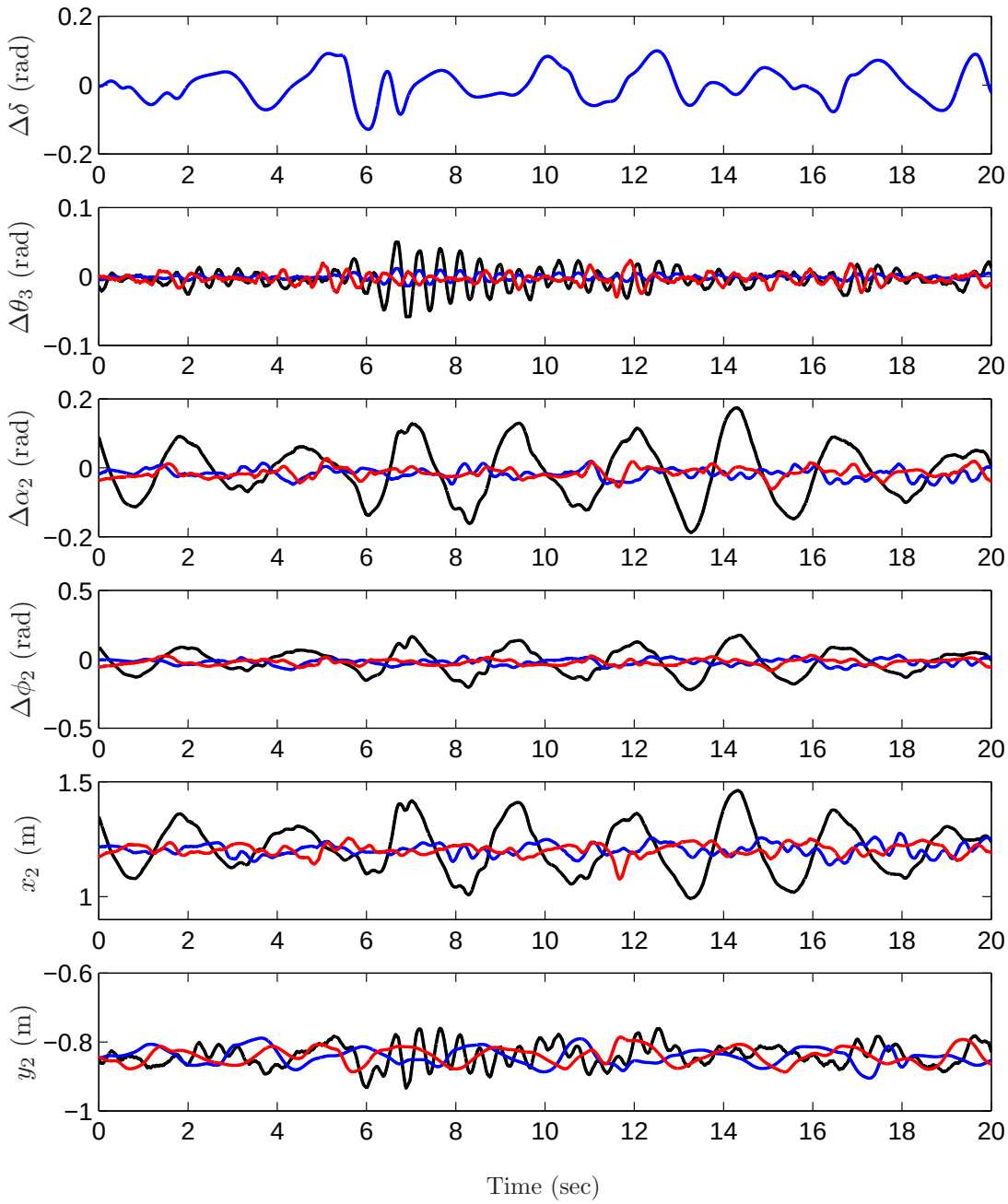

Figure 5.19: Experimental response due to chaotic rolling —— uncontrolled —— controlled (camera), —— controlled (strain gauge)

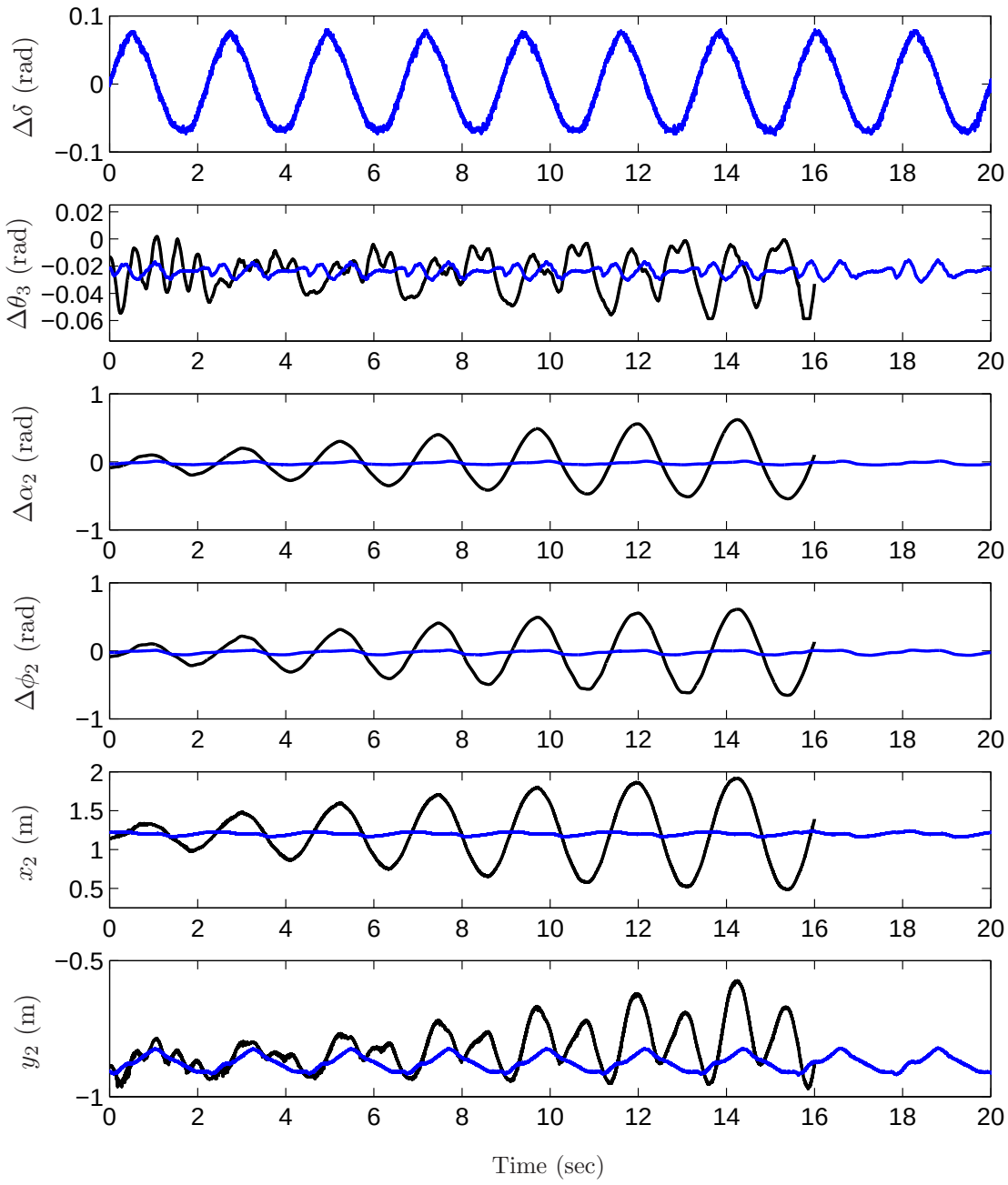

Figure 5.20: Experimental response due to sinusoidal rolling ±5 degree, (10 kg payload) —— uncontrolled —— controlled

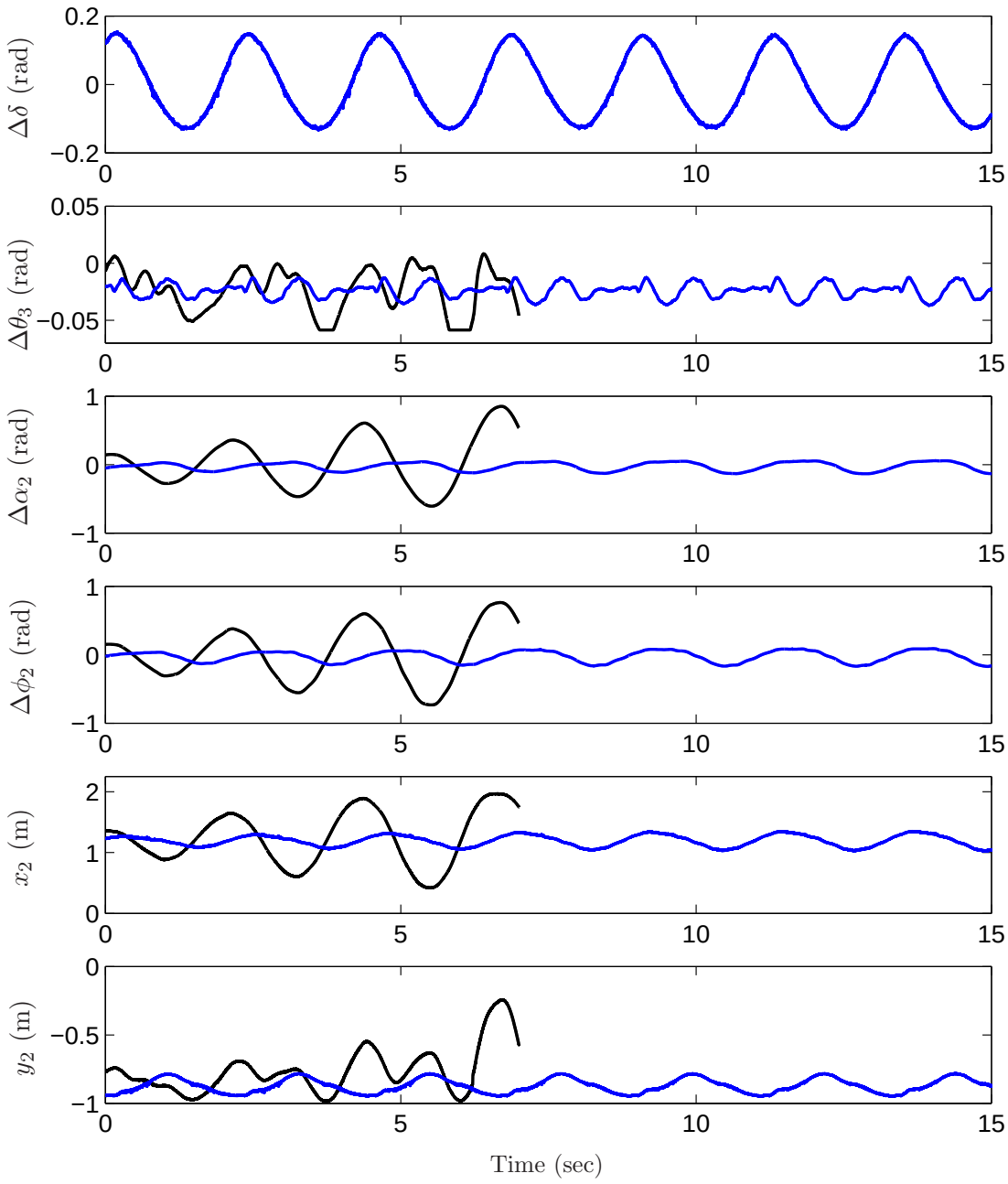

Figure 5.21: Experimental response due to sinusoidal rolling ±10 degree, (10 kg payload) —— uncontrolled —— controlled

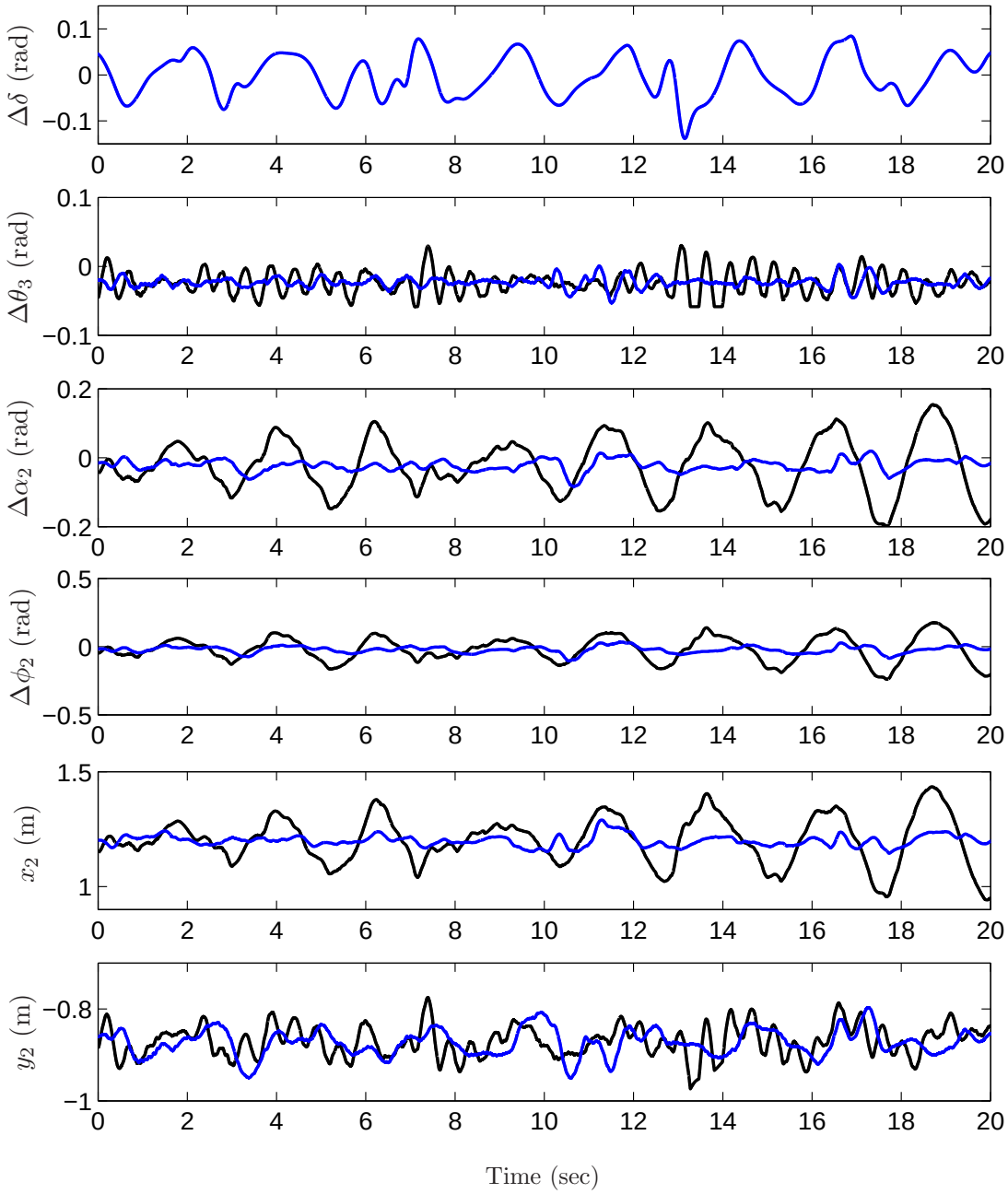

Figure 5.22: Experimental response due to chaotic rolling (10 kg payload) —— uncontrolled —— controlled

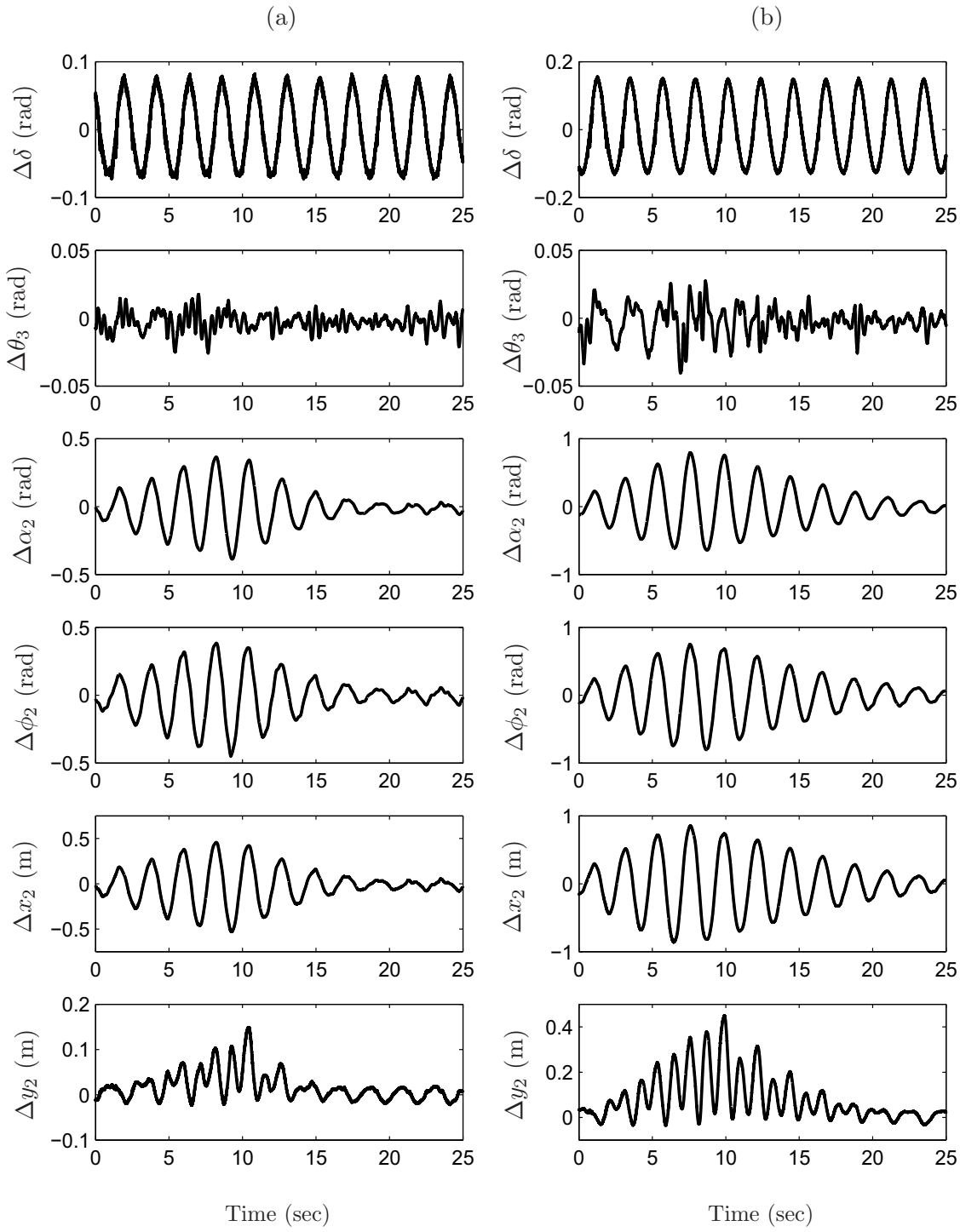

Figure 5.23: Experimental response due to sinusoidal rolling ±5 degree, (7.5 kg payload), controller turned on at the $10th$ second, (a) ± 5 Deg rolling , (b) ± 10 Deg rolling

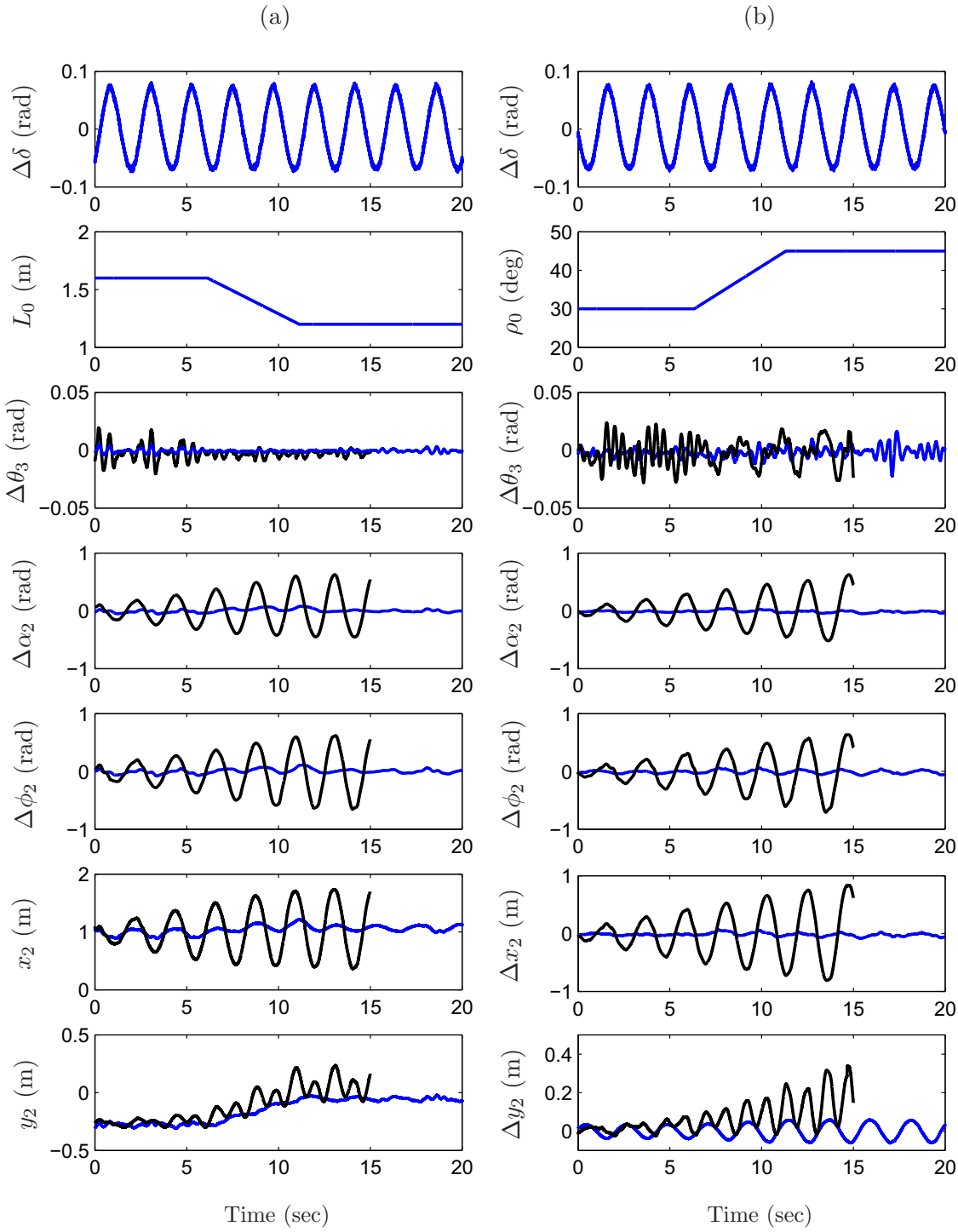

Figure 5.24: Experimental response due to sinusoidal rolling: (a) ±5 degree, length of the cable changes during operation, (b) ±10 degree, luff angle changes during the operation, —— uncontrolled —— controlled

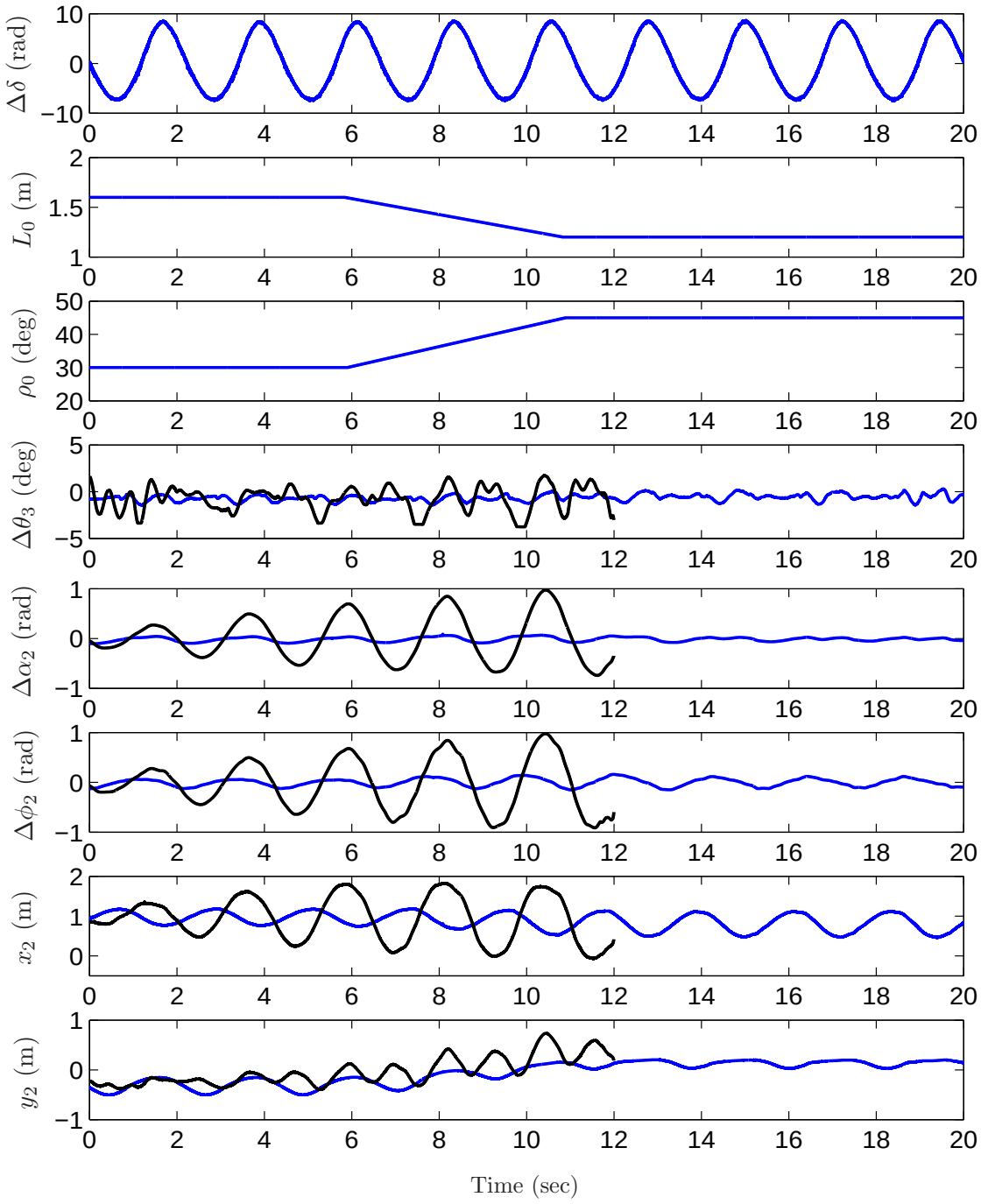

Figure 5.25: Experimental response due to sinusoidal rolling (7.5 kg payload), —— uncontrolled —— controlled

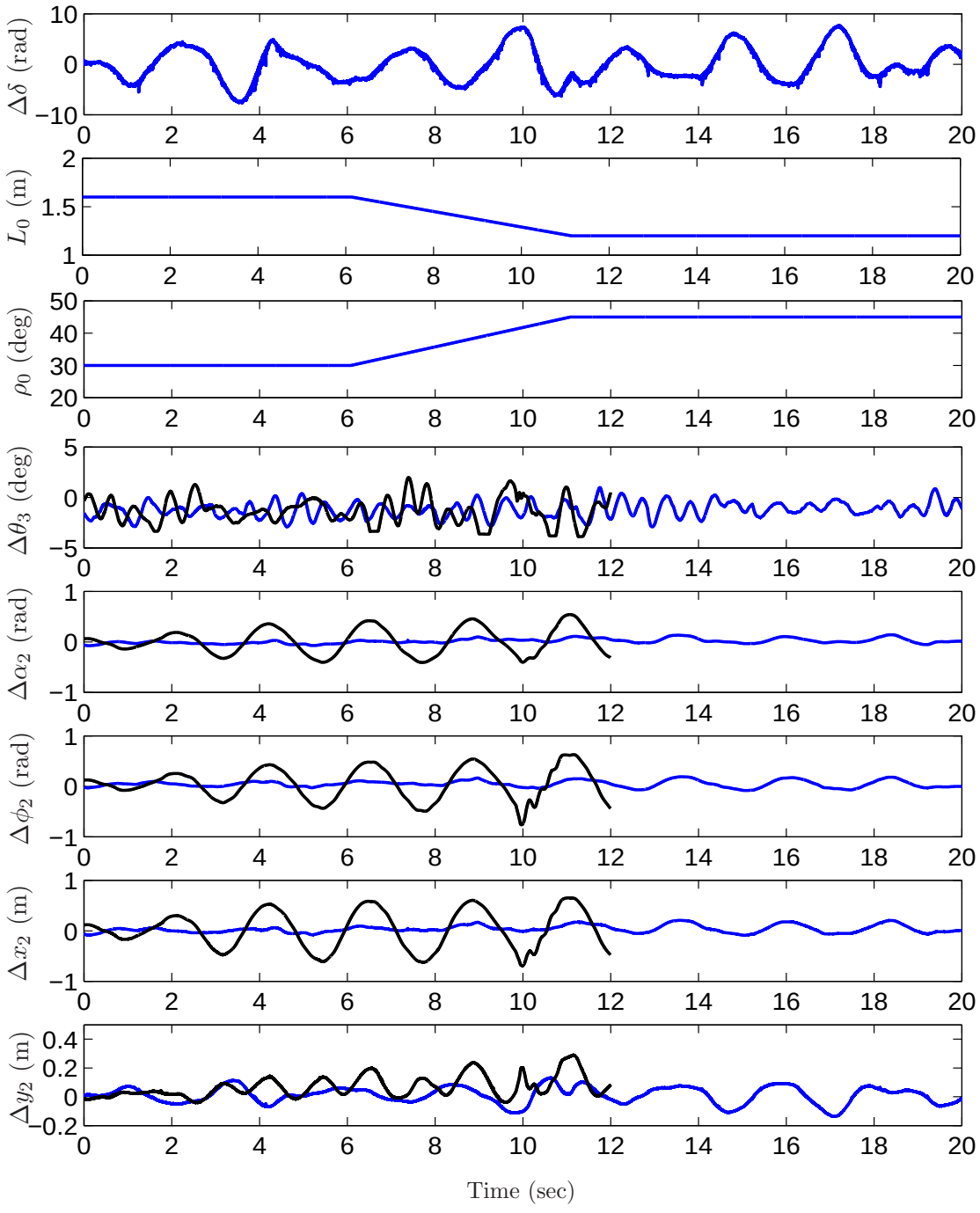

Figure 5.26: Experimental response due to sinusoidal rolling (10 kg payload), —— uncontrolled —— controlled

5.4 Summary

In this chapter the experimental realization of the visual servoing for elastic ship-mounted crane was presented. The components of the elastic crane system test-rig are presented in detail. Also the camera setup in the system, the model of the camera used in the experiments, and the camera calibration are explained. The intrinsic and extrinsic parameters of the camera are addressed. The image processing procedure (i.e. deflection measurements using camera) is presented. Several experiments regarding control of the payload of the elastic crane have been done, in order to ensure that the combination of the two measurement devices is reliable. The approach of using two variable gain observers presented in the last chapter is tested. The results show that the estimation of the dynamic states of the elastic crane works effectively and removes the effects of noise and time delay. It is also important to report that the crane system works very robust using only the measurements of the camera, this results mainly from the ability of the Kalman filter system to remove the effects of noise and time delay.

6 Summary, Conclusion, and Recommendations

6.1 Summary and conclusion

In this thesis the control of flexible link robot using vision sensor data, is studied. The dynamic state variable estimation process using camera measurements have been deeply examined, which is the core of the state feedback control process used in the control of flexible link robot. The main two inherent problem related to vision sensor measurements have been solved in case of state estimation process. Despite time delay and presence of noise in camera measurements; the suggested estimation approach has proved reliability and the dynamics state variables estimated within acceptable accuracy. A traditional state estimator is proposed, which is combined with an augmented Kalman filter to estimate dynamic states of the model.

The dynamic model of the flexible link in chapter 3 is separated to slow and fast dynamics based on assumed camera specification. Two observers are designed using the fast and slow dynamics, the first one to estimate the higher modes of the vibration using strain gauges, the second one representing an estimator using the camera as a sensor to estimate a modal set of slow dynamics based on the frequency of the system states. The proposed method for state estimation is used later for the more complex system, by integrating the flexible link with the overall dynamics of the elastic ship-mounted crane.

In chapter 4 and chapter 5 the elastic ship-mounted crane system is studied. The dynamic model of flexible link which is re-derived based on a two element flexible beam to simplify the observer and controller design problem. The higher modes of vibration of the flexible beam has no large effects on the tip deflection estimation. Two observers are designed, the first (PI-observer) is used to estimate displacement variables and disturbances using potentiometer, the second represents an augmented Kalman filter using the camera as a sensor to estimate displacement variables. Based on a multi-model approach, variable gain observers and controller are designed, in order to cover all the operation conditions of the elastic crane. The states from the second variable estimator are combined with the states estimated using the first observer using minimum mean squared error. The effect of the noise and time delay can be effectively removed from the estimated states after applying this approach. The observer-based control works well and mitigate the error in the estimated states due to the unknown initial conditions rapidly, the controller based on the estimated states attenuates the vibration and suppresses the swing of the payload. Several simulations for the both cases have been applied. And in order to verify the effectiveness of the proposed approach the experimental tests are carried out using elastic crane test rig and CCD camera.

Consequently, the vision sensor (camera) beside other types of measurements can be used effectively to estimate the dynamic state variables of the system, if the

number of modes considered in the model are in the bound of the camera frame rate. It can be shown from the results addressed in this work that the vision sensors represent a good substitute by "slow dynamics" for strain gauges. The idea of using vision as sensing device can be easily extended to other cases due to the fact that no extra measurement equipments is required (different from the case of using strain gauges); which represents another advantage for complex structures with flexible components.

In this thesis for the first time the following results are obtained:

- The state variables estimation for flexible link robot can be estimated using camera measurements if the considered modes of vibration are in the range of camera frame rate.
- When the observer is appropriately designed, noisy measurements have no effect on the estimated states.
- The time delay in the measurements can be compensated successfully using an accounting dynamic term related to the time delay.
- The state estimation process for complex mechanical systems can be optimized based on different types of measurements.

6.2 Recommendations

To extend the "results of this thesis", the following points are recommended as further development:

1. The velocity measurement of the tip-deflection using the camera can be included for the dynamic state variable estimation of flexible link.
2. Instead of CCD sensor and LED markers, IR-camera and IR-markers can be used to increase the measurement quality.
3. The measurements of the camera can be extended to include the other two outputs in the elastic ship-mounted crane case.
4. The neuro-fuzzy intelligent control methods based on camera measurements for flexible link robot can be used.

Bibliography

[AJSMM10] A. Assa, F. Janabi-Sharifi, B. Moshiri, and I. Mantegh, "A data fusion approach for multi camera based visual servoing," in *International Symposium on Optomechatronic Technologies*, Toronto, Canada, 2010, pp. 1–7.

[ASS07] Y. Al-Sweiti and D. Söffker, "Modeling and control of an elastic ship-mounted crane using variable gain model-based controller," *Journal of Vibration and Control*, vol. 13, no. 5, pp. 657–685, 2007.

[Bou] J. Y. Bouguet. Camera calibration toolbox for matlab. Vision Laboratory of California Institute of Technology. USA. Accessed 19 August, 2012. [Online]. Available: www.vision.caltech.edu/bouguetj

[BR03] L. Bascetta and P. Rocco, "Task space visual servoing of eye-in-hand flexible manipulators," in *IEEE/ASME International Conference on Advanced Intelligent Mechatronics*, Politecnico di Milano, Italy, 2003, pp. 1442–1448.

[BR04] ——, "Tip position control of flexible manipulators through visual servoing," in *6th Conference of Dynamics and Control of Systems and Structures in Space*, Riomaggiore, Italy, 2004, pp. 673–682.

[BR06a] ——, "End-point vibration sensing of planar flexible manipulators through visual servoing," *Mechatronics*, vol. 16, pp. 221–232, 2006.

[BR06b] ——, "Two-time scale visual servoing of eye-in-hand flexible manipulators," *IEEE Transactions on Robotics*, vol. 22, pp. 818–830, 2006.

[CCPK09] M. Choi, J. Choi, J. Park, and W. K.Chung, "State estimation with delayed measurements considering uncertainty of time delay," in *IEEE International Conference on Robotics and Automation*, Kobe, Japan, May 2009, pp. 3987–3992.

[CH08] F. Chaumette and S. Hutchinson, *Visual Servoing and Visual Tracking: Handbook of Robotics*. Springer, 2008.

[Cha98] F. Chaumette, "Potential problems of stability and convergence in image-based and position-based visual servoing," in *Conference of Vision and Control*, vol. 237, 1998, pp. 66–78.

[CLG+06] L. Cuvillon, E. Laroche, H. Garnier, J. Gangloff, and M. Mathelin, "Continuous time model identification of robot flexibilities for fast visual servoing," in *IFAC Symposium on System Identification*, Newcastle, Australia, 2006, pp. 1264–1269.

[CLG+12] ——, "A multivariable methodology for fast visual servoing of flexible manipulators moving in a restricted workspace," *Advanced Robotics*, vol. 26, pp. 1771–1797, 2012.

[CLGM05] L. Cuvillon, E. Laroche, J. Gangloff, and M. Mathelin, "GPC versus H-infinity control for fast visual servoing of a medical manipulator including flexibilities," in *IEEE International Conference on Robotics and Automation*, Barcelona, Spain, 2005, pp. 4044–4049.

[Cor11] P. Corke, *Robotics, Vision and Control: Fundamental Algorithms in MATLAB*. Springer, 2011.

[DDM09] G. Dubus, O. David, and Y. Measson, "Vibration control of a flexible arm for the ITER maintenance using unknown visual features from inside the vessel," in *IEEE/RSJ International Conference on Intelligent Robots and Systems*, Interactive Robot Unit, CEA, Fontenay-aux-Roses, France, 2009, pp. 5697–5704.

[DDM10] ——, "A vision-based method for estimating vibrations of a flexible arm using on-line sinusoidal regression," in *IEEE International Conference on Robotics and Automation*, Anchorage Convention District, Anchorage, Alaska, USA, 2010, pp. 4068–4075.

[DE06] S. Dwivedy and P. Eberhard, "Dynamic analysis of flexible manipulators, a literature review," *Mechanism and Machine Theory*, vol. 41, no. 7, pp. 749–777, 2006.

[DJSW02] L. Deng, F. Janabi-Sharifi, and W. Wilson, "Stability and robustness of visual servoing methods," in *IEEE International Conference on Robotics and Automation*, vol. 2, no. 2, Washington, DC, USA, 2002, pp. 1604–1609.

[DlB08] A. De-luca and W. Book, "Robots with flexible elements," *Springer Handbook of Robotics*, pp. 287–319, 2008.

[Dub10] G. Dubus, "On-line estimation of time varying capture delay for vision-based vibration control of flexible manipulators deployed in hostile environments," in *IEEE/RSJ International Conference on Intelligent Robots and Systems*, Taipei, Taiwan, 2010, pp. 3765–3770.

[Esp93] B. Espiau, "Effect of camera calibration errors on visual servoing in robotics," in *3rd International Symposium on Experimental Robotics*, vol. 200, 1993, pp. 187–193.

[FS04] A. Ferrara and R. Scattolini. (2004) Control of a robot manipulator for aerospace applications. [Online]. Available: http://naca.central.cranfield.ac.uk/dcsss/2004/E22_Ferrara_a.pdf

[GBB+09] L. Gargiulo, P. Bayetti, V. Bruno, J.-C. Hatchressian, C. Hernandez, M. Houry, D. Keller, J.-P. Martins, Y. Measson, Y. Perrot, and F. Samaille, "Operation of an ITER relevant inspection robot on tore supra tokamak," *Fusion Engineering Design*, vol. 84, no. (2-6), pp. 220–223, 2009.

[GH07] N. Gans and S. Hutchinson, "Stable visual servoing through hybrid switched-system control," *IEEE Transaction on Robotics*, vol. 23, no. 3, pp. 530–540, 2007.

[Has03] K. Hashimoto, "A review on vision-based control of robot manipulators," *Advanced Robotics*, vol. 17, no. 10, pp. 969–991, 2003.

[HDAG08] T. Heitzmann, C. Doignon, C. Albitar, and P. Graebling, "Position-based visual servoing using a coded structured light sensor," in *IEEE International Workshop on Robotic and Sensors Environments*, Ottawa-Canada, 2008, pp. 126–131.

[HDRT04] F. Heijden, R. Duin, D. Ridder, and D. Tax, *Classification, Parameter Estimation and State Estimation, An Engineering Approach using MATLAB*. John Wiley and Sons, 2004.

[HHC96] S. Hutchinson, G. Hager, and P. Corke, "A tutorial on visual servo control," *IEEE Transactions on Robotics and Automation*, vol. 12, no. 5, pp. 651–670, 1996.

[HJ07] A. H. A. Hafez and C. V. Jawahar, "Visual servoing by optimization of a 2d/3d hybrid objective function," in *IEEE International Conference on Robotics and Automation*, Roma, Italy, 2007, pp. 1691–1696.

[HP79] J. Hill and W. Park, "Real time control of a robot with a mobile camera," in *Proceedings of the 9th International Symposium on Industrial Robots*, Washington DC, USA, 1979, pp. 233–246.

[HS12a] M. T. Hussein and D. Söffker, "State variables estimation for control of elastic crane using vision sensor data," in *Joint Conference MOVIC and ASME DSCC (Dynamic Systems and Control Conference)*, Ft. Lauderdale, FL, USA, 2012, pp. 65–72.

[HS12b] ——, "State variables estimation of flexible link robot using vision sensor data," in *Proceedings of 7th Vienna Conference on Mathematical Modeling on Dynamical Systems MATHMOD 2012*, vol. 7, no. 1. Vienna, Austria: IFAC, 2012, pp. 193–198.

[HS12c] ——, "Variable gain control of elastic crane using vision sensor data," in *International Conference on Control, Automation, Robotics and Vision, ICARCV 2012*, Guangzhou, China, 2012, pp. 1783–1788.

[Hut01] P. C. S. Hutchinson, "A new partitioned approach to image-based visual servo control," *IEEE Transactions on Robotics and Automation*, vol. 17, no. 4, pp. 507–515, 2001.

[JAB12] M. Jörn, S. P. Anh, and T. Bertram, "Scene adaptive rgb-d based oscillation sensing for a multi flexible link robot arm in unstructured dynamic environments," in *IEEE/RSJ International Conference on Intelligent Robots and Systems*, Vilamoura, Algarve, Portugal, 2012, pp. 1017–1022.

[JAR+10] M. Jörn, S. P. Anh, F. Rene, H. Frank, and T. Bertram, "Markerless visual vibration damping of a 3-dof flexible link robot arm," *ISR/ROBOTIK 2010, Munich, Germany*, pp. 401–408, 2010.

[JAT12a] M. Jörn, S. P. Anh, and B. Torsten, "A multi-link-flexible robot arm catching thrown balls," *ROBOTIK 2012, Munich, Germany*, pp. 411–416, 2012.

[JAT12b] ——, "Predictive delay compensation for camera based oscillation damping of a multi-link flexible robot," *Intelligent Robotic and Applications Lecture notes in Computer Science*, vol. 7508, pp. 93–102, 2012.

[JE07] Z. Jiang and T. Eguchi, "Vision feedback based end-effector motion control of a flexible robot arm," in *IEEE International Conference Systems, Man, and Cybernetics*, Hiroshima, Japan, 2007, pp. 2413–2419.

[JF09] C. M. Jaime and R. C. Fernando, "Visual servoing controller for robot manipulators," in *International Conference on Electrical, Communications, and Computers*, Puebla, Mexico, 2009, pp. 153–158.

[JG05] Z. Jiang and A. Goto, "Visual sensor based vibration control and end-effector control for flexible robot arms," in *IEEE International Conference on Industrial Technology*, Hiroshima, Japan, 2005, pp. 383–388.

[Jia08] Z. Jiang, "Vision-based cartesian space motion control for flexible robotic manipulators," *International Journal of Modelling, Identification and Control*, vol. 4, no. 4, pp. 406–414, 2008.

[JKU06] X. Jiang, A. Konno, and M. Uchiyama, "Visual servoing experiment using a 3d flexible-link manipulator," in *IEEE/RSJ International Conference on Intelligent Robots and Systems*, Tohoku University, Sendai, Japan, 2006, pp. 1224–1229.

[JKU07] ——, "A vision-based endpoint trajectory and vibration control for flexible manipulators," in *IEEE International Conference on Robotics and Automation*, Roma, Italy, 2007, pp. 3427–3432.

[JS02] F. Janabi-Sharifi, *Opto-Mechatronic Systems Handbook*. Boca Raton, Florida: CRC Press, 2002.

[JU05] S. J. Julier and J. Uhlmann, "Fusion of time delayed measurements with uncertain time delays," in *American Control Conference*, Portland, OR, USA, 2005, pp. 4028–4033.

[JYKU08] X. Jiang, Y. Yabe, A. Konno, and M. Uchiyama, "Vibration suppression control of a flexible arm using image features of unknown objects," in *IEEE/RSJ International Conference on Intelligent Robots and Systems*, Tohoku University, Sendai, Japan, 2008, pp. 3783–3788.

[KC02] D. Kragic and H. Christensen, "Survey on visual servoing for manipulation," Royal Institute of Technology, Sweden, Sweden, Technical Report, January 2002.

[KMM10] J. G. Katz, S. Mohan, and D. W. Miller, "On-orbit assembly of flexible space structures with SWARM," in *AIAA Infotech Conference*. Atlanta, GA, USA: AIAA, 2010.

[KPB04] H. Küçük, G. Parker, and E. Baumgartner, "Robot positioning of flexible-link manipulator using vision," *Robotica*, vol. 22, pp. 301–307, 2004.

[LD04] M. D. Lichter and S. Dubowsky, "State shape and parameter estimation of space objects from range images," in *IEEE International Conference on Robotics and Automation*, New Orleans, LA, USA, 2004, pp. 2974–2979.

[LD05] ——, "Shape, motion, and parameter estimation of large flexible space structures using range images," in *IEEE International Conference on Robotics and Automation*, Barcelona, Spain, 2005, pp. 4487–4492.

[LF04] J. Larsen and N. Ferrier, "A case study in vision based neural network training for control of a planar, large deflection, flexible robot manipulator," in *IEEE/RSJ International Conference on Intelligent Robots and Systems*, Madison, NJ, USA, 2004, pp. 2924–2929.

[LS13] G. Ligorio and A. M. Sabatini, "Extended Kalman filter-based methods for pose estimation using visual, inertial and magnetic sensors: Comparative analysis and performance evaluation," *Sensors*, vol. 13, pp. 1919–1941, 2013.

[LUD06] M. D. Lichter, H. Ueno, and S. Dubowsky, "Vibration estimation of flexible space structures using range imaging sensors," *International Journal of Robotics Research*, vol. 25, no. 10, pp. 1001–1012, 2006.

[LZW+08] X. Lu, H. Zhang, H. Wang, W. Wang, and L. Xie, "Kalman filtering for continuous-time systems with multiple delayed measurements," *IET Signal Processing*, vol. 2, pp. 37–46, 2008.

[Mal02] E. Malis, "Survey of vision-based robot control," European Naval Ship Design Short Course, Captain Computer IV Forum, ENSIETA, Brest, France, 2002.

[MC02a] E. Malis and F. Chaumette, "Theoretical improvements in the stability analysis of a new class of model-free visual servoing methods. ." *IEEE Transactions on Robotics and Automation*, vol. 18, no. 2, pp. 176–186, 2002.

[MC02b] E. Marchand and F. Chaumette, "Virtual visual servoing: a framework for real-time augmented reality," in *Eurographics*, vol. 21, no. 3, Saarbrücken, Germany, 2002, pp. 289–298.

[MCB99] E. Malis, F. Chaumette, and S. Boudet, "2&1/2-d visual servoing." *IEEE Transactions on Robotics and Automation*, vol. 5, no. 2, pp. 238–250, 1999.

[MKU03] T. Miyabe, A. Konno, and M. Uchiyama, "Automated object capturing with a two-arm flexible manipulator," in *IEEE International Conference on Robotics and Automation*, Sendai, Japan, 2003, pp. 2529–2534.

[MKU04] ——, "An approach toward an automated object retrieval operation with a two-arm flexible manipulator," *International Journal of Robotics Research*, vol. 23, no. 3, pp. 275–291, 2004.

[OB96] K. Obergfell and W. Book, "Vision sensor for control of long-reach flexible manipulators." in *Japan-U.S.A. Symposium on Flexible Automation*, Boston, MA, USA, 1996, pp. 945–950.

[OB99] ——, "Control of flexible manipulators using vision and modal feedback," in *International Conference on Recent Advances in Mechatronics*, Istanbul, Turkey, 1999, pp. 71–86.

[PCT07] J. Pomares, F. Chaumette, and F. Torres, "Adaptive visual servoing by simultaneous camera calibration," in *IEEE International Conference on Robotics and Automation*, Roma, Italy, 2007, pp. 2811–2816.

[Rob86] A. P. Roberts, "State estimation when some measurements are delayed," *IMA Journal of Mathematical Control and Information*, vol. 3, pp. 299–310, 1986.

[SMGP13a] M. Sabatini, R. Monti, P. Gasbarri, and G. Palmerini, "Adaptive and robust algorithms and tests for visual-based navigation of a space robotic manipulator," *Acta Astronautica*, vol. 83, pp. 65–84, 2013.

[SMGP13b] ——, "Deployable space manipulator commanded by means of visual-based guidance and navigation," *Acta Astronautica*, vol. 83, pp. 27–43, 2013.

[SMSC08] G. P. Sequeira, L. Mendonça, J. Sousa, and P. J. Caldas, "Uncalibrated eye-to-hand visual servoing using inverse fuzzy model," *IEEE Transaction on Fuzzy Systems*, vol. 16, no. 2, pp. 341–353, 2008.

[SMVP99] M. Stieber, M. McKay, G. Vukovich, and E. Petriu, "Vision-based sensing and control for space robotics applications," *IEEE Transactions on Instrumentation and Measurement*, vol. 48, no. 4, pp. 807–812, 1999.

[SY09] X. Shen and R. Yin, "Fuzzy control for a visual servoing system," in *Global Congress on Intelligent Systems*, Shanghai, China, 2009, pp. 93–97.

[SYM95] D. Söffker, T. J. Yu, and P. C. Müller, "State estimation of dynamical systems with nonlinearities by using proportional-integral observer," *International Journal of System Science*, vol. 26, pp. 1571–1582, 1995.

[Tew02] A. Tewari, *Modern Control Design With MATLAB and SIMULINK*. John Wiley and Sons, 2002.

[TWL90] P. Tang, H. Wang, and S. Lu, "A vision-based position control system for a one-link flexible arm," in *IEEE International Workshop on Intelligent Motion Control*, Istanbul, Turkey, 1990, pp. 523–528.

[WHB96] W. Wilson, C. Hulls, and G. Bell, "(1996) relative end-effector control using cartesian position-based visual servoing." *IEEE Transactions on Robotics and Automation*, vol. 12, no. 5, pp. 684–696, 1996.

[WLW08a] H. Wang, Y. Liu, and Z. Wang, "Adaptive visual servoing using angle and distance," in *7th World Congress on Intelligent Control and Automation*, Chongqing, China, 2008, pp. 479–484.

[WLW08b] ——, "Uncalibrated dynamic visual servoing using line features," in *IEEE/RSJ International Conference on Intelligent Robots and Systems*, Nice, France, 2008, pp. 3046–3051.

[WLZ08] H. Wang, Y. Liu, and D. Zhou, "Adaptive visual servoing using point and line features with an uncalibrated eye-in hand camera," *IEEE Transaction on Robotics*, vol. 24, no. 4, pp. 843–857, 2008.

[XR09] Y. Xu and E. Ritz, "Vision based flexible beam tip point control," *IEEE Transaction on Control Systems Technology*, vol. 17, no. 5, pp. 1220–1227, 2009.

[YOK01] T. Yoshikawa, A. Ohta, and K. Kanaoka, "State estimation and parameter identification of flexible manipulators based on visual sensor and virtual joint model," in *IEEE International Conference on Robotics and Automation*, Kyoto, Japan, 2001, pp. 2840–2845.

[ZLC06] H. Zhang, X. LU, and D. Cheng, "Optimal estimation for continuous-time systems with delayed measurements," *IEEE Transactions on Automatic Control*, vol. 51, pp. 823–827, 2006.

Conference contributions

This thesis is based on the results and development steps published in the following citations presented in the corresponding conferences.

[HS12a] M. T. Hussein and D. Söffker, "State variables estimation for control of elastic crane using vision sensor data," in *Joint Conference MOVIC and ASME DSCC (Dynamic Systems and Control Conference)*, Ft. Lauderdale, FL, USA, 2012, pp. 65–72.

[HS12b] ——, "State variables estimation of flexible link robot using vision sensor data," in *Proceedings of 7th Vienna Conference on Mathematical Modeling on Dynamical Systems MATHMOD 2012*, vol. 7, no. 1. Vienna, Austria: IFAC, 2012, pp. 193–198.

[HS12c] ——, "Variable gain control of elastic crane using vision sensor data," in *International Conference on Control, Automation, Robotics and Vision, ICARCV 2012*, Guangzhou, China, 2012, pp. 1783–1788.